
THE UNIVERSITY
*of* EDINBURGH

# Effects of AMPK deletion on the response to hypoxia

Utibe–Abasi Sunday Udoh


PhD by Research

The University of Edinburgh

2015

# Declaration

I declare that this thesis is entirely my own composition and the work is my own unless clearly indicated as done in collaboration where I made a significant contribution. This work has not been submitted for any other degree or professional qualification except as specified.

# Acknowledgements

I am deeply grateful to my principal supervisor, Prof. Mayank B. Dutia for his guidance, assistance and support throughout the entire period of this work. Prof. Dutia took time to teach me a lot of things that were helpful both for the theoretical and practical aspects of this project, without which this work would not have been possible – thank you so much Prof.

I will also like to express my appreciation to my co-supervisors Prof. Mark Evans and Prof. Gareth Leng for all their support and encouragement during the course of my studies at the University of Edinburgh. Prof. Mark Evans out of his benevolence gave me all the mice that I used for this project and was deeply involved in the day to day progress of this work while on the other hand Prof. Gareth Leng who as the Head of the Edinburgh University School of Biomedical Sciences for a greater part of my study provided me with all the support I needed for the successful completion of this work.

My sincere gratitude goes to Drs. Nancy Sabatier, Vicky Tobin and Amira Mahmoud, for teaching me amongst other things the techniques of immunohistochemistry and plethysmography. My thanks also go to all the past and present members of the Evans lab for all their support especially Dr. Oluseye Ogunbayo and Dr Jorge Navarro-Dorado for their help and assistance. This acknowledgement will be incomplete without me extending my appreciation to all the members of the NCS group, Centre for Integrative Physiology and my office mates. All of you have been so helpful and supportive – thanks so much.

My sincere gratitude also goes to my wife and son for all their encouragement, emotional and financial support, and endurance throughout the course of my study. You are treasures to me.

Finally I will like to appreciate my parents who guided me into the paths of intellectual accomplishment and the Nigerian government for their sponsorship of my studies.

# Abstract

The enzyme adenosine monophosphate activated protein kinase (AMPK), a critical regulator of energy metabolism in the body, is activated by a rise in the cellular AMP: ATP ratio in response to metabolic stresses such as hypoxia. The work in this thesis arises from the recent characterization by Mahmoud, A. (PhD thesis, University of Edinburgh, 2015) of the response to hypoxia of mice lacking the α1 and α2 isoforms of the catalytic subunit of the AMPK molecule. Targeted conditional deletion of the genes encoding the α1 and/or α2 subunits of AMPK in catecholaminergic cells (including cells in the carotid body and the brain) was achieved by crossing mice expressing Cre-recombinase under the control of the tyrosine hydroxylase (TH) promoter, with mice in which either or both α subunits of AMPK were flanked by loxP sequences. AMPKα1/α2-/- mice showed a profoundly abnormal ventilatory response to hypoxia, compared to AMPKα1/α2fl/fl controls. Interestingly however, in vitro recordings from the CSN in isolated carotid body preparations from AMPKα1/α2-/- mice showed that the carotid body afferent response to hypoxia was completely normal in these mice. The abnormal response to hypoxia in AMPKα1/α2-/- mice appears therefore to be due to a deficit in the central, catecholaminergic brainstem neurons involved in respiratory control, where a lack of AMPK activation appears to inhibit the normal hypoxia-induced hyperventilation. While the importance of the peripheral carotid body chemoreceptors in oxygen-sensing has long been established, these findings indicate that the synergistic activation of AMPK in central brainstem neurons by the hypoxic metabolic stress, is also required for the normal response to hypoxia.

In this thesis, the responses to hypoxia of AMPKα1/α2-/- mice, AMPKα2-/- mice and AMPKα1/α2fl/fl controls were studied using whole-body plethysmography. The findings showed that AMPKα1/α2-/- mice displayed a respiratory phenotype of longer and increased number of apnoeas coupled with hypoventilation in comparison to both the AMPKα2-/- mice and AMPKα1/α2fl/fl controls confirming the earlier results of Mahmoud (2015). In addition TH immunostaining in the carotid bodies of AMPKα1/α2-/- mice and AMPKα1/α2fl/fl controls was compared to determine if there was any change in the number or density of TH-positive cells in the AMPKα1/α2-/- animals, and the gross result showed a 2-fold decrease in the number of TH- immunopositive cells in the AMPKα1/α2-/- mice as compared to the AMPKα1/α2fl/fl. Intriguingly, if this observation is statistically confirm coupled with the unattenuation of the normal afferent discharge from the carotid bodies of AMPKα1/α2-/- mice then it is plausible that a certain degree of redundancy operates in the physiology of the carotid body with regards to oxygen sensing or the glomus cells type lost may be those not involved in mediating the response to hypoxia.

In the main part of this work, c-fos and TH immunohistochemistry were used to investigate the activation of brainstem catecholaminergic neurons by hypoxia, in AMPKα1/α2-/- mice, AMPKα2-/- mice and AMPKα1/α2fl/fl controls. Significant differences in c-fos immunostaining of TH+ve neurons were observed in the SubP

region of the NTS, and the C2 region and the A1 region of the ventral respiratory group, implicating these specific regions in the abnormal hypoxic ventilatory response in AMPKα1/α2-/- animals. Catecholaminergic neurons in these brainstem regions are known to play key role in the control of breathing as a loss of these neurons or decrease in their catecholamine content results in severe respiratory abnormalities including respiratory arrhythmias and apnoeas as seen in the Rett syndrome.

A significant hyperplasia of the brainstem stem catecholaminergic neurons was also observed in both the AMPKα1/α2-/-and AMPKα2-/- mice consistent with the known inhibitory effects of AMPK activation on cell growth and proliferation. Finally a pilot study was carried out to determine if the respiratory phenotype observed in AMPKα1/α2-/- mice could be replicated using a viral vector to deliver Cre-recombinase to targeted areas in the brainstem in AMPKα1/α2fl/fl mice, to knock out AMPK in specific neuronal subgroups. Although the data obtained from this set of experiments were encouraging, the animals did not show the respiratory phenotype as observed in the conditional knockout mice maybe due to poor targeting of specific brainstem neuronal populations including the SubP region or inadequate transfection of these cells due to low viral titre. One advantage of this pilot work was that responses due to compensatory mechanisms as may be the case in the conditional knock out animals were eliminated.

These findings are of interest in understanding the neural control of respiration in hypoxia and acclimatization to altitude, and may also suggest new avenues for therapeutic intervention in breathing disorders such as non-obstructive sleep apnoea. It also raises the possibility that AMPK may be a useful therapeutic tool for disease conditions whose etiology is based on cellular proliferation, such as various forms of cancer and even atherosclerosis.

# Lay Summary

Adenosine monophosphate activated protein kinase (AMPK) is an important cellular enzyme that is involved in the regulation of energy metabolism by regulating the supply of ATP in all tissues of the body. In this work the role of AMPK in the response of mice to low oxygen tension (hypoxia) was studied, using a mouse model in which the α–catalytic subunit of the AMPK molecule had been deleted. In contrast to normal animals that showed marked hyperventilation upon exposure to hypoxia, in AMPK-deficient mice the hyperventilatory response was reduced and interspersed with apnoeas. The areas of the brain that may be responsible for this abnormal ventilatory response in the AMPK-deficient mice were investigated using immunohistochemical staining for c-fos, a marker for neuronal activation, following exposure to hypoxia. The results identified several areas of the brainstem where this abnormal ventilatory response may arise, and showed that AMPK in these brainstem areas plays an important part in producing the normal hyperventilatory response to hypoxia. These findings throw more light on the understanding of the control of breathing during hypoxia, and may also be of value in the management or treatment of breathing disorders such as non-obstructive sleep apnoea.

# List of Abbreviations

| | |
|---|---|
| A1 | A1 noradrenergic cell group |
| A2 | A2 noradrenergic cell group |
| AAV | adeno-associated virus vector |
| ADP | adenosine diphosphate |
| AICAR | 5-aminoimidazole-4-carboxamide-1-beta-4-ribofuranoside |
| AMP | adenosine monophosphate |
| AMPK | adenosine monophosphate activated protein kinase |
| AP | area postrema |
| AP-1 | activator protein -1 |
| ATP | adenosine triphosphate |
| BotC | Botzinger complex |
| C2 | C2 adrenergic cell group |
| C3 | C3 adrenergic cell group |
| CaMKKβ | $Ca^{2+}$/Calmodulin-dependent protein kinase kinase β |
| CB | carotid body |
| CBS | cystathionine-β-synthase domains |
| CC | central canal |
| CPG | respiratory central pattern generator |
| Cre | Cre-recombinase |
| CSN | Carotid sinus nerve |
| CVL | caudal ventrolateral medullary nucleus |
| cVRG | caudal ventral respiratory group |
| DFlox | AMPK double-floxed animal (AMPK $\alpha1^{fl/fl}$ $\alpha2^{fl/fl}$) |
| DKO | AMPK double-knockout animal (AMPK $\alpha1^{-/-}$ $\alpha2^{-/-}$) |
| DNA | deoxyribonucleic acid |

| | |
|---|---|
| DRG | dorsal respiratory group |
| FRAs | Fos-related antigens |
| GFP | green fluorescent protein |
| IV | fourth ventricle |
| K-F | Kolliker-Fuse nucleus |
| LKB1 | liver kinase B1 (tumor suppressor kinase) |
| LPBr | lateral parabrachial region |
| LRt | lateral reticular nucleus |
| LV | lentivirus |
| mRNA | messenger ribonucleic acid |
| NAd | nucleus ambiguus, dorsal division |
| NTS | nucleus of the solitary tract |
| PCR | polymerase chain reaction |
| pFRG | parafacial respiratory group |
| PGCI | retrofacial paragigantocelullar nucleus, lateral part |
| Pn | ventral pontine nucleus |
| PP2A | protein phosphatase 2A |
| PP2C | protein phosphatase 2C |
| PreBotC | preBotzinger complex |
| PRG | pontine respiratory group |
| RTN | retrotrapezoid nucleus |
| RVL | rostral ventrolateral medullary nucleus |
| rVRG | rostral ventral respiratory group |
| SO | superior olivary nucleus |
| SolC | nucleus of the solitary tract (commissural) |
| SolM | nucleus of the solitary tract (medial) |
| SolV | nucleus of the solitary tract (Ventral) |

| | |
|---|---|
| SolVL | nucleus of the solitary tract (Ventrolateral) |
| SubP | nucleus of the solitary tract (SubP) |
| TAK1 | TGF-β-activated kinase 1 |
| TH | tyrosine hydroxylase |
| TH+ve | tyrosine hydroxylase immunopositive cells |
| V | motor nucleus of the trigeminal nerve |
| Vll | motor nucleus of the facial nerve |
| VLM | ventrolateral medulla |
| VRC | ventral respiratory column |
| VRG | ventral respiratory group |
| X | dorsal nucleus of the vagus nerve |
| XII | hypoglossal motor nucleus |
| α2-KO | AMPK α2 knockout mice (AMPK $\alpha1^{+/+}$ $\alpha2^{-/-}$) |

# Contents


| | |
|---|---|
| Declaration | i |
| Acknowledgements | ii |
| Abstract | iii-iv |
| Lay Summary | v |
| List of Abbreviations | vi-viii |

**Chapter 1: General Introduction**

| | |
|---|---|
| 1.1 Background | 1 |
| 1.2 Literature Review Part 1: AMPK | 3 |
| 1.3 Literature Review Part 2: Oxygen sensing in the carotid bodies | 12 |
| 1.4 Literature Review Part 3: Central control of breathing by brainstem respiratory centres | 17 |
| Chapter 1 Figures 1.1 – 1.4 | 23-26 |

**Chapter 2: Activation of brainstem areas during hypoxia in AMPK-deficient mice**

| | |
|---|---|
| 2.1 Introduction | 27 |
| 2.2 Materials and Methods | 32 |
| 2.3 Results | 42 |
| *2.3.1 Ventilatory response of mice following exposure to hypoxia* | *42* |
| *2.3.2 Activation of brainstem catecholaminergic neurons by hypoxia and the effects of AMPK deletion* | *48* |
| 2.4 Discussion | 53 |
| 2.5 Conclusion | 61 |
| Chapter 2 Figures 2.1 – 2.12 | 62-74 |

**Chapter 3: The effects of AMPK deletion on the peripheral carotid body**

3.1 Introduction 75

3.2 Materials and Methods 76

3.3 Results 79

3.4 Discussion 80

Chapter 3 Figures 3.1-3.3 84-87

**Chapter 4: Pilot Study to develop virus-targeted AMPK knock-out in brain areas**

4.1 Introduction 88

4.2 Materials and Methods 93

4.3 Results 96

4.4 Discussion 100

Chapter 4 Figures 4.1 – 4.7 104-110

Chapter 5: General Discussion 111

Chapter 5 Figures 5.1-5.2 122-124

List of References 125

# Chapter 1

## General Introduction

### *1.1 Background*

The moment-to-moment control of energy metabolism in the body is essential for the survival of all organisms. In mammalian cells, the enzyme adenosine monophosphate activated protein kinase (AMPK) has been recognized as the critical regulator of this energy homeostasis (Viollet et al., 2010, Carling et al., 2011; Hardie et al., 2012; Miyamoto et al., 2015). AMPK is activated by a rise in the cellular adenosine 5'- monophosphate (AMP) : adenosine 5'- triphosphate (ATP) ratio in response to metabolic stresses such as hypoxia, ischemia, glucose deprivation, starvation, heat shock and muscle contraction (Kahn et al. 2005; Towler and Hardie, 2007; Fisslthaler and Fleming, 2009, Viollet et al., 2010; Figure 1.1). On activation AMPK switches on ATP generating processes such as glycolysis in the heart , mitochondrial biogenesis in the muscle and fatty acid uptake and oxidation in multiple tissues, while switching off ATP–consuming biosynthetic pathways such as fatty acid and protein synthesis, cholesterol synthesis in the liver, cell growth and proliferation (Towler and Hardie, 2007; Viollet et al., 2010; Figure 1.1).

The work in this thesis is based on the recent characterization by Mahmoud, A. (PhD Thesis, University of Edinburgh; Mahmoud 2015a) of the response to hypoxia of mice lacking the α1 and α2 isoforms of the α-catalytic subunit of the AMPK molecule in catecholaminergic cells (including cells in the carotid body and the

brain), which are known to be involved in the control of breathing (Urena et al.,1994; Montoro, et al.,1996; Lopez-Barneo et al.,2008; Hirooka et al., 1997; Erickson and Millhornm 1994; Teppema et al.,1997; Greenberg et al; 1999). Targeted conditional deletion of the genes encoding the α1 and α2 catalytic subunits of AMPK (AMPK $\alpha1^{-/-}$ $\alpha2^{-/-}$ animals, herein referred to as double-knockout or DKO animals) was achieved by crossing mice expressing Cre-recombinase under the control of the tyrosine hydroxylase (TH) promoter (TH-Cre mice), with mice in which either or both of the isoforms of the α subunit of the AMPK were flanked by loxP sequences (AMPK $\alpha1^{fl/fl}$ $\alpha2^{fl/fl}$ , herein referred to as double-floxed or DFlox mice).

Upon exposure to hypoxia (8% $O_2$, 0.05% $CO_2$, balanced with $N_2$), Mahmood (2015a) demonstrated that AMPK knockout (DKO) mice showed marked abnormal ventilatory responses that were characterized by apnoeas and hypoventilation, in contrast to the hyperventilation that was observed in DFlox controls. It is well established that the carotid body is the primary sensory organ that detects changes in the partial pressure of oxygen in the arterial blood and that during hypoxia it transmits afferent signals through the carotid sinus nerve (CSN) to brainstem neurons to elicit the hypoxic hyperventilatory response (Prabhakar, 2000; Lui et al., 2009; Lopez-Barneo et al.,2009). Strikingly however, *in vitro* recordings from the CSN in isolated carotid body preparations of DKO mice showed that the carotid body sensory response to hypoxia was normal (Mahmoud et al., 2015a). The observed abnormal response to hypoxia in DKO animals is therefore not due to an abnormal carotid body response, but instead AMPK deletion appears to precipitate a

deficit in the central brainstem respiratory control network, which fails to respond correctly to the hypoxia signaled by the CSN afferents. In this work, I therefore investigated the brainstem catecholaminergic neurons which are known to be involved in the control of respiration, to determine the effects of AMPK deletion on their response to hypoxia in DKO mice.

The central regulation of ventilation occurs in the brainstem respiratory centres, which contains well-defined catecholaminergic neuronal populations such as the A1/A2 noradrenergic neurons and the C1/C2 adrenergic neurons that are involved in respiratory control (Li and Nattie, 2006; Buller et al., 2008; Li et al., 2008; Soliz et al., 2008; Smith, et al., 2013; Guyenet et al.2013; Zoccal et al., 2014). The abnormal response to hypoxia observed in DKO mice may therefore be due to a deficit in any or all of these central catecholaminergic brainstem neurons, where the deletion of AMPK may result in the loss of the normal hyperventilatory response to hypoxia. This possible importance of AMPK and its activation by hypoxia in central brainstem neuronal pathways is potentially of great interest, as it may be relevant in certain disorders of breathing such as some types of sleep apnoeas, and in the physiological adaptations to living at altitude. In the main part of this thesis, I therefore investigated the areas of the brainstem in which AMPK may mediate this important functional modulation of the hypoxic ventilatory response.

### *1.2 Literature Review Part 1: AMPK*

AMPK belongs to the family of protein kinases that have been highly conserved in all eukaryotic cells (Stein et al., 2000; Hardie et al., 1998; Hardie et al., 2003; Motoshima et al., 2006; Towler and Hardie, 2007; Xiao et al., 2007; Emerling et al., 2009; Hardie, 2004; Viollet et al., 2010; Xiao et al., 2011; Hardie, et al., 2012; Hardie, 2013). It is homologous to the *saccharomyces cerevisiae* protein kinase Snf1 which is required for yeast survival during conditions of glucose starvation (Celenza and Carlson, 1986; Hardie et al., 1994; Woods et al., 1994; Steinberg and Kemp, 2009; Viollet et al., 2010).

AMPK is activated by a rise in the cellular AMP: ATP ratio resulting from metabolic stresses that deplete ATP either by interfering with its production (e.g hypoxia, ischemia, glucose deprivation, starvation and heat shock) or accelerating its consumption (e.g muscle contraction, vigorous exercise)(Kahn et al. 2005; Motoshima et al., 2006; Towler and Hardie, 2007; Fisslthaler and Fleming, 2009, Viollet et al., 2010). Upon activation, AMPK turns off ATP-consuming processes such as lipid and glycogen synthesis, cell growth and proliferation, while turning on ATP-generating processes such as fatty acid oxidation and glycolysis (Carling 2004; Towler and Hardie, 2007; Emerling et al., 2009). Thereby making energy available for use under conditions where ATP is limited (Emerling et al., 2009).

#### *1.2.1 Structure of mammalian AMPK*

AMPK is a heterotrimeric complex, consisting of an α-catalytic subunit and two regulatory, noncatalytic β and γ subunits (Carling, 2004; Evans, 2006; Wyatts and

Evans,2007; Evans et al., 2009; Viollet et al., 2010; Carling et al., 2012; Ruderman et al., 2013; Miyamoto et al., 2015). In mammals isoforms of each subunit exist, α (α1 and α2), β (β1and β2), γ (γ1,γ2 and γ3) and they are products of different genes (Fryer and Carling, 2005 ; Viollet et al., 2010; Carling et al., 2012; Ruderman et al., 2013; Miyamoto et al., 2015). There are 2 or 3 genes that encode for each subunit, resulting in at least 12 possible heterotrimeric complexes (Fryer and Carling, 2005; Towler and Hardie, 2007; Viollet et al., 2010). Also alternative splicing of some of the genes ( e.g γ2 and γ3 isoforms) and the use of different promoters further increase the diversity and complexity of AMPK system (Carling, 2004; Fryer and Carling, 2005; Towler and Hardie, 2007; Viollet et al., 2010). There are indications that the different isoforms give rise to both tissue specificity, and the specificity in response to a specific type of stimulus (metabolic stress) by AMPK (Fryer and Carling, 2005; Viollet et al., 2010). For example the γ3 isoform expressed predominately in the fast-twitch type II fibres of the skeletal muscles, appears to play a role in the control of fuel utilization in these tissues (Barnes et al., 2004; Mahlapuu et al., 2004; Fryer and Carling, 2005).

The AMPKα1 isoform is richly expressed in the adipose tissue, pancreas, lung, spleen and kidney and is predominantly in the cytoplasm (Towler and Hardie, 2007; Fisslthaler and Fleming, 2009; Viollet et al., 2010). In the other hand, the AMPKα1 isoform in carotid body type I cells is associated with the plasma membrane, while in the airway epithelial cells it is also associated mainly with its apical membrane (Hallows et al., 2003; Evans et al., 2005; Towler and Hardie, 2007). The AMPKα2-subunit is found in the nucleus of several cell types, such as the pancreatic β cells,

neurons, skeletal and cardiac muscles (Salt et al., 1998; Turnley et al., 1999; Towler and Hardie, 2007; Fisslthaler and Fleming, 2009; Viollet et al., 2010).

The are several amino acid residues in the α subunit that can be phosphorylated both *in vitro* and *in vivo* and one of such is Threonine 172, whose phosphorylation is required for AMPK activation (Carling, 2004) (see Figure 1.2). The α1 and /or α2 subunit is the catalytic domain of the AMPK molecule and thus it full functionality depends on the intact presence of this domain. Studies in high- altitude dwellers (e.g Andean populations) have shown that the gene for the AMPK-α1 subunit (*PRAKK1*) has been modified by natural selection through single nucleotide polymorphisms (Bigham et al., 2014; Mahmoud et al., 2015b). Therefore it has been hypothesized that the body through natural selection may be utilizing AMPK to synchronise responses arising from oxygen deficits (hypoxia) in animals and its α1- subunit is the principal mediator of this function (Evans, 2006; Mahmoud et al., 2015b).

The β subunit contains two characteristic regions, a central (glycogen- binding) domain and a C-terminal domain (Hudson et al., 2003; Polekhina et al., 2003; Iseli et al., 2005; Townley and Shapiro, 2007; Viollet et al., 2010; Carling et al., 2012). The physiological role of the central domain is unclear, although it is found in enzymes that metabolise starch and glycogen and there is speculation that the domain could be involved in binding AMPK to glycogen, as well as providing a mechanism for the regulation of AMPK by glycogen (Hudson et al., 2003; Polekhina et al., 2003; Carling, 2004; Fryer and Carling, 2005; Viollet et al., 2010; Carling et al., 2012). The c-terminal domain on the other hand is required for functional binding with the β and

γ subunits (Hudson et al., 2003, Iseli et al., 2005; Fryer and Carling, 2005; Townley and Shapiro, 2007; Carling et al., 2012; see Figure 1.2).

The γ-subunit contains a variable N-terminal domain that is followed by four domains which are known as CBS (cystathionine-β-synthase) domains (Bateman, 1997; Fryer and Carling, 2005; Towler and Hardie, 2007; Viollet et al., 2010). The CBS domain in AMPK forms the adenine nucleotides (AMP, ADP, ATP)-binding (regulatory) sites (Viollet et al., 2010; Carling et al., 2012; see Figure 1.2).

### *1.2.2 Regulation of AMPK*

The activity of AMPK can be regulated via various ways and these include:

***Allosteric Regulation:***

In mammals, AMPK activity is allosterically activated by AMP (Emerling et al., 2009; Viollet et al., 2010; Xiao, et al., 2011; Hardie, 2011; Carling et al., 2012). AMP binds to the regulatory γ subunit and this binding result in a 2 to 5 fold increase in the kinase activity (Hardie et al., 1999; Viollet et al., 2010; Carling et al., 2012). The nature of the α and γ- isoforms that make up the AMPK complex, markedly affect the level of its activation by AMP (Cheung et al., 2000; Viollet et al., 2010; Carling et al., 2012). It has been reported that complexes containing the γ3 isoform are weakly activated by AMP, while those containing the α2 and γ2 subunits show the greatest degree of activation (Cheung et al., 2000; Viollet et al., 2010). When AMP binds to the γ-subunit of AMPK, it leads to a change in the shape of the enzyme that indirectly affects its catalytic activity (allosteric activation) and this conformational change in the protein kinase also protects it from dephosphorylation by protein phosphatases, as well as promoting phosphorylation by upstream kinases (Davies et al., 1995; Suter et al., 2006; Sanders et al., 2007; Oakhill et al., 2010; Viollet et al., 2010). ATP in high concentrations, has been shown to antagonise the effects of AMP on AMPK (Davies et al., 1995; Hardie et al., 1999; Viollet et al., 2010; Carling et al., 2011), indicating that it is a change in the intracellular AMP/ATP ratio, rather than the AMP concentration, that regulates AMPK activity (Viollet et al., 2010; Carling et al., 2011).

***Regulation via phosphorylation / dephosphorylaton:***

The major way of regulating AMPK activity is through reversible phosphorylation (Stein et al., 2000; Viollet et al., 2010; Xiao et al., 2011; Carling et al., 2012). The phosphorylation of the amino acid residue Threonine 172 of the α subunit, by upstream kinases activates AMPK (Stein et al., 2000; Emerling et al., 2009; Xiao et al., 2011; Carling et al., 2012; Miyamoto et al., 2015). The phosphorylation of Thr172, leads to a several-hundred-fold increase in the activity of AMPK (Suter et al., 2006; Sanders et al., 2007; Xiao et al., 2011). It has been reported that, the combination of the allosteric and phoshorylation activation of AMPK, produces more than a 1000- fold increase in its activity (Suter et al., 2006; Hardie, 2011). In mammalian cells, the principal upstream kinases that phosphorylate (Thr172) AMPK, include the tumor suppressor kinase, LKB1 (liver kinase B1) and $Ca^{2+}$/Calmodulin-dependent protein kinase kinase β (CaMKKβ) (Woods et al., 2003; Hawley et al., 2005; Hurley et al., 2005; Woods et al., 2005; Viollet et al., 2010; Carling et al. 2011; Carling et al. 2012) . In addition to the above, a number of other upstream kinases may be involved in the phosphorylation of AMPK in vivo (Carling et al., 2008; Viollet et al., 2010).

*In vitro* studies have shown that AMPK can be de-phosphorylated by the protein phosphatases PP2A and PP2C (Davies et al. 1995; Viollet et al., 2010).The ability of the phosphatases to dephosphorylate AMPK at Thr-172 is inhibited when AMP binds to the γ- subunit (Davies et al., 1995; Sanders et al., 2007; Viollet et al., 2010).

***Regulation by ADP***

Recent studies have shown that ADP also plays a role in the regulation of the activity of AMPK. ADP can bind to any one of two nucleotide (AMP/ADP/ATP) binding sites on the regulatory fragment of the AMPK complex (Xiao et al., 2011). This binding protects the enzyme from dephosphorylation, but does not lead to its allosteric activation (Xiao et al., 2011; Carling 2012). Previous studies have shown that in normal conditions AMPK mainly exists in its inactive form in a complex with Mg-ATP (Xiao et al., 2007, Xiao et al., 2011). The mammalian AMPK binds more tightly to ADP and AMP (about 10 –fold ) than to Mg-ATP, so despite the higher physiological concentration of Mg-ATP the competitive binding of either ADP or AMP offsets the Mg-ATP from the regulatory binding sites of the enzyme (Carling et al., 2011; Xiao et al., 2011). Therefore under most conditions AMPK activity is regulated by the ATP: ADP ratio via changes in phosphorylation at Thr172 (Carling et al., 2011). However, during severe stress conditions, when the concentration of AMP is very high, the additional allosteric activation by AMP may function as a further device, which ensures that all AMPK molecules are fully phosphorylated resulting in maximum activation (Carling et al., 2011).

***Regulation of AMPK at whole- body level***

Various hormones, cytokines, nutrients and substances play a role in the regulation of AMPK activity at whole body level. AMPK plays a role in the hypothalamus,

where it acts as a central regulator of food intake by mediating various orexigenic and anorexigenic signals (Kola et al., 2006; Kola et al., 2008; Blanco et al., 2011). Studies have shown that AMPK activity in the hypothalamus increases during fasting and drop during refeeding (Minokoshi et al., 2004; Kola et al., 2008). Leptin, when administered *in vivo* results in a fall in hypothalamic AMPK activity and reduced food intake (Minkoshi et al., 2004; Andersson et al., 2004) , while ghrelin, an orexigenic hormone on the other hand activates hypothalamic AMPK and increases food intake (Andersson et al., 2004; Blanco et al., 2011). Other hormones include adiponectin which increases AMPK activity in the arcuate nucleus of the hypothalamus leading to increased feeding (Yamauchi et al, 2002; Blanco et al., 2011; Hardie et al., 2012). Studies have also shown that anorectic hormones and factors such as cilliary neurotrophic factor, insulin, estradiol, glycogen-like peptide-1 inhibit hypothalamic AMPK activity (Watt et al., 2006; Blanco et al., 2011), while orexigenic signals such as glucocorticiods, cannabinoids and the neuropeptide agouti-related protein increases hypothalamic AMPK activity (Blanco et al., 2011). Hypothalamic AMPK activity is also modulated by nutrients such as glucose, whose administration suppresses AMPK activity and citrate, lactate, and amino acids such as leucine which have inhibitory influences on AMPK activity resulting in anorexigenic responses (Blanco et al., 2011).

AMPK plays a role in skeletal muscle metabolism, where it mediates the non-insulin dependent- glucose uptake in skeletal muscle cells during exercise (Merrill et al., 1997; Kola et al., 2008). AMPK mediates this action mainly in the glycolytic, fast-twitch (white) muscles and not in the oxidative, slow-twitch (red) muscles (Kola et

al., 2008; Hardie et al., 2006). In the liver, AMPK activation causes the inhibition of gluconeogenesis, fatty acid, triglyceride, cholesterol and protein synthesis, while it stimulates fatty acid oxidation (Kola et al., 2008). In line with the above its activation in the adipose tissue causes decreased fatty acid uptake, decreased triglyceride synthesis and increased fatty acid oxidation (Kola et al., 2008).

### *1.3 Literature Review Part 2: Oxygen-sensing in the carotid bodies*

In mammals the ventilatory response to hypoxia originates from the carotid bodies (Teppema and Dahan, 2010). The carotid bodies are small sensory organs located bilaterally within the carotid bifurcation (Kumar, 2007; Lopez-Barneo et al., 2009). It is now fully established that the carotid bodies are the primary peripherial arterial chemoreceptors, although the molecular sensor that couples decrease in oxygen tension during hypoxia to its activation is still unknown (Prabhakar, 2000; Prabhakar and Peng, 2004; Liu, et al., 2009; Lopez- Barneo et al., 2008).

The afferent (sensory) nerve supply of carotid body is via the carotid sinus nerve (CSN), which is a branch of the glossopharyngeal nerve (cranial nerve IX), with its cell bodies located in the petrosal ganglion (Figure 1.3). The carotid body afferents project to the nucleus of the tractus solitarius (NTS) of the medulla in the brainstem, where information is integrated to control both cardiopulmonary and autonomic reflex responses (Kumar, 2007; Figure 1.3).

The efferent innervations to the carotid body include a sympathetic input from the closely located superior cervical ganglion and a parasympathetic efferent from the

vagus nerve (Kumar, 2007). The carotid body is a highly vascular organ, receiving its blood flow through a branch arising from the external carotid artery (Kumar, 2007; Lopez-Barneo et al., 2008). The capillary network across the carotid body consists of both the typical diameter capillaries (about 7-8 μm) and wider diameter penetrating sinusoid vessels (18μm) that lie in very close contact with the type I cells (Kumar, 2007) . Apart from the capillary network, arterio-venous shunts are also present in the carotid bodies and these allow for multiple routes of blood flow through the organ. The approximate blood flow through the carotid body is (2000ml/100g-$^{1}$.min-$^{1}$, at normal blood gases and blood pressure), amounting to about 10-15 times that received by the brain, relative to its size (Kumar, 2007).

The parenchyma of the carotid body is organised into clusters of cells (3-5 in each cluster) in intimate contact with capillaries and nerve fibers (glomeruli) (Kumar, 2007; Lopez-Barneo et al. 2009). Among the various cells types in the glomerulus, the most abundant ones are the neuron-like type I or glomus cells (8-12μm in diameter), and enveloping them are the processes of the sustentacular (glia-like) type II cells (Prabhakar, 2000; Kumar, 2007; Lopez-Barneo et al., 2009). Autonomic neurons and fibers which appear to have efferent regulatory action on the type 1 cells are also found in the carotid body (Lopez-Barneo et al., 2008). The type I cells have been identified as the primary oxygen–sensing cells in the carotid body, while type II cells are regarded as being supportive in nature (Prabhakar, 2000; Prabhakar and Peng, 2004; Lahiri et al., 2006; Kumar, 2007; Lopez-Barneo et al., 2008, 2009). The type II cells also act as *in vivo* precursors of new glomus cells during hypoxic conditions (Pardal et al., 2007; Lopez-Barneo et al., 2008).

The glomus cells contain secretory vesicles that are packed with a variety of both excitatory and inhibitory neurotransmitters and neuromodulators, which have been hypothesized to be involved in the chemosensory function of the carotid body (Nurse, 2005; Kumar, 2007; Lope-Barneo et al., 2008). These include amines (e.g dopamine, norepinephrine and acetylcholine), neuropetides (e.g substance P), purines (e.g ATP and adenosine), amino acids (e.g γ-aminobutyric acid (GABA) and gas signalling molecules (e.g nitric oxide and carbon monoxide) (Nurse, 2005; Kumar, 2007; Lope-Barneo et al., 2008, 2009). Dopamine has been suggested to play an autocrine role in the function of the carotid body via its inhibition of the glomus cell $Ca^{2+}$ channels, while on the other hand ATP and ACh appear to be the main neurotransmitters that mediate the glomus cell–afferent chemo-transmission in the carotid body (Nurse, 2005; Lope-Barneo et al., 2009).

### *1.3.1 Oxygen sensing in the carotid body*

Almost all mammalian cells sense oxygen, but the carotid body is a specialised oxygen sensing organ that can detect and transduce modest falls in the partial pressure of oxygen in the arterial blood ($PaO_2$) to a neural signal that is beneficial for the overall maintenance of oxygen homeostasis in the body (Prabhakar, 2000; Prabhakar and Peng, 2003; Lahiri et al., 2006; Kumar, 2007; Lope-Barneo et al., 2008).

It is well established that the glomus cells are the chemoreceptive elements in the carotid body and upon exposure to hypoxia, these cells release excitatory

neurotransmitters that act on nearby sensory nerve fibers resulting in an increase in the afferent traffic through the carotid sinus nerve (CSN) (Prabhakar, 2000; Prabhakar and Peng, 2003; Lahiri et al., 2006; Lope-Barneo et al., 2008; Lope-Barneo et al., 2009; Evans et al., 2009; Lui et al., 2009). The CSN afferents project to the brainstem where they elicit appropriate adjustments in the breathing patterns until the partial pressure of oxygen ($PO_2$) in the blood is restored to normal (Prabhakar, 2000; Prabhakar and Peng, 2003; Lahiri et al.,2006; Lope-Barneo et al., 2008, 2009; Evans et al., 2009; Lui et al., 2009). Many classes of $O_2$- sensitive $K^+$ channels are found in the glomus cells and it has been reported that during hypoxia their opening probability (modulated by an unknown oxygen transducer) decreases resulting in the depolarization of the glomus cell membrane (Peers and Buckler, 1995; Lopez-Berneo et al., 2001; Weir et al., 2005; Lopez- Berneo et al., 2008). Some of these channels include, the voltage –dependent $K^+$ channel, the $Ca^{2+}$-dependent maxi- $K^+$ and the twin pore acid-stimulated $K^+$ channel-like background channel (Lope-Barneo et al., 2008). It is worth noting that there are species differences in the type of $O_2$- sensitive $K^+$ channels that are expressed and also that within species there may be an expression of more than one type of $O_2$- sensitive $K^+$ channels (Peers et al., 2010) . Apart from $K^+$ channels the type 1 cells also express a wide range of voltage–dependent $Na^+$ and $Ca^{2+}$ channels (Lope-Barneo et al., 2009).

The basic mechanism for the carotid body chemotransduction during hypoxia involves, the inhibition of specific $K^+$ channels via the action of a molecular sensor which leads to glomus cell membrane depolarization, with a resultant increase in

firing rates of the cells resulting in $Ca^{2+}$ channel opening and transmembrane $Ca^{2+}$ influx into the cell, which elicits neurotransmitter release (Lopez- Barneo et al., 2008, 2009; Peers et al., 2010). This basic sensory process of the carotid body chemotransduction during hypoxia is referred to as the membrane hypothesis for oxygen sensing (Lopez- Barneo et al., 2008; Peers et al., 2010). The generated neural signal is then conveyed through the CSN to the NTS in the medulla of the brainstem (Kumar, 2007).

Although there have been great advances in understanding the cellular physiology of the carotid body, the molecular mechanisms (and/or sensor) that underpin the type1 cell oxygen sensing (i.e. the precise mechanism(s) through which deviation in oxygen tension is translated into the inhibition of $K^+$ channel in the glomus cells) is still largely unknown (Wyatt and Evans, 2007; Lopez- Barneo et al., 2008; Peers et al., 2010). While several hypotheses have been put forward to explain this oxygen sensing mechanism(s) of the carotid body, the two principal ones are the mitochondrial hypothesis and the Membrane hypothesis (Lahiri et al. 2006; Wyatt and Evans, 2007).

The mitochondrial hypothesis suggests a possible role of the mitochondria in the carotid body chemotransduction following hypoxia and this is in line with the early findings of Heymans et al. (1931) that potassium cyanide stimulates respiratory reflexes when introduced into the carotid sinus, an effect similar to that which is observed during hypoxia (Wyatt and Evans, 2007). Cyanide is an inhibitor of mitochondrial complex IV (Lopez- Barneo et al., 2008) and several reports have shown that similar to hypoxia, inhibitors of the electron transport chain (ETC) or

mitochondrial uncouplers increase the afferent discharge of the carotid sinus nerve (Mills and Jobsis, 1972; Lopez-Barneo et al., 2008). Thus traditionally several investigators have considered the mitochondria to be the site of oxygen sensing in type I cells of the carotid body (Lopez-Barneo et al., 2008). On the other hand, the membrane hypothesis as earlier noted explains that hypoxia causes the inhibition of specific $K^+$ channels in glomus cells leading to their depolarisation and a resultant opening of voltage-gated $Ca^{2+}$ channels and $Ca^{2+}$ influx which triggers the release of neurotransmitters (Urena et al., 1994; Buckler and Vaughan-Jones,1994; Peers et al., 2010). At present the membrane hypothesis is generally accepted, but there are many divergent views concerning how hypoxia leads to the inhibition of $K^+$ channel activity (Peers et al., 2010) and thus there is an ongoing search for the oxygen sensor.

One of such postulated $O_2$ sensors is AMPK (Evans et al., 2005; Evans, 2006; Evans et al., 2009; Wyatt et al., 2007; Wyatt and Evans, 2007; Peers et al., 2010). The AMPK hypothesis, suggests that hypoxia increases the AMP/ATP ratio in the glomus cell as a result of metabolic stress and that this leads to the activation of AMPK, resulting in the inhibition of specific $K^+$ (e.g BKca and leak $K^+$) channels (Evans et al., 2005; Evans, 2006; Evans et al., 2009; Wyatt et al., 2007; Wyatt and Evans, 2007; Peers et al., 2010). This hypothesis suggests a unifying basis between the mitochondrial and the membrane hypotheses (Wyatts and Evans, 2007; Peers et al., 2010).

However recently the hypothesis that AMPK is necessary for the carotid body chemosensory response during hypoxia has fallen into disfavor, following the demonstration that AMPK deletion in the glomus cells of mice had no effect on the

oxygen sensitivity and afferent discharge from the carotid body (Mahmoud et al., 2015a,b). It is possible that other postulated $O_2$ sensors such as Heme oxygenase -2 may be the key players in mediating chemotransduction at the level of the carotid body (Lopez-Barneo et al., 2008; Peers et al., 2010). Interestingly though, in characterizing the response of AMPK- deficient mice to hypoxia, it was observed that these animals did show significant breathing disorders even though the carotid body function was normal. This suggests that AMPK deletion results in a hitherto unsuspected deficit in the central brainstem response to hypoxia despite a normal afferent input from the carotid body. The work in this thesis aims to further characterize this central deficit causing abnormal breathing in AMPK–deficient animals.

### *1.4 Literature Review Part 3: Central control of breathing by brainstem respiratory circuitry*

The principal point of termination of the chemosensory afferents from the carotid body is in the caudal regions of nucleus tractus solitarius in the brainstem (Teppema et al., 1997; Cruz et al., 2010; Alheid, et al., 2011; Smith et al., 2013; Zoccal et al., 2014). The brainstem contains spatially and functionally organised neural circuits that generate breathing movements, which are innate, rhythmic motor patterns that occur automatically and continuously throughout life (Alheid et al., 2011; Smith et al., 2013).

These brainstem neural circuits, which make up the respiratory central pattern generator (CPG) consist of excitatory and inhibitory interneurons within a ventral respiratory column (VRC), that is located bilaterally on each side of the medulla (Alheid et al., 2011; Smith et al., 2013) (see Figure 1.4). Structures that make up the VRC include, the retrotrapezoid nucleus (RTN), the Botzinger (BotC) and Pre-Botzinger (Pre-BotC) complexes, the rostral ventral respiratory group (rVRG) and the caudal ventral respiratory group (cVRG; Smith et al., 2013). These microcircuits in the respiratory CPG are in the other hand, modulated by several afferent systems, some of which include sensory information from caudal nuclei of the solitary tract (NTS; Smith, et al., 2013), as well as inputs from pontine and supra-brainstem nuclei e.g motor and sensory cortices, basal ganglia, cerebellum and hypothalamus (Smith et al., 2013). The efferent outflow from these circuits are relayed via premotor networks to the cranial motor neurons that innervate the upper airways as well as to the spinal motorneurons (phrenic, intercoastal and lumbar) that supply the diaphragm, thoracic and abdominal pump muscles respectively ( Smith et al., 2013).

Overall, the structures that make up the brainstem respiratory network are arranged bilaterally from the rostral pons to the caudal medulla and these include, the pontine respiratory group (PRG, comprising the Kolliker–Fuse (K-F) nucleus and the prabrachial nuclei), the retrotrapezoid nucleus/ parafacial respiratory group, the Botzinger complex, the pre-Botzinger complex, the rostral respiratory group, the caudal respiratory group, the nucleus tractus solitarius and the brainstem raphe nuclei (Gracia III et al., 2011; Smith et al., 2013; see Figure 1. 5).

The NTS is located in the dorsomedial portion of the medulla oblongata and is made up of heterogeneous groups of neurons, including catecholaminergic neurons that serves as critical integrating sites in control of breathing (Buller et al., 2008; Alheid, et al., 2011; Zoccal et al., 2014). The NTS acts as an entry point for multiple sensory afferents such as the pulmonary mechanoreceptor, peripheral chemoreceptor (carotid body) and other visceral sensory afferents (Alheid et al., 2011; Smith et al., 2013; Zoccal et al., 2014). Studies have shown that the caudal NTS regions (cNTS) alongside with the associated dorsal respiratory group (DRG) are involved in mediating the afferent control of breathing through their projections to the pontine and VRC components of the brainstem respiratory network (Alheid, et al., 2011; Smith et al., 2013; Zoccal et al., 2014).

The caudal NTS contains well–defined neurochemical cell groups, particularly the A2 noradrenergic neurons which along with the close by C2 adrenergic neurons play major roles in respiratory control (Buller et al., 2008). Additionally in the ventrolateral medulla (VLM) are distinct populations of catecholaminergic neurons namely, the A1 noradrenergic neurons and the C1 adrenegic neurons (Buller et al., 2008), which form part of the respiratory central pattern generator. The importance of these catecholaminergic neuronal groups in the control of respiration is emphasized for example by the profound disorders of breathing seen in Rett syndrome, associated with a loss of central catecholaminergic neurons. The Rett syndrome is an X-linked neurodevelopmental disorder that occurs in females and is caused by mutation of the methyl CpG binding protein 2 (*MECP2*) gene, which encodes the transcription factor MECP2 (Ravn et al., 2005; Viemari et al., 2006;

Stettner et al., 2007; Smith 2013). Patients with Rett syndrome suffer from bioaminergic deficiencies (noradrenalin and serotonin), and display episodes of breath-holding and life-threatening breathing arrhythmias which may result in sudden death (Viemari et al., 2006; Stettner et al., 2007; Roux and Villard 2010; Smith 2013). It has been reported that twenty–six percent of the deaths that occurs in girls with Rett syndrome could be attributed to the sudden respiratory arrhythmia that occurs in these patients (Viemari et al., 2006; Stettner et al., 2007). Several studies using mouse models in which the *MECP2* gene has been knocked-out (*mecp2-/y)* has been carried out to uncover the origin of these respiratory abnormalities (Viemari et al., 2006; Smith 2013). *Mecp2-/y* mice at birth showed normal breathing and normal number of TH neurons in the medulla, but at about one month of age there was a variability in the duration of respiratory cycles coupled with a significant reduction in the number of medullary TH neurons and noradrenalin content which progressed into severe respiratory disturbances including high variability in breathing cycle period and frequent apneas. Finally a fatal respiratory arrest occurred at about two months of age with a drastic reduction in the numbers of TH neurons, noradrenalin and serotonin (5-HT) content in the medulla (Viemari et al., 2006). Thus a deficit of the catecholaminergic and serotonergic modulation of the medullary respiratory network, is believed to result in an excessive expiratory activity, and profound abnormalities in breathing pattern (Viemari et al., 2006; Stettner et al., 2007; Smith 2013).

A more detailed description of the A1/C1 and A2/C2 catecholaminergic neurons and their activation during hypoxia is given in Chapter 2 of this work.

In contrast to hypoxia, ventilation during normal conditions is driven by changes in the partial pressure of carbon dioxide ($CO_2$) and pH of the blood and cerebrospinal fluid. These stimuli are detected by central chemoreceptors (with varying degree of chemosensitivity) located in multiple areas in the brainstem as well as in the cerebellum (Nattie, 1999; Putman et al., 2004; Dean and Nattie, 2010). Changes in blood $pCO_2$ and pH are also sensed by peripheral chemoreceptors in the aortic and carotid bodies, and their afferent projections to the brainstem respiratory neurons contribute to the control of breathing during normal conditions (Nattie, 1999).

In mammals the normal value for the arterial $pCO_2$ is 40mmHg at blood pH of 7.4 and small increases above this value produce dramatic increases in ventilation, while on the other hand small decreases in $pCO_2$ below the normal value can decrease breathing to apnea as may be observed during anesthesia and sleep (Nattie, 1999).

Overall, although the control of respiration during eupneic (normal) breathing is largely understood the regulation of ventilation during hypoxia remains controversial and moreover there is limited information with regard to the location and cellular mechanisms of oxygen sensing neurons in the brainstem (Neubauer and Sunderram, 2004). In this thesis I look at the possible location(s) of these neurons and the functional role of AMPK in the ventilatory response to hypoxia.

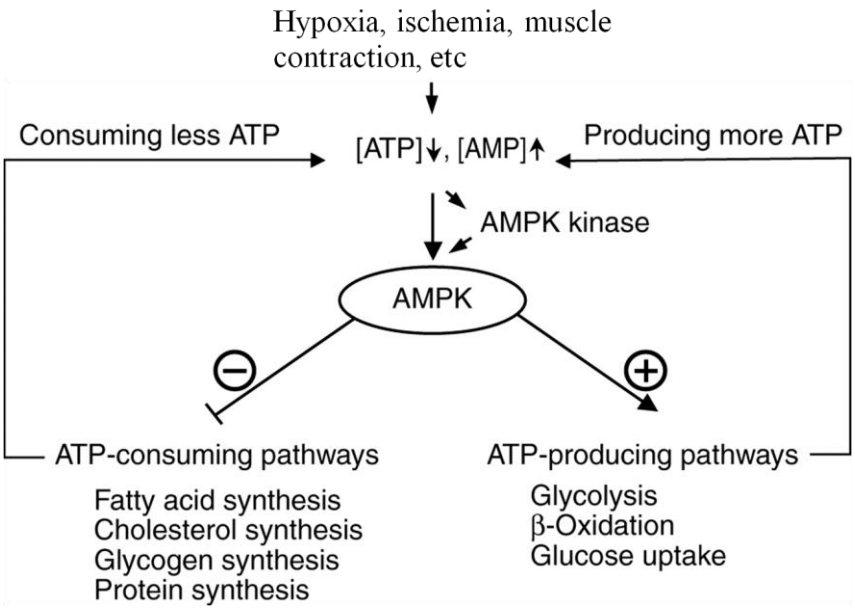


**Figure 1.1 : Activation of AMPK by hypoxia and other metabolic stressors**.

Hypoxia and other stressors such as ischemia and muscle contraction leads to a fall in the cellular ATP levels, while causing a rise in cellular AMP level and this activates the AMPK either directly (allosteric activation) or indirectly via phosphorylation by upstream kinases. Once activated AMPK accelerates all ATP producing pathways while inhibiting all ATP-consuming pathways. Thus AMPK activation preserves the cellular ATP level. Adapted from Frederich et al., 2008.

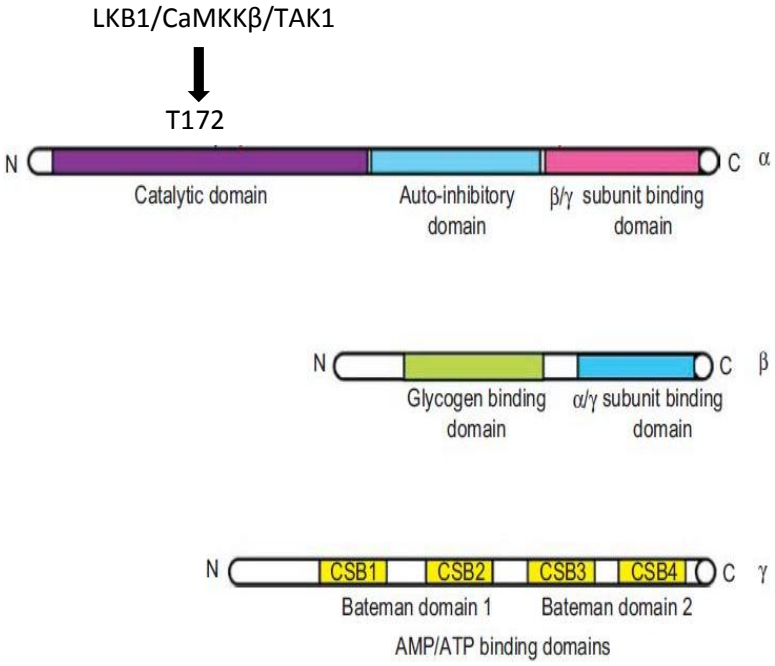


**Figure 1.2 : Organization of the AMPK (α, β and γ) subunit domains.**

Threonine 172 residue phosphorylated by LKB1, CaMKKβ and TAK1 is shown within the α-subunit. The CBS domains also called the Bateman domains are shown in the γ- subunit (Adapted from Viollet et al., 2010).

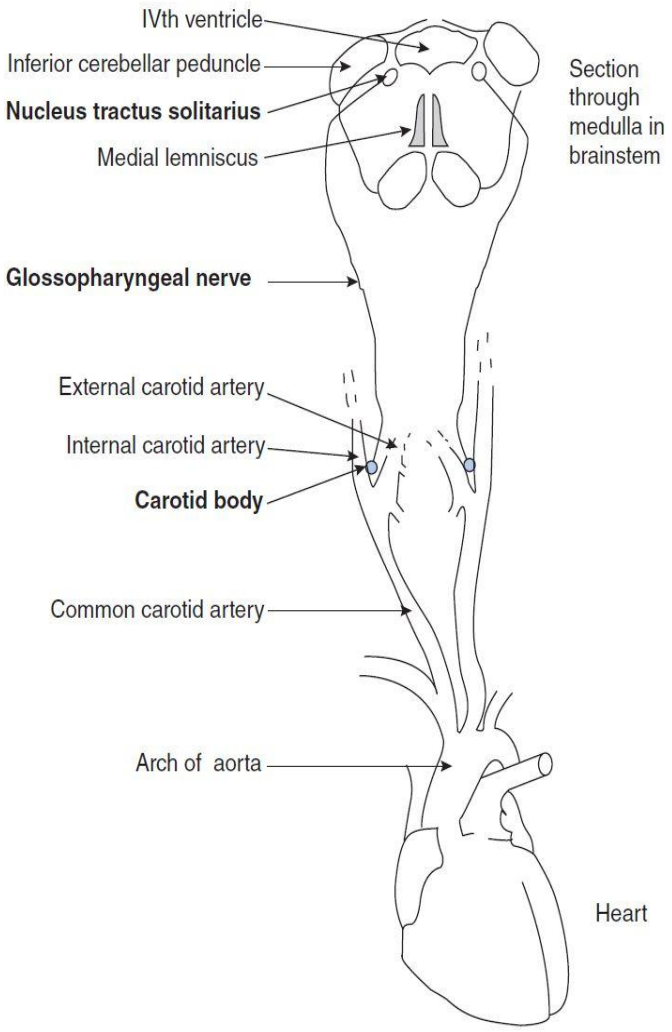


**Figure 1.3: Diagram showing the anatomical location of the carotid bodies with their sensory innervation**. Carotid bodies are located bilaterally at the bifurcation of the common carotid arteries. Their sensory nerve supply is via the glossopharyngeal nerve (sinus branch) which transmits chemosensory information into the NTS in the medulla of the brainstem (Kumar, 2007).

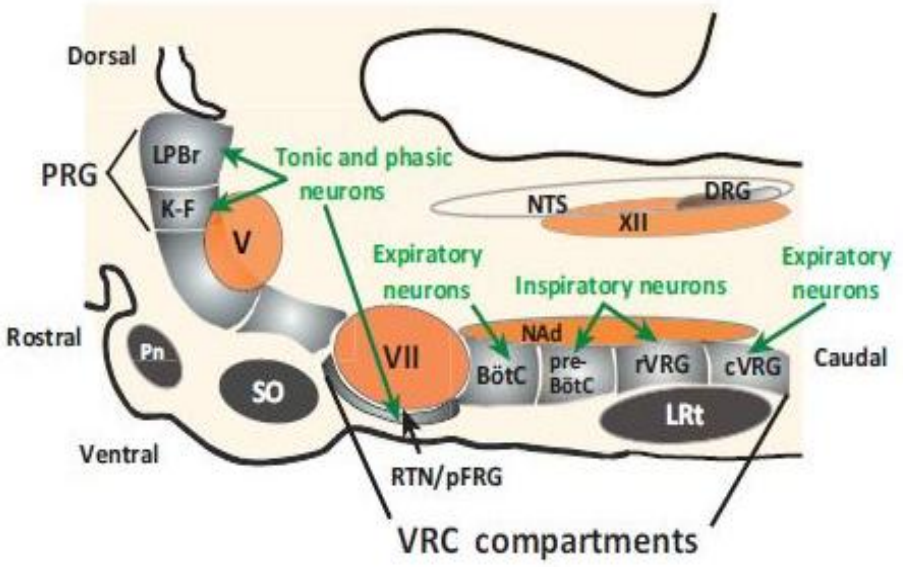


**Figure 1.4: A parasagittal section through one side of the rat brainstem showing the bilateral distribution of the brainstem respiratory network arranged from the rostral pons to the caudal medulla**. Areas of predominant inspiratory, expiratory, tonic and respiratory modulated (phasic) interneurons are indicated. The nucleus tractus solitarius (NTS) in the dorsal brainstem strongly modulates the activity of the neural pattern generators in the ventral respiratory column (VRC). Abbreviations are as stated in the list of abbreviations page. (Adapted from Smith et al., 2013).

# Chapter 2

## Activation of brainstem areas during hypoxia in AMPK deficient mice

### 2.1 Introduction

Previous studies in experimental animals such as rats and rabbits have identified neuronal populations, associated with the control of breathing, in the brainstem that are activated in response to a hypoxic stimulus (Erickson and Millhorn, 1994; Teppema et al., 1997; Hirooka et al.,1997). In this Chapter I investigated the activation upon exposure to hypoxia of brainstem areas in AMPK DKO mice, in comparison to DFlox control mice, using c-Fos as a neuronal marker of activation, with the aim of identifying any differences in DKO animals that may underlie the hypoxia-induced hypoventilation and apnoeas seen in these animals.

The aim of these experiments was to identify specific areas of the brainstem where the deletion of AMPK in TH+ve neurones, leads to a change in their response to the hypoxic stimulus, which may then be associated with the abnormal hypoxic response seen in the DKO animals.

#### *2.1.1 c-fos*

The most widely used neuronal activation marker *in vivo* is Fos, the protein product of the immediate -early gene c-fos (Sagar et al., 1988; Hoffman et al., 1993., Thiele et al., 2000, Morgan and Curran, 1991; Kovacs, 1998; Han et al., 2003). c-fos is a member of the two proto-oncogenes families consisting of the fos family (c-fos, fosB, fra-1 and fra-2) and the jun family (c-jun, junB and junD) which are referred to as cellular immediate-early genes, because a variety of extracellular stimuli cause their rapid and transient induction (Pelto-Huikko et al., 1995 Kovacs, 1998). c-fos is a transcriptional regulatory factor that is expressed within neurons following voltage-

gated calcium entry into the cell in response to electrical , chemical or environmental stimuli (Peng et al., 1995; Han et al., 2003). The transcription product of c-fos, the Fos protein is regarded as a messenger molecule that couples short term extracellular signals with long term changes in cell function after neuronal activation (Han et al., 2003). When neurons are not activated the transcriptional activity of the c-fos gene is low with a resultant low level of the Fos protein production and thus an increase in cfos expression following stimulation is an indication of neuronal excitation (Hoffman et al., 1993; Thiele et al., 2000).

It is worth noting that c- Fos was the first to be characterized among the Fos family of proteins and it forms complexes (dimers) with other members of the Fos and Jun protein families (Hoffman et al., 1993; Gao and Ji, 2009). Such complexes include the c-Fos/c-Jun and c-Fos/Jun B dimers (Hoffman et al., 1993; Gao and Ji, 2009). These complexes bind to AP-1 sites on the DNA to induced gene transcription and thus c- Fos is involved in a signal transduction network that connects extracellular events to intracellular changes (Hoffman et al., 1993; Gao and Ji, 2009). The binding of these complexes to the AP-1 specific binding sites on the DNA is responsible for the nuclear staining that is observed during the localization of c-Fos or c-Jun via immunocytochemistry (Hoffman et al., 1993). At the cellular level c-fos expression can be studied either with the detection of c-fos mRNA via in situ hybridization, or through its nuclear phosphoprotien Fos, using immunohistochemistry (Peng et al., 1995; as in this work, see Results). Studies have shown that maximal c-Fos protein expression is achieved at 60- 90 minutes after exposure to stimuli and persists for 2-5 hours, while the cellular level of the c-fos messenger RNA peaks at 30- 60 minutes before declining to basal levels at 180 minutes (Morgan et al,. 1987; Hoffman et al., 1993; Gao and Ji, 2009).

The use of c-Fos as a marker for neuronal activation is further advantageous since Fos is found in the nucleus, and it is possible to identify the phenotype of the activated neurones through substances located in their cytoplasm with the use of double-labelling immuno-histochemical techniques (Gao and Ji, 2009; Hoffman et al., 1993). Moreover c-Fos immuno-histochemical procedure is relatively easy to carry out using commercially available antibodies and can be quantified (Gao and Ji, 2009). However there are also some limitations in the use of c-Fos as a neuronal activation marker. c-Fos may not be valuable as an investigating tool for inhibitory systems, or systems with reduced tonic activity, since it is typically expressed following excitation. Also persistent or recurring (chronic) stimuli do not lead to c-Fos expression, thereby hindering the elucidation of neuronal activation in such conditions (e.g. during suckling, Hoffman et al., 1993). It is believed that when neurons are repeatedly stimulated they may activate intracellular mechanisms that result in the inhibition of chronic c-Fos expression. A few other pitfalls include the possibility that a neuronal population may express another immediate early gene product and not necessarily c-Fos when stimulated, and that the threshold for c-Fos induction may differ from neuron to neuron, and the induction of c-Fos in a given neuron may be dependent on the activating neurotransmitter or second messenger involved (Hoffman et al., 1993). In spite of the foregoing, c-Fos is still widely accepted and used as a robust marker for neuronal activation. Studies have shown that other immediate–early gene proteins such as members of the Jun protein family (e.g c-Jun) and Fos-related antigens (FRAs) can also serve as markers for neuronal activation (Hoffman et al., 1993), but these are not as widely used as c-Fos.

### *2.1.2 Brainstem areas activated by hypoxia*

Previous studies using the expression of c-Fos as an index of neuronal activation have shown that single and chronic–intermittent exposure to hypoxia in various experimental animals, results in Fos-like immunoreactivity in discrete brainstem areas associated with the integration of visceral (including respiratory) sensory inputs (Sica, et al., 2000).

The classical works of Erickson and Millhorn (1994) and Teppema et al.(1997) in rats and that of Hirooka et al.(1997) in rabbits have clearly identified specific brainstem areas that are activated following hypoxia. Exposure of these animals to a single episode of moderate hypoxia (7-10% $O_2$; balanced with $N_2$) resulted in the distribution of c-Fos in the following brainstem areas:

*Medulla.*

In the medulla c- Fos immunopositive neurons were found bilaterally in the NTS, predominantly in the commissural, medial and dorsomedial subdivisions of the NTS (including the SubP region), with some labelling in the ventrolateral portion (Erickson and Millhorn, 1994; Teppema et al., 1997; Hirroka et al.,1997). Fos–like immunoreactive neurons were also present in the area postrema (AP) and in the intermediate reticular formation (Erickson and Millhorn, 1994; Teppema et al., 1997; Hirooka et al., 1997).

c-Fos was also expressed bilaterally in many neurons located throughout the rostrocaudal length of the ventrolateral medulla (VLM). In the caudal VLM the majority of the c-Fos immunopositve cells were located in and close to the A1 noradrenergic neuronal group (Erickson and Millhorn, 1994; Teppema et al., 1997; Hirroka et al., 1997). In the intermediate VLM immunoreactive cells were present in

areas surrounding the nucleus ambiguus with the highest density in the ventrolateral part (Hirooka et al., 1997). In the rostral VLM including the C1 region, c-Fos immunopositive cells were present mainly in the retrofacial paragigantocelullar nucleus (Teppema et al., 1997; Hirooka et al., 1997). Other areas in the medulla that have been reported to show Fos-like immunoreactivity following hypoxia include the raphe nuclei, the gigantocellular nucleus, the parapyramidial region in rostral medulla, the cochlear nucleus and in anesthetized rats, the medial vestibular nucleus (Erickson and Millhorn, 1994; Teppema et al., 1997; Hirooka et al.,1997).

*Pons*

In the pons an array of cells were also shown to express c-Fos in experimental animals upon exposure to hypoxia. c-Fos immunoreactive neurons were present in the parabrachial complex and the Kolliker-Fuse nucleus, the locus coeruleus and subcoerulus region (Erickson and Millhorn, 1994; Teppema et al., 1997; Hirooka et al.,1997). Immunopositive cells were equally encountered bilaterally in the A5 noradrenergic cell group in the caudal ventrolateral pons as well as in the raphe magnus nucleus (Erickson and Millhorn, 1994; Teppema et al., 1997; Hirooka et al., 1997).

Studies have also shown that experimental animals exposed to a paradigm of chronic intermittent hypoxia expressed Fos-like immunoreactivity in similar brainstem nuclei as discussed above (Greenberg et al., 1999; Ma et al., 2008).

*c-Fos and TH neurons in the brainstem*

As discussed in Chapter 1, brainstem catecholaminergic neurons play an important role in the control of respiration with a net excitatory effect on ventilation (Li and Nattie, 2006; Li et al., 2008), and the loss of these neurons causes severe breathing

abnormalities including breath-holding, apnoeas and a loss of the drive to breathe, in Rett syndrome. The activation of catecholaminergic neurons following hypoxia in different regions of the brainstem has also been characterized, using double immunohistochemistry for c-Fos and tyrosine hydroxylase (TH), which is the rate-limiting enzyme in the biosynthesis of catecholamines. Hirooka et al. (1997) showed that upon exposure to hypoxia one quarter of the c-Fos immunoreactive cells in the NTS were immunopositive for TH, while half of c-Fos expressing cells in the VLM also stain for TH, amounting to 45% - 65% of all the TH+ve neurons in this region. These observations were similar to the earlier results of Erickson and Millhorn (1994), where they observed co-localization of c-Fos and TH-immuno positive staining both in the A2/C2 and A1/C1 neuronal groups in rats that were exposed to hypoxia.

In this study, I therefore investigated the response of brainstem TH+ve neurones to hypoxia, to determine if the breathing disorders observed in the AMPK DKO animals were due to differences in the numbers or activation of TH+ve neurones during hypoxia.

## 2.2 Materials and Methods

### *2.2.1 Animals*

AMPK mutant mice weighing between 31-43g (8-10 weeks old) were used for experiments in this thesis. All mice (a gift from Prof. Mark Evans, with the mice colony under the management of Dr. Oluseye Ogunbayo) were bred and housed in the BRR animal facility, Centre for Integrative Physiology, School of Biomedical Sciences, University of Edinburgh. All procedures were carried out in accordance

with the University of Edinburgh guidelines for animal research and in conformity with the UK Animals (Scientific procedures) Act 1986.

*2.2.2 Generation of AMPK deficient mice*

In this work I compared the response to hypoxia of mice in which the α1- and α2-catalytic subunits of AMPK were conditionally deleted (DKO animals, genotype AMPK $\alpha1^{-/-}$ $\alpha2^{-/-}$), with controls in which the α1- and α2- encoding genes of AMPK were flanked by inserted loxP sequences but not deleted (DFlox animals, genotype AMPK $\alpha1^{fl/fl}$ $\alpha2^{fl/fl}$). I also compared the response to hypoxia of animals in which only the α2- catalytic subunit of AMPK was conditionally deleted (α2-KO animals, genotype AMPK $\alpha1^{+/+}$ $\alpha2^{-/-}$), in order to determine the role of the α2 isoform of AMPK in the hypoxic response. All the transgenic AMPK mice used in this work were kindly provided by Prof Mark Evans, Centre of Integrative Physiology, University of Edinburgh. The breeding programme, genotyping and maintenance of the colony of transgenic animals were carried out by members of the Evans laboratory (Mahmoud et al 2015a).

In the DKO mice, conditional deletion of the α1 and/or α2 AMPK genes was achieved using the Cre-recombinase conditional gene targeting technique. Basically this technique is carried out by first generating a transgenic mouse line in which two loxP sequences in the same direction are added to the ends of the target gene (Floxed mice). To achieve unconditional deletion of the target gene, the Floxed mice can then be cross-bred with mice carrying the Cre-recombinase gene. The Cre-recombinase recognizes the loxP sites in the DNA and excises the DNA segment between them (Metzger and Chambon, 2001; Kos, 2004; Gaveriaux-Ruff and Kieffer, 2007; Deng, 2012; Miao, 2013; Mahmoud, 2015a; see Figure 2.1).

However, as in this work, this strategy can also be used to produce conditional knockout of the targeted gene(s) in specific tissues, by the fusion of the Cre-recombinase gene with a suitable tissue-specific promoter. The Cre-recombinase is therefore activated conditionally after birth (Metzger and Chambon, 2001; Kos, 2004; Gaveriaux-Ruff and Kieffer, 2007; Deng, 2012; Miao, 2013).

In this work, DFlox mice were used where both the α1- and α2- domains of the AMPK gene were flanked by loxP sequences and α2-Flox mice where only the α2-domain was flanked by loxP sequences. These animals were cross-bred with mice in which Cre-recombinase was coupled to a promoter for tyrosine hydroxylase (TH; TH-Cre mice), to generate animals in which Cre-recombinase was expressed selectively in catecholaminergic, TH-expressing cells. Mating of DFlox mice with TH-Cre mice resulted in litters which included animals in which both the α1- and α2-subunits of AMPK were deleted (DKO mice), and mating of α2- Flox mice with TH-Cre mice resulted in litters which included animals in which only the α2- subunits of AMPK were deleted (α2-KO mice). The genotype of each of the animals used in this work was confirmed by direct PCR of DNA samples extracted from ear or tail clips from the mice after weaning, to confirm the deletion of the target genes in each case (procedures carried out by members of the Evans laboratory, Centre for Integrative Physiology; Mahmoud et al 2015a).

The success of the deletion of the AMPKα1 and /or α2 cataytic subunits in tyrosine hydroxylase expressing cells was confirmed by performing single cell end point reverse transcription- polymerase chain reaction (RT-PCR) on isolated carotid body type 1 cells and adrenomedullary chromaffin cells and also by whole brain quantitative real –time PCR( qPCR) (Mahmoud et al., 2015a, b).The initial step in performing these procedures was the designing of primers using primer-BLAST

(NCBI) to target the excised regions of the AMPK gene which included; exons 4-7 of the AMPKα1 gene and exons 5-7 of the AMPKα2 genes and thereafter the validity and the specificity of these primers were tested against complement DNA (cDNA) of the adrenomedullary chromaffin cells from wild type mice (C57/BL6) to ascertain that only single amplicons with the expected band length were generated (Mahmoud et al., 2015a). These primers were designed because pre-designed primers from Qiagen for the AMPK α-subunits were not used due to the fact that they detect areas of the genes that are not within the floxed loxp sites which may results in the appearance of false positives if mRNA transcript is still produced regardless of whether the catalytic domains have been excised (Mahmoud et al., 2015a)

In carrying out single cell end point RT-PCR, amplification was achieved by adding GoTaq DNA polymerase (Promega) to 2.5µl of cDNA that was obtained from individual cells (including carotid body type 1 cells from wild type and AMPK transgenic mice as well as those of the wild type adrenomedullary chromaffin cells). The procedure was carried out in parallel with positive and negative controls. Positive controls were the samples from wild type adrenomedullary chromaffin cells while the negative controls included aspiration from the extracellular medium used during the collection of the cells, PCR controls and control aspirants, lacking reverse transcriptase (Mahmoud et al., 2015a, b).

The actual PCR protocol involves an initial denaturing phase at $94^{o}$c for 5mins followed by a second denaturing step at $94^{o}$c for 30s before proceeding to the annealing stage at $60^{o}$c for 45s and an extension stage for 60s at 72 $^{o}$c which was followed by the final extension step for 7mins at $72^{o}$c. 15 cycles were carried out initially and were then followed by reaction and dilution for a further 38 cycles. To

detect the expression of tyrosine hydroxylase in both the carotid body and adrenomedullary chromaffin cells primers obtained from Qiagen (Quantitect Primer Assay, QT00101962) were utilized with an expected band length of 92bp while on the other hand AMPK was detected by using two primers, *forward* and *reverse* to generate the expected band length of 92bp (Mahmoud et al., 2015a, b). 15µl sample together with a 100bp DNA ladder (GeneRuler$^{TM}$, Fermentas) were run on 2% agarose gels that was made with SYBR®Safe DNA Gel stain (Invitrogen). The gels were imaged with the use of a Genius Bio Imaging system and GeneSnap Software (Syngene). The RNA for both the isolated carotid body type1 cells and adrenomedullary chromaffin cells were extracted using the High pure RNA Tissue Kit (Roche) in accordance with the manufacturer's guidelines and the concentration was determined by the use of the Nanodrop 1000 spectrophotometer (Thermoscientific). cDNA synthesis was performed by the use of Transcriptor High Fidelity cDNA kit (Roche) in accordance with the manufacturer's guidelines (Mahmoud et al., 2015a, b).

For the brain tissue, RNA extraction and cDNA synthesis were carried out using the same techniques as stated above. The qPCR was performed by the method outlined in Mahmoud et al. (2015 b); 2.5 µl of cDNA in RNase free water was made up to 25µl by the addition of FastStart Universal SYBR Green Master (ROX, 12.5 µl, Roche), 8µl of Ultra Pure Water ( Sigma) and forward and reverse primers for AMPK α1 and α2. After that the sample was centrifuged and the 25µl added to a microAmp$^{TM}$ Fast optical 96-well Reaction Plate (Greiner bio-one), the plate was sealed with an optical adhesive cover (Applied Biosystems) and then centrifuged. The reaction was thereafter run on a sequence detection system (Applied Biosystems) using AmpliTaq Fast DNA Polymerase with an initial step of 2min at

50$^{o}$c that was followed by a second step of 10 min at 95 $^{o}$c and then a 15s step at 95 $^{o}$c ( this step was repeated 40 times). These were followed by a dissociation stage which consisted of a 15s step at 95 $^{o}$c followed by a 20s step at 60 $^{o}$c and finally a 15s step at 95 $^{o}$c.

The negative controls that were used included as in RT-PCR, cell aspirants to which no reverse transcriptase was added, PCR controls and aspiration of the extracellular medium (Mahmoud et al., 2015b).

### *2.2.3 Plethysmography*

*Principles*

In this work I utilized a barometric unrestrained whole- body plethysmography (UWBP) to determine the ventilatory responses of the DKO, α2-KO and DFlox mice to hypoxia.

UWBP is non-invasive technique that allows for precise and quantitative measurements of respiratory parameters such as tidal volume, breath frequency and minute ventilatory volume (DeLorme and Moss, 2002; Glaab et al., 2007; Lim et al., 2014). This procedure involves placing a mouse in a closed chamber and recording the pressure fluctuations that occur during the breathing cycle. The instrument consists of two chambers, the main chamber where the mouse is placed and a reference chamber. And with the help of a pressure transducer the pressure differences between the main chamber and the reference chamber are assessed during the breathing cycle (DeLorme and Moss, 2002; Glaab et al., 2007; Mahmood 2015a; Figure 2.2). This procedure is useful because it overcomes the challenges of using anesthesia or restraints which are employed in invasive methods of assessing respiratory functions such as invasive plethysmography (DeLorme and Moss, 2002; Glaab et al., 2007; Lim et al., 2014). Anesthesia suppresses ventilatory functions, alter heart rate and is challenging to control while restraints can elicit an increase in ventilation due to additional stress (Lim et al., 2014).

*Plethysmography recording*

For this work, mice were placed in the main plethysmography chamber (Buxco Research Systems apparatus, UK) and pressure variations due to respiratory

movements of the mice relative to the reference chamber were recorded using a Halcyon low-noise pneumotachograph, and FinePointe acquisition and analysis software (Buxco Electronics Inc, USA). The experimental protocol consisted of an initial exposure of mice to 10 minutes of normoxia in the plethysmography chamber (Medical grade air; delivered at a flow rate of 3L/min to the main chamber), followed by another 10 minutes of exposure to a single episode of hypoxia (8% $O_2$, 0.05% $CO_2$, balanced with $N_2$). The plethysmograph and associated software produced an output file of pressure values recorded every millisecond, and a log of breath frequency, tidal volume, and minute ventilation values averaged over successive 2 second periods. The pressure values were analysed using scripts written in Python by Professor Mayank Dutia. The pressure values were plotted as for example in Figures 2.3 – 2.6, and the inter-breath intervals were measured. Apnoeas were identified in these recordings as inter-breath intervals which were greater than 0.6 sec, as shown for example in Figures 2.4 – 2.6.

*Processing of brain tissue for immunohistochemistry*

Upon completion of the plethysmography protocol and the single exposure to hypoxia, the mice were returned to their home cages for ninety minutes to allow for c-Fos expression. At the end of the ninety minutes the mice were administered an overdose of sodium pentobarbital (0.2ml i.p.; Pentojet, Animal Care Ltd, York, UK) and transcardially perfused with heparinised saline (prepared by dissolving 129mg of heparin (Sigma- Aldrich, UK) in 1000mls of normal saline; approx. 120 mls, administered over 10mins) followed by fixation with 4% paraformaldehyde in 0.1 phosphate buffer (approx.100ml; administered over 10mins; pH 7.4) with the use of a peristaltic pump. The brain was then dissected out en bloc and post-fixed overnight in vials containing 15% sucrose in 4% paraformaldehyde at 4$^{o}$C. The brains were

then cryoprotected by immersing them in 30% sucrose in 0.1M phosphate buffer at a temperature of 4$^{o}$C for 24 hours, until the brains sank. They were then frozen in dry ice in tin foil. Coronal brainstem sections were subsequently cut using a freezing microtome (Leica CM 1325, Leica, set at - 17 to -18$^{o}$C.) at 44µm. Alternate brainstem sections from each mouse were collected in two pots that were filled with 0.1M phosphate buffer. The sections were then stored at -20$^{o}$C in cryoprotectant (Ethylene glycol/glycerol in 0.2M phosphate buffered saline, PBS) for immunohistochemistry.

*Immunohistochemistry (c-Fos and tyrosine hydroxylase immunofluorescence)*

Cryoprotected sections were processed for both c-Fos and TH immunoreactivity following the protocol described below. This protocol is well established in our lab and has been developed by Dr Vicky Tobin, Dr. Nancy Sabatier and others for use in a variety of brain areas.

The sections were first of all washed 4 times (10 mins per wash) in 0.1M phosphate buffer by the use of cell strainers inserted in to 6 –well plates placed on a shaker at room temperature. This was followed by incubation in 0.1M glycine diluted in 0.1M Phosphate buffer (PB) for 30mins to stop the fixation reaction of paraformaldehyde after which the sections were again exposed to another washing phase comprising of four washes of 10 mins each. This was followed by incubation with 3% normal goat serum (NGS) in 0.1M phosphate buffer with 0.3% Triton X-100 (PB-T) for 30 mins to block non-specific binding. Triton X-100 was added to enhance tissue penetration of the antibodies. Thereafter sections were incubated in primary antibodies (anti–Fos polyclonal, raised in rabbit, used at 1 : 10000, Calbiochem, San Diego, CA, USA or

1: 50000 for anti–Fos rabbit polyclonal, Synaptic Systems, Gottingen, Germany and anti- tyrosine hydroxylase , raised in mouse, used at 1: 1000, Millipore, Ternecula, CA, USA) diluted in PB-T with 3% NGS . The sections were left overnight on the shaker at 4$^{o}$C. Following this the sections were washed four times (15 mins each) with 0.1M PB and then incubated for 1 hour in biotinylated secondary anti–rabbit antibody raised in goat ( 1:500; Vector Laboratories, Inc, Burlingame, CA, USA) diluted in a mixture of 0.1M PB with 0.05% Tween which served to amplify the c-Fos staining. The sections were again washed with 0.1M PB for four times with a 15 minutes duration per wash before being incubated for 1 hour in vials containing secondary conjugated antibodies (Alexa Flour® 488- Streptavidin and Alexa Flour® 568; (Molecular Probes, Inc.) Life Technologies, Oregon, USA, used at 1: 500) diluted in a mixture of 0.1M PB with 0.05% Tween. The final washing of the sections was then carried out (4 times; 15 mins per wash) and the sections were mounted serially onto gelatinized microscope slides, coverslipped using Vectashield hard set mounting medium (Vector laboratories Inc. Burlingame, CA, USA) and left to dry for 1 hour at room temperature before being wrapped in foil and kept in the dark at 4$^{o}$C to preserve the fluorescence signal. It is worth noting that from the stage at which the secondary antibodies were added the sections were protected from light to prevent bleaching of the immunofluorescence signal.

*Microscopy and brainstem areas of interest*

After about 12-15 hours images of the brainstem sections were acquired using a Leica digital camera, controlled by Leica acquisition software (AIS) attached to an upright Leica microscope (LEICA DMR). Images were captured with both x10 and x20 objectives. The x20 images were used for the counting of the immunopositive cells.

c-Fos and/or TH-immuolabelled neurons in the brainstem areas of interest were counted using Image J software (Fiji ; an open source platform for biological –image analysis). The brainstem areas of interest included the caudal NTS with its subdivisions (SubP, Medial, ventral and ventrolateral, all of which contain the A2 noradrenergic cells) as well the rostral NTS containing the C2 adrenergic neurons and regions of the ventrolateral medulla containing both the A1 and C1 catecholaminergic neurons (see Results, below for further details of the regions of interest). C-Fos +ve and double-labelled neurons in the central (widest) area of each neuronal group were counted in the alternate brainstem sections for each mouse. The counts from each region of interest per section were normalized using the area of the region of interest, to give cells/100μm$^2$.

*Statistical analysis*

Values in texts and tables are presented as mean± SEM, except where otherwise stated. Statistical comparison between groups was carried out with the use of GraphPad prism 6. A one-way ANOVA statistical test was used to ascertain the statistical differences between groups and this was followed by Tukey's post hoc test to determine the actual differences between each of the groups. $P \leq 0.05$ was considered to be statistically significant.

## 2.3 Results

### *2.3.1 Ventilatory response of mice following exposure to hypoxia*

*Baseline recordings*

The breathing patterns of the control DFlox mice in normoxia, recorded in the first part of the protocol prior to their exposure to the episode of hypoxia, showed brief

periods of regular normal breathing but these were frequently interrupted by irregular, high-frequency patterns of pressure changes in the plethysmography chamber which were due to the mice moving around, sniffing, and exploring the novel chamber, as exemplified in the recording from one animal shown in Figure 2.3. These observed patterns made it difficult in almost all cases to obtain resting (baseline) values for breathing parameters (frequency, tidal volume, minute ventilatory volume), that could be used as a standard for comparing respiratory deviations upon exposure to hypoxia.

This was in contrast to the previous work of Mahmood (2015a), where baseline breathing parameters were successfully obtained for each of the mouse groups (DFlox, DKO and α2-KO) by training each mouse, via repeated exposures to the plethysmography chamber to become accustomed to the chamber, and the breathing patterns were recorded only after the animals had settled down (e.g. 20 - 30 minutes or longer after being placed in the chamber). Interestingly there was no statistical difference in the baseline respiratory parameters between the three groups of animals (see Table 2.1 below; Mahmood, A. (PhD thesis, University of Edinburgh, 2015)

**Table 2.1: Baseline respiratory parameters in DFLox, DKO and α2-KO mice**

| GROUP | FREQUENCY (breaths/min) | TIDAL VOLUME (mL) | MINUTE VENTILATION (mL/min) | NUMBER OF ANIMALS |
|---|---|---|---|---|
| DFLox | 215.9 ± 1.9 | 0.3631 ± 0.01 | 79.52 ± 2.7 | 31 |
| DKO | 211.2 ± 2.5 | 0.3574 ± 0.02 | 74.62 ± 2.4 | 22 |
| α2-KO | 216.2 ± 4.1 | 0.3694 ± 0.02 | 80.48 ± 5.5 | 8 |

Since the aim of the present study was to compare patterns of c-Fos expression in the brainstem after a standardised protocol of exposure to hypoxia, the same for each animal, baseline values for the respiratory parameters in these animals were not obtained. Instead, in this work each mouse was exposed to hypoxia after the fixed normoxia period (10mins) without necessarily waiting to obtain a baseline breathing record. The more reliable resting values obtained by Mahmoud (2015a) for each group of animals were used to give the baseline against which the response to hypoxia was compared (e.g. Figure 2.7).

Very shortly after exposure to hypoxia (i.e. switching the air flow inlet valve from Medical grade normal air (21% $O_2$ with 0.05% $CO_2$, balanced with $N_2$) to the hypoxic gas mixture (8% $O_2$ with 0.05% $CO_2$, balanced with $N_2$), the animals stopped exploratory and other behaviours and typically kept still or lay down on the floor of the plethysmography chamber. This enabled clean breathing records to be obtained uncontaminated by the movement artifacts that were seen in the normoxia

period (see Figures 2.4 – 2.6). The switching of the gas mixture created a large pressure artifact in the plethysmograph recordings. The recordings shown in Figures 2.4 – 2.6 begin immediately after the end of this pressure artifact, so that time 0 in these Figures corresponds to the start of the exposure of the animals to the hypoxic gas mixture.

Upon exposure to hypoxia DFlox mice displayed an initial hyperventilatory response over the first minute or more of hypoxia (Figure 2.4, upper three panels). This was followed by a prolonged period of steady hypoxic breathing at a slower rate, with occasional larger breaths presumably corresponding to gasps (Figure 2.4). With continued hypoxia, the animal showed a number of clear short apnoeas which followed a gasp, indicated by asterisks in Figure 2.4.

By contrast, AMPK DKO mice upon exposure to hypoxia showed an initial hyperventilatory response similar to DFlox animals, but typically containing more irregular breathing such as the short sequences of larger and more frequent breaths shown in Figure 2.5 (upper two panels). Soon after this initial hyperventilatory response, the DKO animals typically developed frequent, long-lasting apnoeas (Figure 2.5, indicated by asterisks). These apnoeas were markedly longer than those seen in the DFlox animals (Figure 2.4).

In AMPK α2-KO mice, exposure to hypoxia evoked an initial hyperventilatory response similar to the pattern observed in the DFlox mice (Figure 2.6).This was followed by a period of steady hypoxic breathing throughout the rest of the experiment, which was interrupted with short apnoeas, that tended to be more frequent in some animals than those typically seen in DFlox animals (indicated by asterisks, Fig. 2.6).

The averaged breathing parameters during exposure to hypoxia for each group of mice are shown in Figures 2.7 and 2.8. All groups of mice showed a similar initial hyperventilatory response for the first one minute after the onset of hypoxia (Figure 2.7A), followed by a decline ("roll-off") to a steady breathing rate in the second minute which remained relatively unchanged throughout the remaining period of the experiment. In both the DFlox and α2-KO mice the steady-state breathing rate was similar to the normal resting (baseline) respiratory frequency established in the earlier systematic characterization by Mahmoud, 2015a (269.3 ± 8.35 breaths per minute). On the other hand the breathing frequency in the DKO mice continued to fall in the second minute after hypoxia, and then remained significantly slower in comparison to the other groups throughout the remaining part of experiment (Figure 2.8A). The averaged breathing frequency of DKO animals over 3-6 minutes after hypoxia (i.e. the initial part of the steady-state response) was 204.7 ± 5.6 breaths per minute (n=5 animals), and this was significantly different from both the DFlox controls (252.3 ± 3.9 breaths per minute, n=4 animals) and the α2-KO animals (241.0 ± 7.6 breaths per minute, n=4 animals; $P<0.05$). This significant difference in breathing rate was also observed in the averaged parameters taken over the last 3 minutes of the steady-state response (7-10 minutes after hypoxia), as shown in Figure 2.8B.

As shown in Figure 2.7B, there was no significant change in the tidal volume of the three groups of mice during exposure to hypoxia, and the tidal volumes remained similar to the baseline volume of 0.35 ± 0.02 mL established by Mahmood (2015a). Thus the hypoxic hyperventilatory response was not accompanied by a significant change in the tidal volume in any of the three groups of mice.

The minute ventilation is a product of both the breathing frequency and the tidal volume. Thus as shown in Figure 2.7C, there was an increase in minute ventilation within the first one to two minutes upon the onset of hypoxia in each of the three mice groups. Similar to breathing frequency, the minute ventilation of both the DFlox and α2-KO mice returned to a value similar to the resting baseline value (Mahmood 2015a) within two minutes of the onset of hypoxia, and remained relatively stable at this level throughout the rest of the experiment. Minute ventilation in AMPK DKO mice did not decline to the baseline value (96.87 ± 5.06 mL/min) as in the other groups but rather was further decreased throughout the remaining part of the experiment after the initial hyperventilation (see Figure 2.7C).

In parallel with the reduced breathing frequency and minute volume in DKO mice during hypoxia, the number of apnoeas recorded per minute during the initial part of the steady-state period (3-6 minutes post hypoxia) was significantly higher in these animals with a value of 22.63 ± 10.18 apnoeas/min compared to 10.3 ± 6.36 apnoeas/min the control DFlox mice and 7.2±4.55apnoeas/min in the α2-KO mice ($P$<0.05, Fig. 2.8). The median apnoea duration was also significantly longer in the DKO mice averaging at 1137.81 ± 405.51 sec, compared to that in DFlox mice (865.5 ± 191.51 msec) and α2-KO mice (813.7 ± 252.10 msec) ($P$<0.05, Figure 2.8). In the later stage of the steady-state response (7-10 minutes post-hypoxia), the number of apnoeas per minute in DKO animals remained higher and the median duration longer than in DFlox and α2-KO mice, but this difference was no longer significant (Figure 2.8).

Thus, a significant hypoventilation (reduced breathing rate), reduced minute volume and a higher number and longer duration of apnoeas were observed in DKO animals, but not α2-KO animals, upon exposure to hypoxia. These findings are in line with

the earlier characterization of breathing parameters in these groups of animals by Mahmood (2015a), and confirm that the animals used in the present study showed the observed phenotype after AMPK deletion in DKO mice. The analysis of brainstem c-Fos expression in these animals (below) can therefore be related to the observed phenotype in each group.

### *2.3.2 Activation of brainstem catecholaminergic neurons by hypoxia and the effects of AMPK deletion*

As detailed in the Methods, following the 10-minute exposure to hypoxia in the plethysmography chamber the animals were moved back to their home cages for ninety minutes, to allow for c-Fos expression in the areas of the brain activated by the hypoxic stimulus. Their brains were subsequently removed after transcardiac perfusion under terminal anaesthesia, and processed for double-immunohistochemistry to visualize TH- and c-Fos immunoreactive neurones in the areas of the brainstem involved in the control of breathing. Differences in the activation (c-Fos immunoreactivity) of these neuronal groups following hypoxia in the different AMPK deficient mice were examined, to identify areas of the brainstem which may be involved in generating the abnormal hypoxic ventilatory response (hypoventilation and apnoeas) seen in the DKO animals.

#### *Localisation of TH+ve neuron groups in the brainstem*

Figure 2.9 shows representative examples of the well-known distribution of TH+ve neurons (red, indicated by arrows) located in the dorsal NTS region (A2 neuronal group; A) and ventral A1 and C1 neuronal groups (B, C) and the dorsal C2 neuronal group (D). The neurons in the A1, C1 and C2 groups were clustered together in clearly identified regions (Figure 2.9 B, C, D), which allowed a clear definition of

the region of interest for cell counting in each case. In the case of the A2 neurons in the NTS however (Figure 2.9 A), the NTS was divided into its sub-regions as indicated, using a brain atlas (Paxinos & Watson, 1998) to define the boundaries of the individual regions. This allowed changes in c-Fos immunoreactivity to be investigated in each sub-region of the NTS, rather than analyzing the NTS as a whole.

*Total numbers of TH+ve neurons in DFlox, DKO and α2-KO mice*

As mentioned in the Introduction, certain important disorders of breathing are caused by the loss of catecholaminergic neurons in the respiratory control centres in the brainstem, such as in Rett syndrome. To investigate the possibility that the apnoeas and hypoxia-induced hypoventilation observed in DKO animals were due to a loss of such neurons in these animals, the total numbers of TH+ve neurons in each of the above regions of the brainstem (A2, C2, A1 and C1 neuronal cell groups) were counted. The counts for the sub-regions of the NTS (A2 neurons) in each of the DFlox (controls), DKO and α2-KO groups of animals are shown in Figure 2.10A, while the counts for the A1, C1 and C2 regions are shown in Figure 2.10B, C and D. In each of these regions of the brainstem, the total number of TH+ve cells were found to be not significantly different between the DFlox animals and the DKO animals, except for the SubP region of the NTS where the DKO animals showed a significantly higher number of TH+ve cells compared to the DFlox controls (Figure 2.10A). Interestingly in the α2-KO animals there was a significantly higher number of TH+ve cells in all regions of the NTS (SubP, medial, SolC, ventral and ventrolateral), as well as in the A1 region in the ventral medulla, compared to DFlox controls. These data therefore exclude the possibility that the abnormal hypoxic

ventilatory response in DKO animals is due to a loss of central brainstem catecholaminergic neurons, as a consequence of the AMPK deletion in these cells.

*Activation of the NTS neurons after exposure to hypoxia*

Following exposure of the DFlox, DKO and α2-KO mice to hypoxia (8% $O_2$; 10mins), c-Fos immunoreactive neurons were found in each of the different subdivisions of the NTS, as shown in Figure 2.11Ai. Co-localization of both the TH (red) and the c-Fos (green) immunoreactivities reveal the A2 neurons that were activated following hypoxia in each subdivision (Figure 2.11 Ai). In each subdivision of the NTS the total number of double-labelled cells (TH + cFos) and the number of cells labelled for cFos alone (non-catecholaminergic cells activated by hypoxia), were counted (Figure 2.11 B).

As seen in the histograms shown in Figure 2.11B, the majority of cFos+ve neurons in each of the areas of interest were also TH+ve. This is in line with expectations from previous work and demonstrates the importance of catecholaminergic neurones in the control of respiration and the response to hypoxia (Erickson and Millhorn, 1994; Teppema et al., 1997; Hirooka et al., 1997).

In SubP subdivision (which lies adjacent to the area postrema, AP; Figure 2,13Ai), the DFlox mice which served as the control group contained 1.09 ± 0.36 Th+cFos double-labelled cells/100μm$^2$ (n= 23 sections, from 4 mice). In DKO mice by contrast the number of TH+cFos neurones was significantly reduced, to 0.27 ± 0.11 cells/100μm$^2$ (n= 22 sections from 5 animals, $P<0.05$). In the α2-KO group, the SubP region contained 1.30 ± 0.20 cells/100 μm$^2$ TH+cFos neurones, which was not significantly different from the DFlox controls (Figure 2.11 B).

In the medial subdivision (SolM), there was no significant difference in the numbers of TH+cFos double-labelled neurones in DKO mice compared to the DFlox controls (2.54±0.31 vs. 2.67±0.04 cells /100µm$^2$ respectively, n= 22 sections from 4 animals in the DFlox controls and 5 animals in the DKO group; Figure 2.11B). In contrast, the medial region in α2-KO mice contained a significantly higher number of TH+cFos neurones (3.88±0.31/100µm$^2$, n= 13 sections from 4 animals), compared to both the DFlox controls and the DKO animals (Figure 2.11B).

In the SolC, ventral (SolV) and ventrolateral (SolVL) subregions of the NTS the number of TH+cFos neurones was significantly higher in DKO mice compared to DFlox controls (Figure 2.11B). Thus the SolC in DFlox mice contained 4.96 ± 0.54 cells/100µm$^2$ (n= 22 sections from 4 mice), while in DKO animals this was significantly increased to a value of 6.24±0.54 cells/100µm$^2$ (n= 23 sections from 5 animals). In the SolV, the number of TH+cFos neurones in the DFlox mice was 5.06±0.70 cells/100µm$^2$ (n=22 sections from 4 animals), while that of the DKO stood at 6.93±0.65 cells/100µm$^2$ (n=23 sections from 5 animals; $P<0.05$). The SolVL, the number of TH+cFos neurones in the DFlox mice was 3.29±0.38 cells/100µm$^2$ (n=22 sections from 4 animals), while in the DKO mice this was increased to 5.32±0.60 cells/100µm2 (n=23 sections from 5 animals; $P<0.05$, Figure 2.11B). In α2-KO animals, these regions of the NTS showed a further increase in TH+cFos double-labelled cells which was significantly higher than in both the DFlox controls and the DKO animals (Figure 2.11B). Thus the SolC in α2-KO mice contained 9.06±0.65 cells/100µm$^2$ (n= 16 sections from 4 mice), while the SolV region contained 8.70 ± 0.68 cells/100µm$^2$ (n= 13 sections), and the SolVL region contained 7.26±0.59 cells/100µm2 (n= 14 sections). These values were all significantly higher ($P\leq0.05$) than the DFlox controls (Figure 2.11B).

*Activation of C2 neurons after exposure to hypoxia*

The C2 adrenergic neurons are located in the rostral part of the NTS in the dorsal medulla (Figure 2.11Aii). As shown in Figure 2.11B, there was a significant reduction in double-labelled Th+cFos neurones in DKO animals (5.48 ± 0.40 cells/100μm$^2$ n= 38 sections from 5 animals) compared to DFlox controls (6.75 ± 0.62 cells/100μm$^2$, n= 29 sections from 4 animals; P<0.05). By contrast, the numbers of double-labelled neurons in the α2-KO mice were not significantly different from the DFlox controls (6.64 ± 0.42 cells/100μm$^2$, n= 23 sections from 4 animals; Figure 2.11B).

*Activation of A1 neurons after exposure to hypoxia*

The A1 noradrenergic neurons are constituents of the ventral respiratory network located in the caudal part of the ventrolateral medulla (Figure 2.11Aiii). As shown in Figure 2.11B, there was a significant reduction in double-labelled Th+cFos neurones in DKO animals (3.88 ± 0.23 cells/100μm$^2$, n= 45 sections from 5 animals) compared to DFlox controls (4.66 ± 0.26 cells/100μm$^2$, n= 47 sections from 4 animals; P<0.05). In contrast, in the α2-KO mice there was a significant increase in double-labelled cells, to 6.86 ± 0.25 cells/100μm$^2$ , n= 45 sections from 4 animals; *P*<0.05; Figure 2.14B).

*Activation of C1 neurons after exposure to hypoxia*

The C1 neurons are a group of catecholaminergic cells that are located in the rostral portion of ventrolateral medulla (Figure 2.11Aiv). In this region, there was a significant increase in double-labelled TH+cFos neurons from 5.05 ± 0.21 cells /100μm$^2$ in the DFlox controls (n= 31 sections from 4 animals) to 6.29±0.30

cells/100μm$^2$ in the DKO mice (n= 30 sections from 5 animals; $P \leq 0.05$; Figure 2.11B). By contrast, the numbers of double-labelled C1 neurons in the α2-KO mice were not significantly different from the DFlox controls (5.38 ± 0.28 cells/100μm$^2$, n= 23 sections from 4 animals; Figure 2.11B).

## 2.4 Discussion

The analysis of total number of catecholaminergic neurons in the A1, A2, C1 and C2 areas of the brainstem (Figure 2.9) in the present study showed that there was no loss of TH+ve neurons in the DKO animals when compared to the DFlox controls. Indeed in the SubP region of the NTS, a significant increase in the total number of TH+ve neurons was observed in DKO animals. Interestingly in A2KO animals, where only the alpha2 isoform of AMPK had been conditionally deleted, there was also a significant increase in the total TH+ve neurons in all parts of the NTS, and in the A1 ventral cell group.

This is an interesting and important finding, as it demonstrates that the hypoxia-induced apnoeas and hypoventilation that are observed in the AMPK DKO mice, are not as a result of a loss of the brainstem catecholaminergic neurons as occurs, for example, in Rett syndrome. As discussed in Chapter 1 and in the Introduction, patients with Rett syndrome display life-threatening breathing arrhythmias with episodes of breath-holding and apnoeas, which may result in sudden death (Viemari et al., 2005; Stettner et al., 2007; Smith 2013). Studies using mouse models have shown that the underlying cause is the progressive loss of brainstem catecholaminergic neurons, as a consequence of a mutation in the *MECP2* gene (Ravn et al., 2005; Viemari et al., 2005; Stettner et al., 2007; Smith, 2013). However,

the present findings show that in DKO animals where AMPK has been conditionally deleted in catecholaminergic neurons, this does not lead to the death and overall loss of these neurons. Therefore the cause of the hypoxia-induced hypoventilation and apnoeas in DKO animals, is not due to an overall loss of TH+ve neurons in these animals. Instead it may be due to an alteration in the physiological function of the catecholaminergic neurons following AMPK deletion, rather than their death and overall loss. Thus for example in the absence of AMPK, it is possible that the ability of the catecholaminergic neurons to cope with metabolic stress (hypoxia) may be compromised, given the importance of AMPK in regulating the production of ATP (Chapter 1). Under these conditions, a compromised catecholaminergic modulation of the facilitatory drive to breathe in the brainstem respiratory networks, may result in the abnormal hypoxia response observed in the DKO animals. Essentially the hypoxic hypoventilation and apnoeas in DKO animals may be due to a compromised physiological response of brainstem catecholaminergic neurons as a result of the AMPK deletion, which is less severe than that seen in for example Rett syndrome, where these neurons are actually lost completely.

An interesting observation in the AMPK α2-KO animals, was a pronounced hyperplasia of the catecholaminergic neurons in all regions of the NTS and in the A1 cell group, when compared to that in DKO and the DFlox groups (Figure 2.9). This is broadly in agreement with the known role of AMPK in regulating cell proliferation in a range of tissues, and suggests that knock-out of the AMPK α2 gene alone (but not both the α1 and α2 genes together), affects the development of the brainstem catecholaminergic neurons in these animals. Activation of AMPK has been shown to suppress cell proliferation in tumor cells, with a sustained activation of AMPK inducing apoptosis in a variety of cell types including pancreatic β- cells

(Motoshima et al., 2006; Fisslthaler and Fleming, 2007). In cultured vascular smooth muscle cells AMPK α2 deletion has been shown to similarly lead to increased cell proliferation, and to accentuate neointimal hyperplasia in intact mouse after mechanical arterial injury (Song et al., 2011). While it is possible that the AMPK α2 isoform has a specific effect on cell proliferation in brainstem catecholaminergic neurons in these mice, the mechanisms involved need to be further investigated. There is also a possibility that the hyperplasia observed in these neurons could be as a result of compensatory changes occurring within the neurons due to AMPK α2 gene deletion or/and could also stem from novel expressions (e.g cytokines) from other brainstem non-catecholaminergic cells that surround the AMPK α2 deficient catecholaminergic neurons as a results of cell –cell communication as well as directly from the AMPKα2 deficient cells. Cytokines amidst other functions play a role in embryonic development, cellular proliferation and differentiation (Goldring and Goldring, 1991). Several regulatory cytokines such as the fibroblast growth factor, platelet-derived growth factor, epidermal growth factor and insulin-growth factor has been postulated to initiate the proliferation of fibroblast and connective tissues cells, while the immunomodulatory ones e.g interleukin-1, tumor necrosis factor –alpha and interferon-gamma are involved in modulating growth response in nonimmune cells (Goldring and Goldring, 1991). Interestingly activation AMPK inhibits an array of interferon –gamma induced cytokines and chemokines in primary astrocytes and microglia an observation that points to a plausible involvement of cytokines in the brainstem catecholaminergic cells hyperplasia as a result of AMPK deletion (Meares et al., 2013).

The analysis of c-Fos expression in the brainstem catecholaminergic groups (A1, C1, A2, C2) in this study (Figures 2.11, 2.12) allows inferences to be made regarding the

sites in the brainstem which may be involved in the abnormal hypoxic ventilatory response seen in DKO animals after AMPK deletion.

Of particular interest are the A2 catecholaminergic neurons in the NTS, because the NTS is the primary central projection target for CSN afferents carrying chemoreceptor inputs from the peripheral carotid bodies, and is the major integration centre which transmits this information via output neurons to other brain regions (such as the ventral respiratory group neurons) that are involved in the control of breathing (Andresen and Medelowitz, 1996; King, et al., 2012; McGinnis et al., 2013). In the NTS the A2 noradrenergic neurons have been reported to be preferentially sensitive to hypoxia (Buller et al., 2008; McGinnis et al., 2013), and are potent modulators of ventilation during hypoxia (Soliz et al., 2008; Buller et al., 2008; Li et al., 2008). The high sensitivity of the NTS to hypoxia is suggested for example in humans via clinical reports (McGinnis et al., 2013). Adults and children who died of hypoxia have been reported to have greater apoptotic index in the NTS, compared to that of the close-by dorsal motor nucleus of the vagus and the hypoglossal nucleus (McGinnis et al., 2013). Furthermore autopsy reports of adults who died of central sleep apnoea (a disease that is characterized by repetitive central apneas with hypoxia) reveal the presence of acute bilateral lesions at the level of the NTS (Parenti et al., 2005).

In the present study of c-Fos expression in the A2 neurons in the NTS after exposure to hypoxia (Figure 2.10), most prominently there was a specific reduction in the activation in the SubP region of the NTS in the DKO animals, as compared to the DFlox controls. The SubP region of the NTS is in close approximation with and surrounding the highly vascularized area postrema (AP). Its blood supply is unusual and consists of short connecting vessels that proceed from the capillaries of the AP,

which then break up into capillaries of normal size in the SubP before supplying the rest of the medulla (in a similar way to a portal system; Fodor et al., 2007; McGinnis et al., 2013). These short vessels convey re-entrant venous blood from the AP into SubP region after a prolonged stay in the AP, resulting in a relatively low $O_2$ saturation at the SubP capillary bed (Fodor et al., 2007; McGinnis et al., 2013). Therefore it is possible that during hypoxia there is a resultant potentiation of this effect, a phenomenon that may lead to an increased sensitivity and greater excitation of the A2 neurons in the SubP region. The SubP A2 neurons may therefore be in a particularly appropriate position to be activated by hypoxia, and by their output projections to drive the hypoxic ventilatory response. The reduced activation of these neurons in DKO animals (Figure 2.10) may be therefore an important factor in generating the apnoeas and hypoventilation seen in DKO animals during hypoxia.

Interestingly, the significantly reduced activation of SubP catecholaminergic neurons was only seen in DKO animals, while the activation of these neurons in α2-KO animals was the same as in the DFlox control group (Figure 2.10B). This suggests either that the complete knock-out of both isoforms of AMPK in SubP neurons is necessary to obtain this effect, while the α2 isoform alone is not sufficient, or possibly that only the α1 isoform is expressed in SubP neurons, so that the α2-KO animals still have a normal AMPK function. Further characterization of AMPK expression in this area of the brainstem is necessary to investigate these possibilities.

The C2 adrenergic neurons are reported to have a net excitatory effect on breathing and chemoreception (Li et al., 2008). Previous studies have shown that the C2 cells in the rostral NTS are activated during hypoxia in various experimental animals (Erickson and Millhorn, 1994; Teppema et al., 1997). In this work there was a significant reduction in the excitation of the C2 neurons in the DKO group compared

to the Floxed , a finding that showed that the lack of AMPK decreased the activation of these neurons and thereby compromised their normal modulation and funneling of the chemoafferents signals to the ventrolateral medullary respiratory neurons ( including the A1 and C1 neurons ) that drives respiration during hypoxia. Apart from the direct effect of AMPK deletion, the decrease excitation observed in these cells may as well be due to a decrease in the facilitatory hypoxic response signals from the subP region. Therefore, in all the deficit in the activation of the C2 neurons in the DKO mice during hypoxia may be a prominent contributing factor to the observed phenotype (hypo ventilation and apnoeas) that was observed in these mice.

In contrast to the marked reduction in activation of the SubP A2 neurons and C2 neurons in the dorsal brainstem by hypoxia in DKO animals, in all of the other regions of the NTS there was either no change in the activation of catecholaminergic neurons compared to DFlox controls (medial region), or a significant increase compared to the DFlox controls (SolC, ventral and ventrolateral regions of the NTS; Figure 2.10B). Furthermore, in all of these regions, it should be noted that in the α2-KO animals this increase in activation after hypoxia was even greater than in the DKO animals (Figure 2.10B). These sub-regions of the NTS are known to be involved in the integration and transmission of chemoreceptor information from the carotid bodies (Andresen and Mendelowitz, 1996; Song et al., 2011; Bathina et al., 2013; Mayer et al., 2015). Previous studies have shown that neuronal groups (including the catecholaminergic A2 cells) in these NTS sub regions are activated during hypoxia (Erickson and Millhorn, 1994; Teppema et al., 1997). In addition, the medial NTS is the first point for the termination of baroreceptor sensory signals entering the central nervous system, and thus these neurons are also importantly involved in the control of cardiovascular reflexes. The increased activation of these

regions of the NTS, therefore, can be interpreted as a secondary consequence of the hypoventilatory response to hypoxia in DKO animals, due to the decreased activation of the SubP neurons, as discussed above. Interestingly, the observation of the increased activation of these regions in the α2-KO animals, compared to the DKO group, suggests that the α2 isoform of AMPK may have a particular role to play in mediating this increased activation during hypoxia in these regions of the NTS.

In the ventrolateral brainstem, the activity of the A1 noradrenergic neurons and the C1 adrenergic neurons is strongly modulated by efferent outputs from the NTS neurons (Figure 2.11A), and they form part of the ventral respiratory column which contains key interacting and excitatory respiratory neurons that generate the breathing rhythm motor pattern (Hirooka et al., 1997; Alheid et al., 2011; Smith et al., 2012). Thus, afferent input from the carotid bodies via the CSN is integrated in the NTS areas in the dorsal brainstem, after which it is transmitted to the downstream A1 and C1 neurons in the ventrolateral brainstem (Figure 2.12A). Therefore the observed changes in the activation of the ventrolateral A1 and C1 neurons in the DKO mice as compared to the DFlox controls during hypoxia (Figure 2.11B), are likely to be due to the changes in the transmission of the chemosensory signals from the NTS in the dorsal brainstem, as discussed above. The reduction in activation of the A1 neurons in DKO animals, may be related to the decreased transmission of efferent signals from the SubP and C2 regions, for example (Figure 2.12B).

The C1 adrenergic neurons, which showed an increased activation during hypoxia in DKO animals, have been reported to be involved in regulating several physiological

functions such as the neuroendocrine responses to infection and inflammation, reproduction, glucose homeostasis, thermoregulation, hypothalamo-pituitary axis-(HPA-) mediated stress responses, food consumption and breathing (Guyenet et al., 2013). Although the physiological role of these neurons is complex, it is generally accepted that hypoxia results in their activation (Erickson and Millhorn, 1994; Hirooka, et al., 1997; Teppema et al., 1997; Greenberg et al., 1999; Guyenet et al., 2013). Previous work has shown that hypoxia excites the C1 adrenergic neurons in the rostral ventrolateral medulla both through a projection from the caudal part of the NTS, and also secondarily by a direct (self–autonomous) or indirect activation (via the release of glial transmitters, e.g ATP) in response to central nervous system hypoxia, an effect that may contribute to the Cushing response (Reis et al., 1994; Guyenet et al., 2013). Therefore the increased activation of the C1 neurons in the DKO mice observed in this work may be as a result of the excitation of these cells via chemosensory inputs to the ventrolateral medulla from the commissural, ventral and ventrolateral NTS subnuclei that were significantly excited during hypoxia in these mice as compared to their DFloxed counterparts, as well be a self –autonomous excitation of a subset of these cells as result of brainstem hypoxia that might have occurred during the period in which the animals were exposed to the hypoxic challenge. It is also possible that the increased excitation observed in the C1 neurons during hypoxia in the DKO mice may be as result of a subset of these neurons mediating other physiological function(s) such as sympathetic nervous system control, or the HPA stress response, during the period of hypoxia.

## 2.5 Conclusion

The analysis of TH and c-Fos expression in the brainstem of DKO mice in comparison with their DFlox controls in this Chapter, shows firstly that the hypoxia-induced apnoeas and hypoventilation seen after AMPK deletion in DKO mice is not due to a loss of brainstem catecholaminergic neurons, as occurs for example in certain breathing disorders such as Rett syndrome. Instead, the deletion of AMPK appears to result in a markedly reduced activation of neurons in the SubP region of the NTS, and to a smaller extent also in the C2 region in the dorsal brainstem, during hypoxia. Since the NTS is known to be the primary site of termination of the carotid body afferent inputs to the brain, the decreased activation of the SubP region in particular shows for the first time that AMPK in specific NTS neurons is necessary for the effective integration and transmission of the chemoafferent signals from the carotid bodies. The reduced integration and onward transmission of the carotid body afferent inputs to the downstream ventrolateral medullary respiratory neurons, is suggested to be the underlying cause of the hypoventilation and apnoeas that are observed in DKO animals.

This finding is potentially of clinical significance, as it illustrates specific sites within the dorsal brainstem where disorders of AMPK expression or function could result in breathing disorders such as, for example, non- obstructive sleep apnoeas, and could also be involved in the physiological adaptation to living at altitude. Further studies of AMPK expression and function in the NTS neurons are necessary to investigate the potential for AMPK as a therapeutic target in the treatment or management of respiratory disorders of central brain origin.

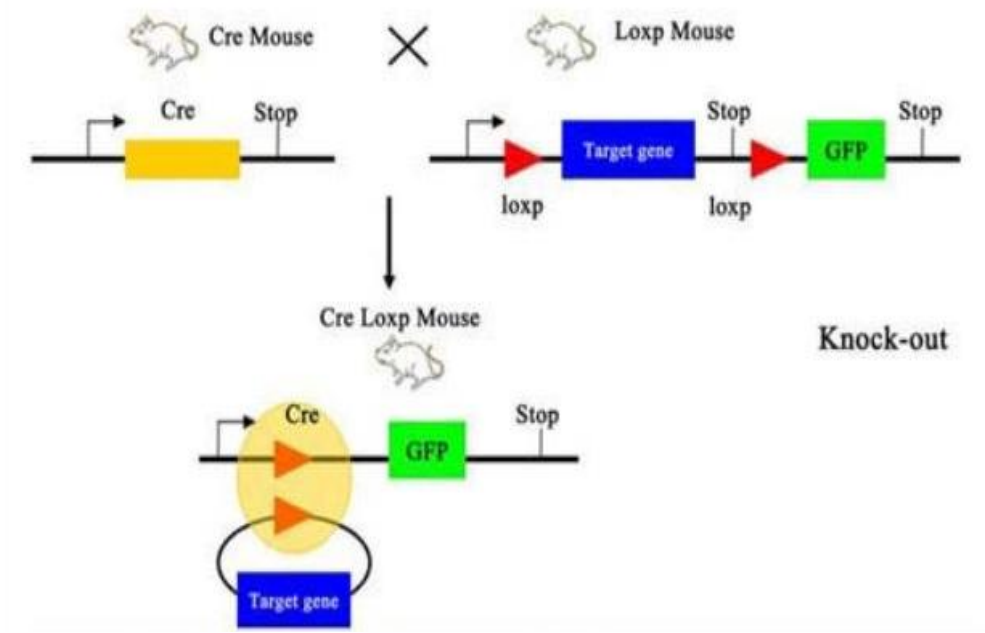


**Figure 2.1:** Schematic diagram showing the use of the Cre–recombinase technique to generate genetic knock-out of a target gene. Cross-breeding a Cre-expressing mouse with a mouse in which the target gene is flanked by two loxp sequences, results in offspring in which the target gene is irreversibly deleted (Adapted from Miao, 2013).

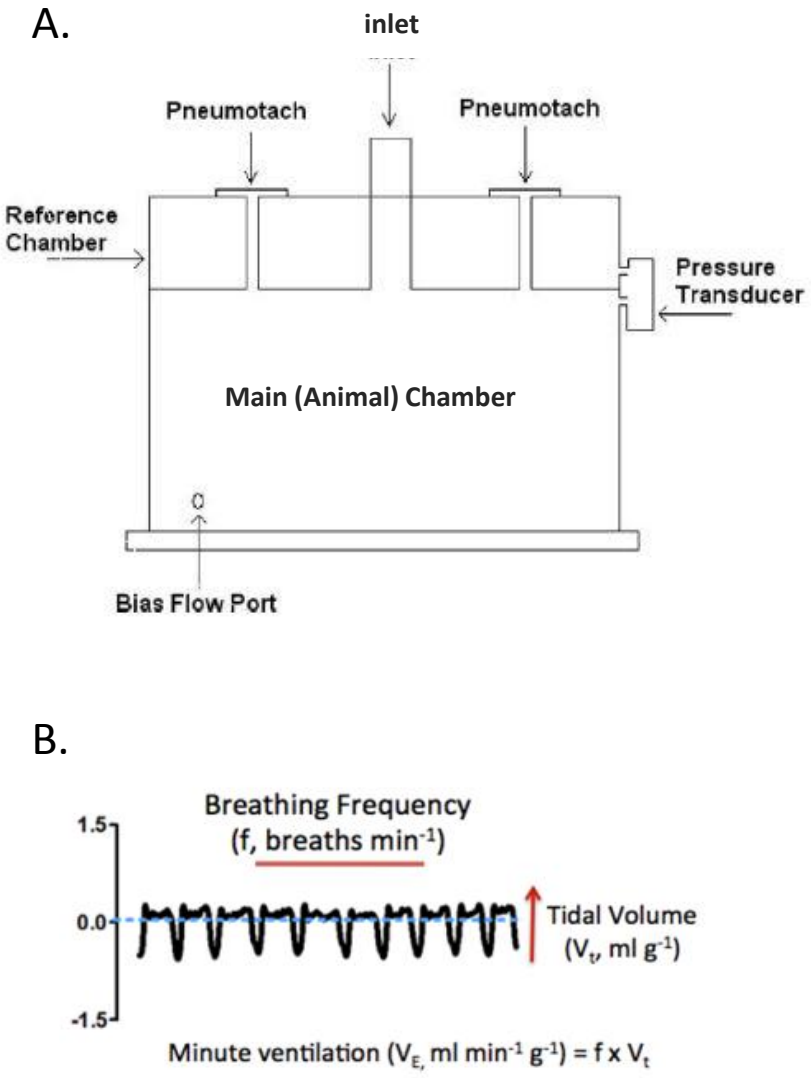


**Figure 2.2: A,** Schematic diagram of the Buxco small animal whole-body plethysmograph, showing the main animal chamber, the reference chamber and the pressure transducer monitoring changes in relative pressure between the two chambers (adapted from DeLorme and Moss, 2002). **B,** example recording of steady breathing of an animal in the main chamber, showing a decrease in recorded pressure during inspiration and conversely an increase in recorded pressure during expiration (see also Figures 2.3 – 2.6). (Adapted from Mahmood, PhD thesis, University of Edinburgh 2015a).

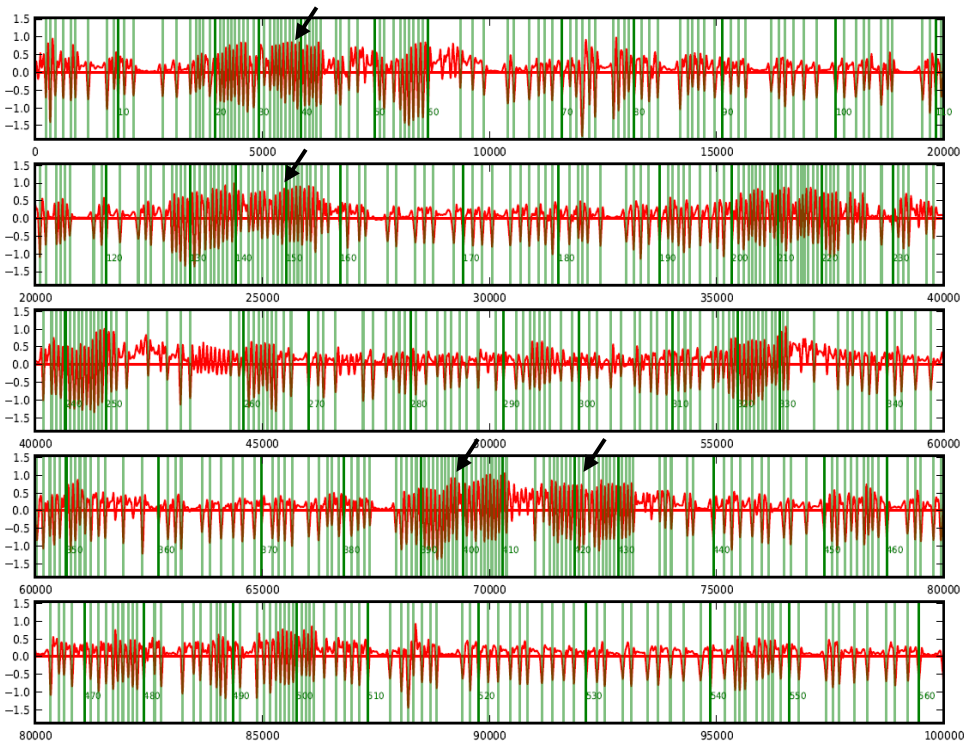

**Figure 2.3. Example plethysmograph recording from an AMPK Dflox control mouse in the initial part of the experimental protocol, in normoxia.** The record begins (time=0, uppermost panel) a few minutes after the animal was first put into the plethysmograph chamber. Each panel follows consecutively. Time on the X-axis is in milliseconds. Green vertical lines indicate the time of peak inspiration for each breath. Note the irregular breathing pattern and periods of high-frequency pressure changes, associated with exploring, sniffing and grooming movements of the animal (arrows), which made it difficult to obtain steady-state baseline breathing records from naïve animals that were not habituated to the plethysmograph chamber.

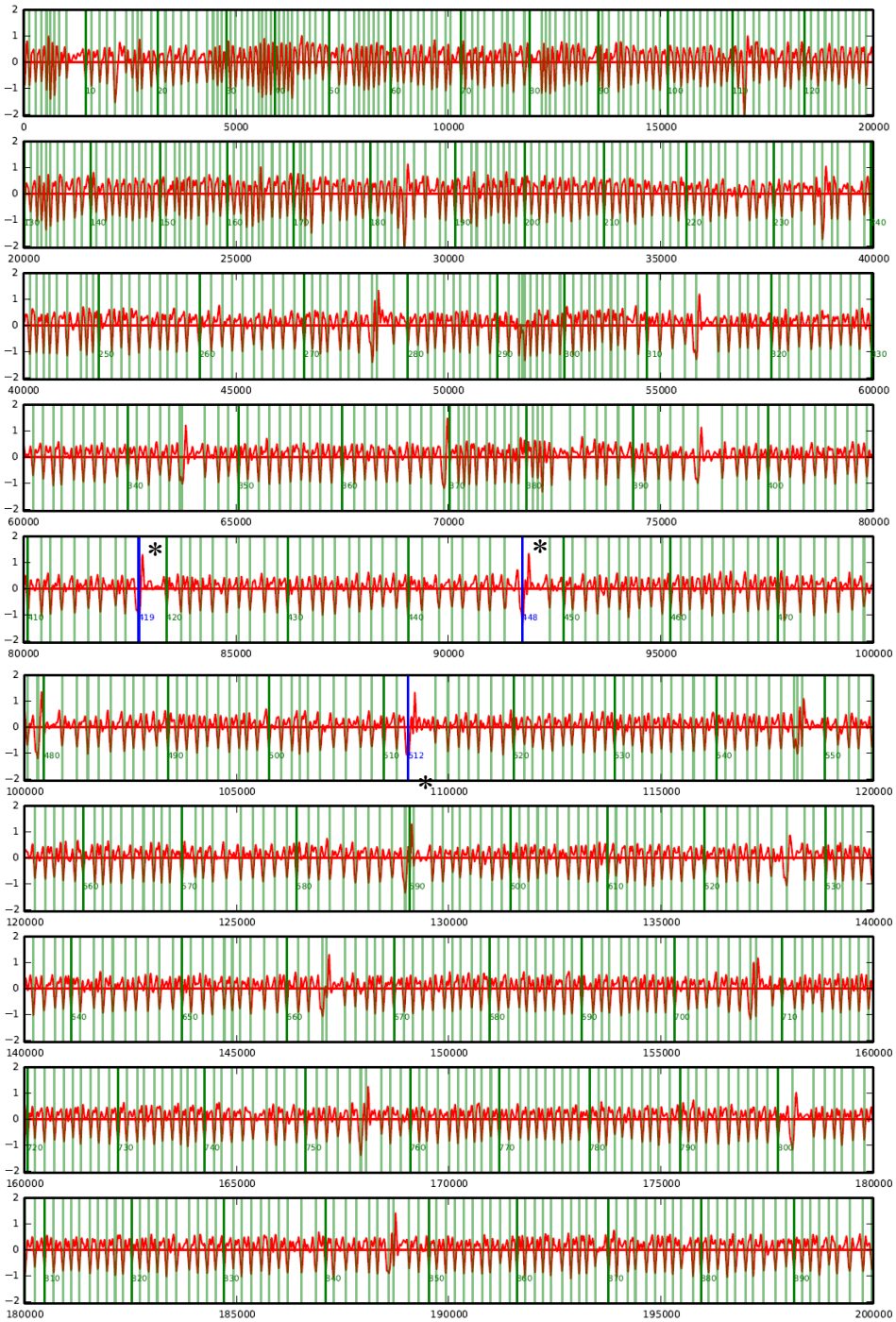

**Figure 2.4. Response of a representative AMPK Dflox control mouse to hypoxia.** Plethysmograph recording from an AMPK Dflox control mouse over the first 3 minutes and 20seconds after the start of the exposure to hypoxia. Time=0 (uppermost panel) is immediately after the end of the pressure artefact caused by the switch to the hypoxia gas mixture. Note initial hyperventilation (uppermost two panels) followed by steady breathing at a lower rate, with occasional apnoeas (blue vertical lines, asterisks). Apnoeas followed gasps, but not all gasps were followed by apnoeas.

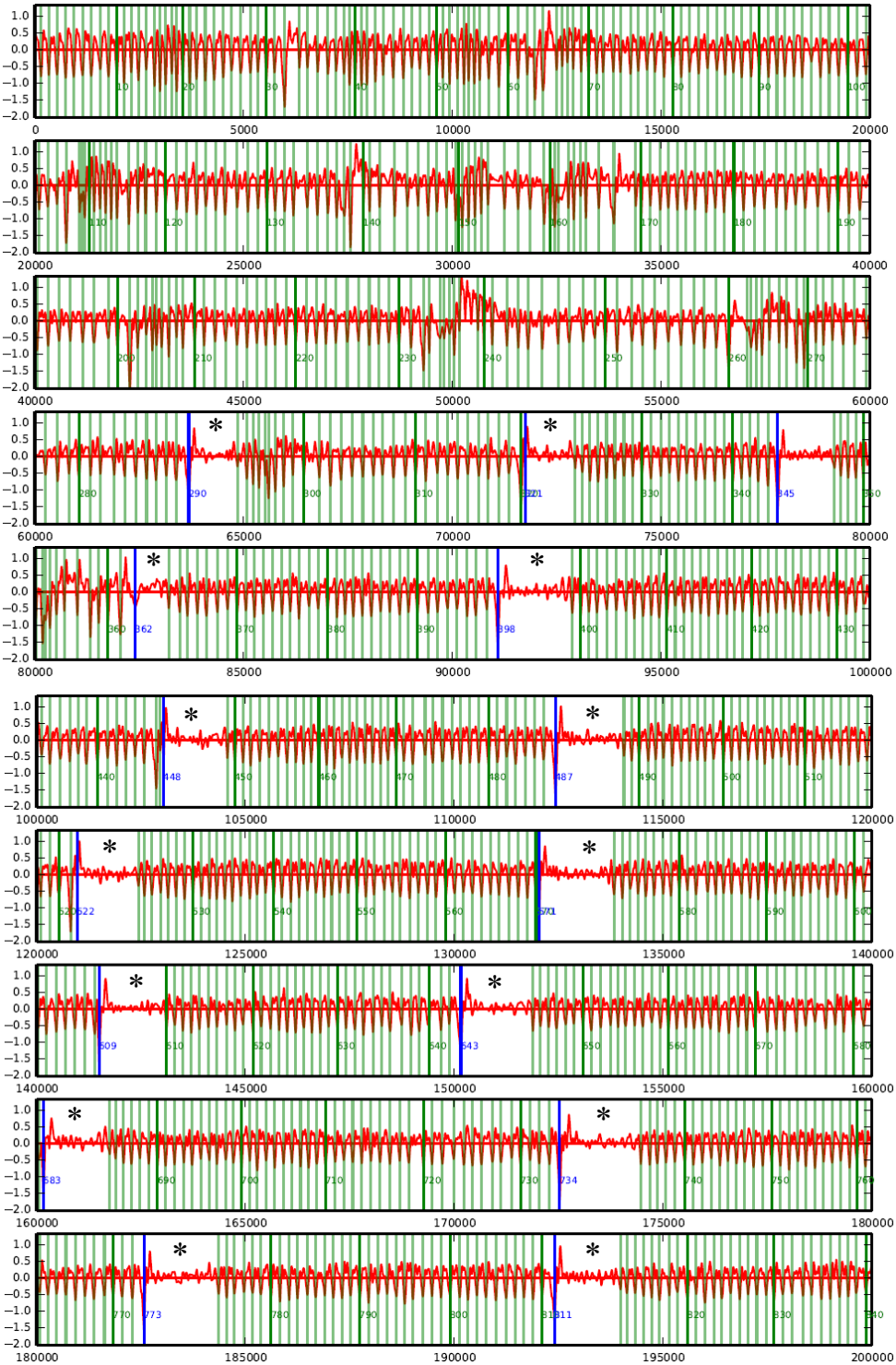

**Figure 2.5. Response of a representative AMPK DKO mouse to hypoxia.** Plethysmograph recording from a DKO animal over the first 3 minutes and 20seconds after the start of the exposure to hypoxia. Time=0 (uppermost panel) is immediately after the end of the pressure artefact caused by the switch to the hypoxia gas mixture. Note initial hyperventilation (uppermost two panels) followed by steady breathing at a lower rate, with occasional apnoeas (blue vertical lines, asterisks). Apnoeas in DKO animals were more frequent and longer in duration, than in Dflox controls.

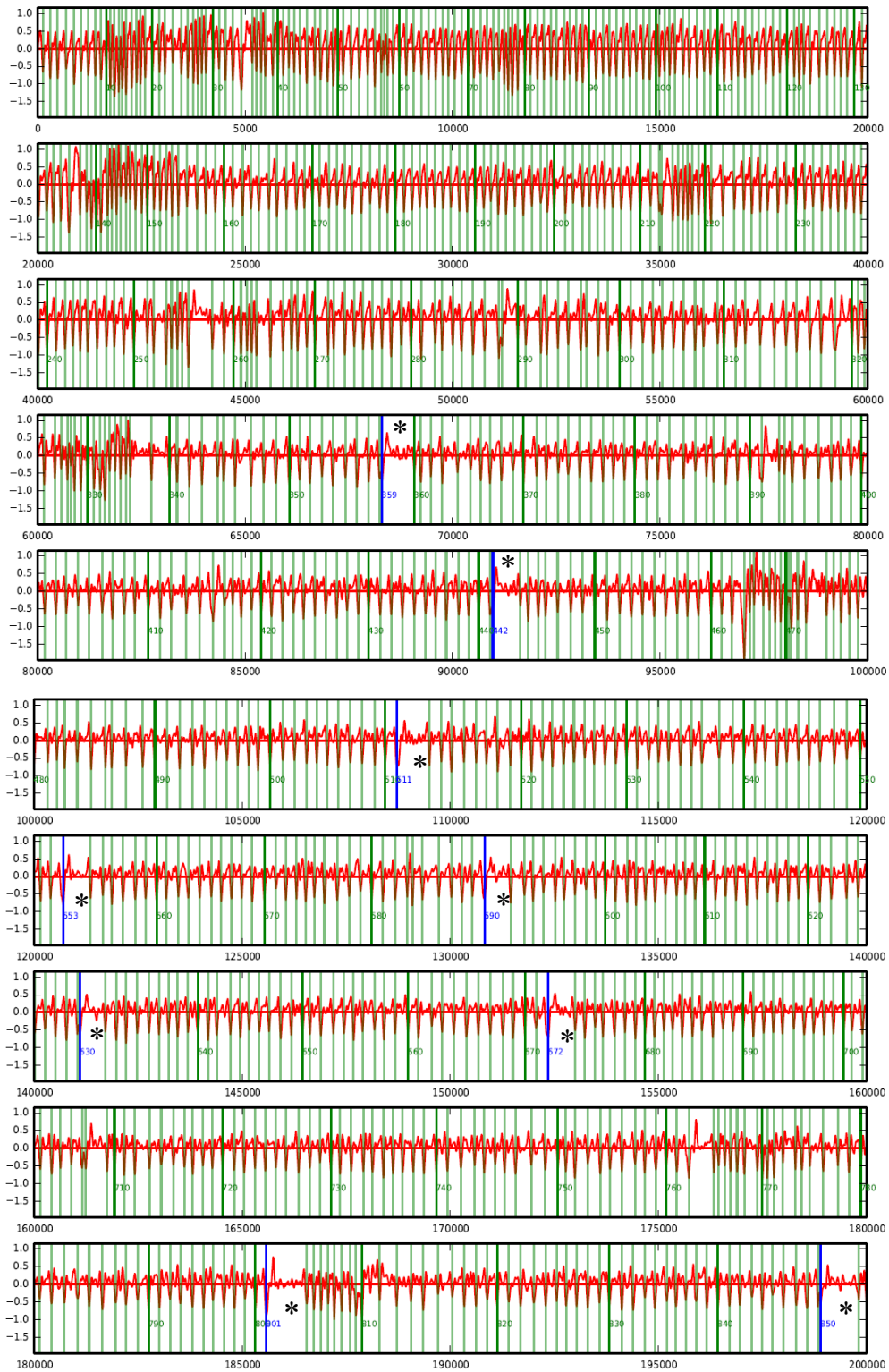

**Figure 2.6. Response of a representative α2-KO mouse to hypoxia.** Plethysmograph recording from a α2-KO mouse over the first 3 minutes and 20 seconds after the start of the exposure to hypoxia. Time=0 (uppermost panel) is immediately after the end of the pressure artefact caused by the switch to the hypoxia gas mixture. Note initial hyperventilation (uppermost two panels) followed by steady breathing at a lower rate, with occasional apnoeas (blue vertical lines, asterisks). Apnoeas were similar in duration to those seen in DFlox controls.

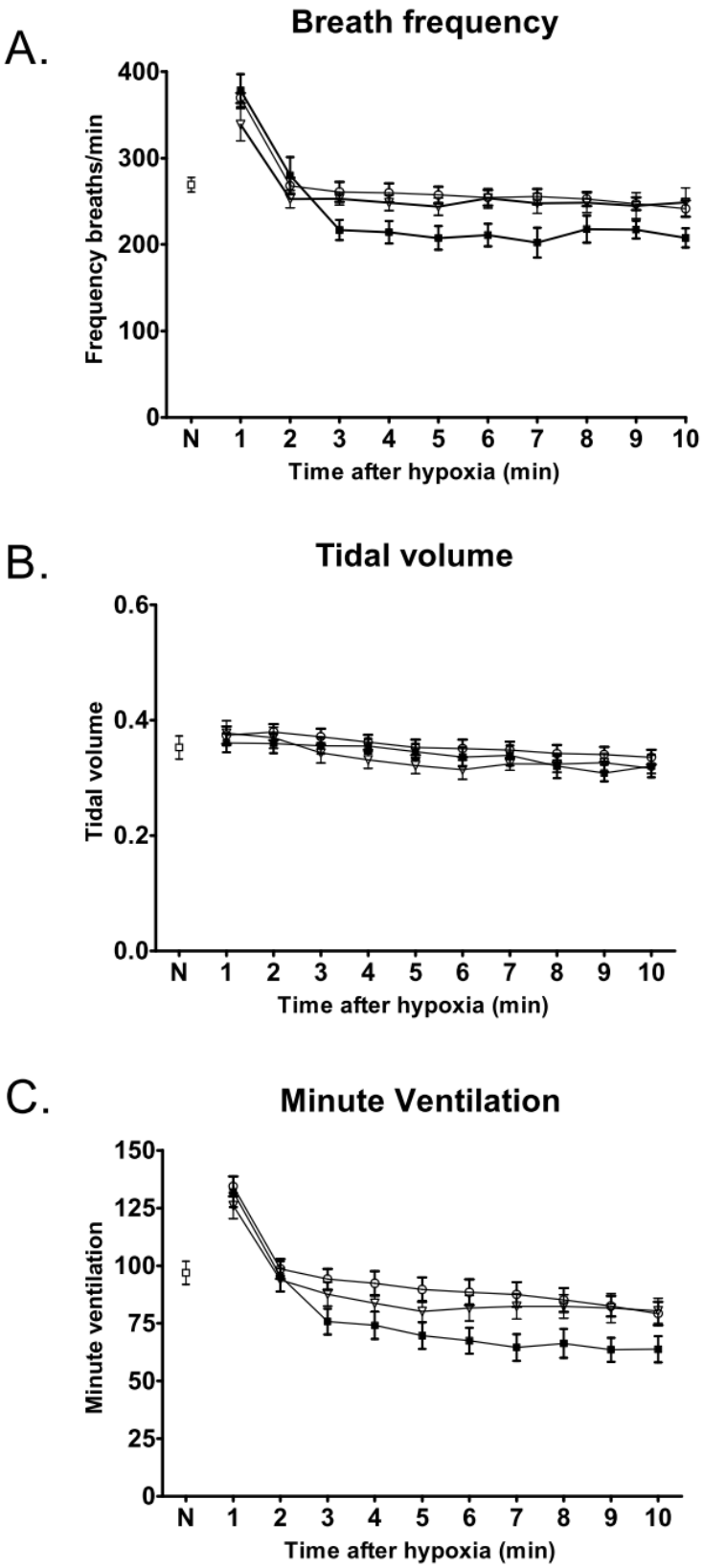


**Figure 2.7. Hypoxic breathing parameters in AMPK Dflox, DKO and α2-KO animals.** Plots show A, breathing frequency (breaths/minute), B, tidal volume (ml) and C, minute ventilation (ml/minute) averaged over each minute after the start of the exposure to hypoxia. Open circles, AMPK Dflox animals (n=4); filled squares, AMPK DKO animals (n=5); open triangles, AMPK α2-KO animals (n=4). **N,** averaged baseline (resting) values obtained by Mahmoud (PhD thesis, 2015a) in control animals that had been habituated to the plethysmograph chamber.

**A. Averages over 3 - 6 minutes of hypoxia**

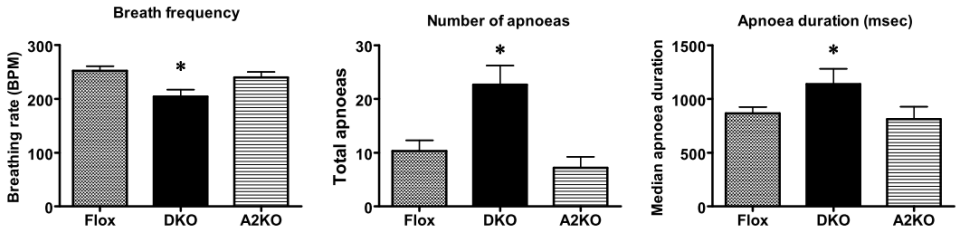


**B. Averages over 7 - 10 minutes of hypoxia**

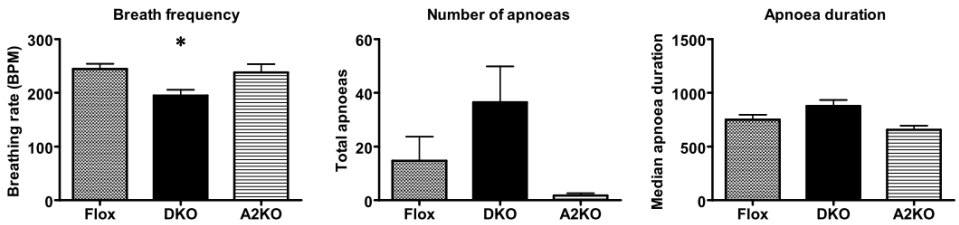


**C. Averages of Minute Ventilation over 3-6 minutes (i) and 7-10 minutes(ii) of hypoxia**

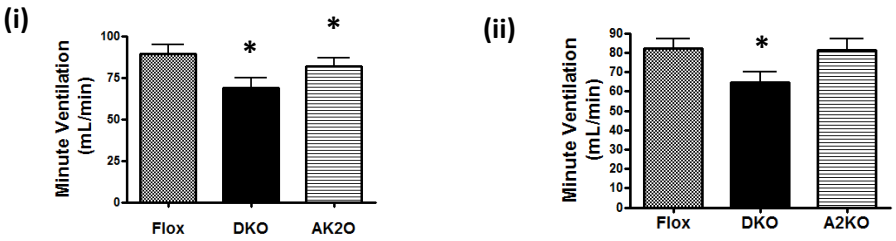


**Figure 2.8. Averages of breathing rate (left), number of apnoeas (middle) and apnoea duration (right) over 3-6 minutes (A), and 7-10 minutes (B), of exposure to hypoxia in each group of animals and (c) averages of Minute Ventilation over 3-6 minutes (i) and 7-10 minutes(ii) of hypoxia.** Note that the DKO animals show a significant sustained hypoventilation over the 10 minutes of hypoxia, and significantly higher numbers of apnoeas, of longer duration, over the initial 3-6 minutes of hypoxia. Similarly the minute ventilation of the DKO mice show a significant reduction throughout the 3-10 minutes of hypoxia but interestingly the A2KO animals show a significant reduction in the initial 3-6 minutes before returning to the normal baseline value in the 7-10minutes of hypoxia.
(* =group significantly different from the controls , $P < 0.05$)

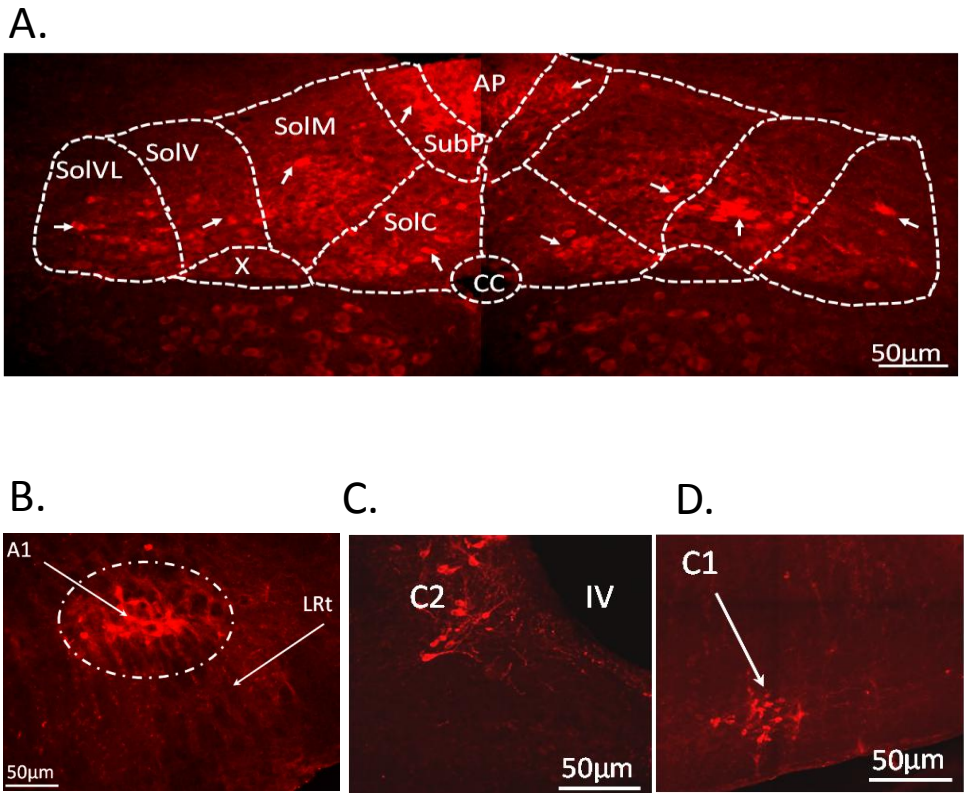


**Figure 2.9. TH-immunoreactive (catecholaminergic) neuronal cell groups in the brainstem. A,** transverse section through the dorsal brainstem showing the nucleus tractus solitarius (NTS) of the left and right sides. Midline is at the centre of the image. CC, central canal; AP, area postrema. The regions of the NTS, defined by the presence of the TH+ve neurons (red, arrows) and with reference to the atlas of Paxinos and Watson (REF), are shown: SubP, medial, central, ventral and ventromedial (SolM, SolC, SolV and SolVL respectively). **B,** the A1 cell TH+ve cell group in the ventral medulla, lying above the lateral reticular nucleus (LRt). **C,** the C2 TH+ve cell group in the dorsal medulla, lying rostral and dorsal to the NTS. **D,** the C1 cell group in the ventral medulla, lying just above the ventral surface of the brainstem.

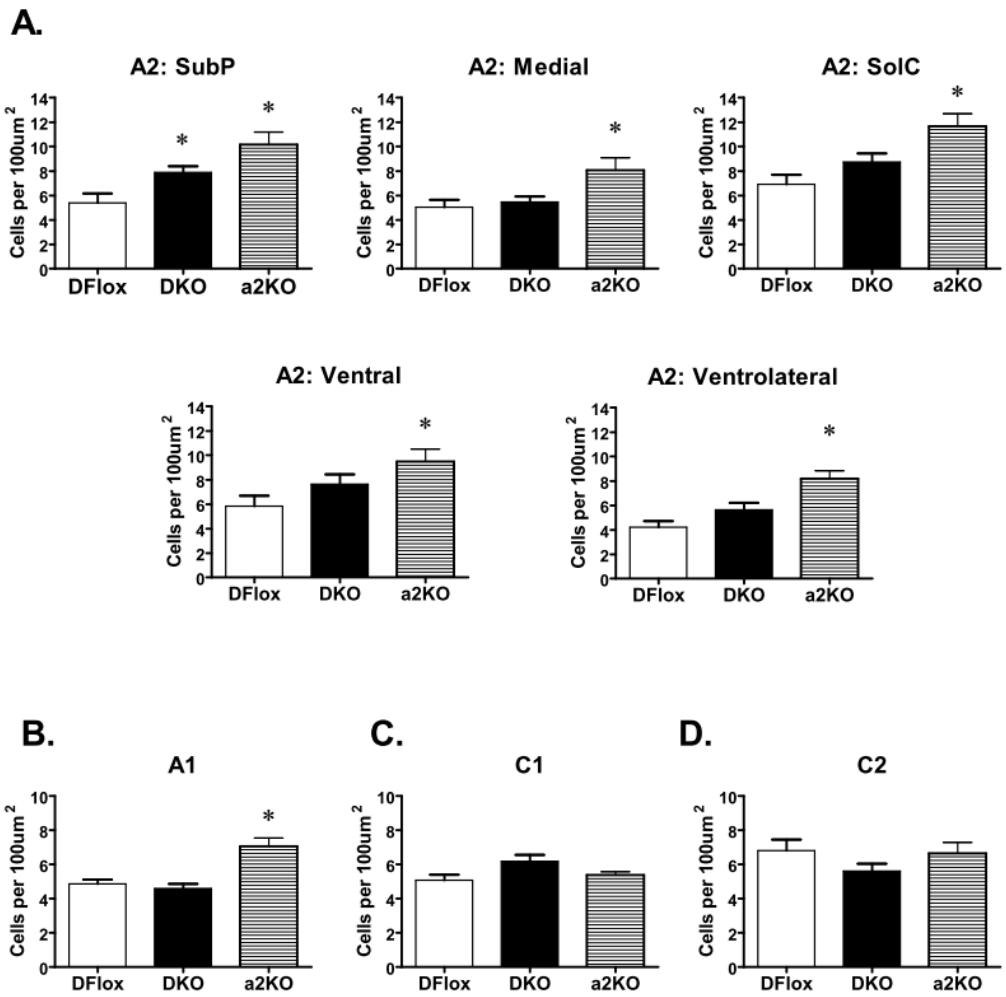


**Figure 2.10. Total numbers of TH-immunopositive (catecholaminergic) neurons in brainstem regions of AMPK Dflox, DKO and α2-KO animals. A,** TH+ve neurons In each sub-region of the the nucleus tractus solitarius (NTS), shown in Figure 2.9. **B, C and D,** TH+ve neuron counts in the A1, C1 and C2 regions of the brainstem (Figure 2.9). Note that there is no loss of catecholaminergic neurons in any of these areas in DKO animals, while in α2-KO animals there is a significant increase in the number of TH+ve cells in the NTS and A1 regions.
(* =group significantly different from the controls , P< 0.05)
Abbrieviations as in Figure 2.9.

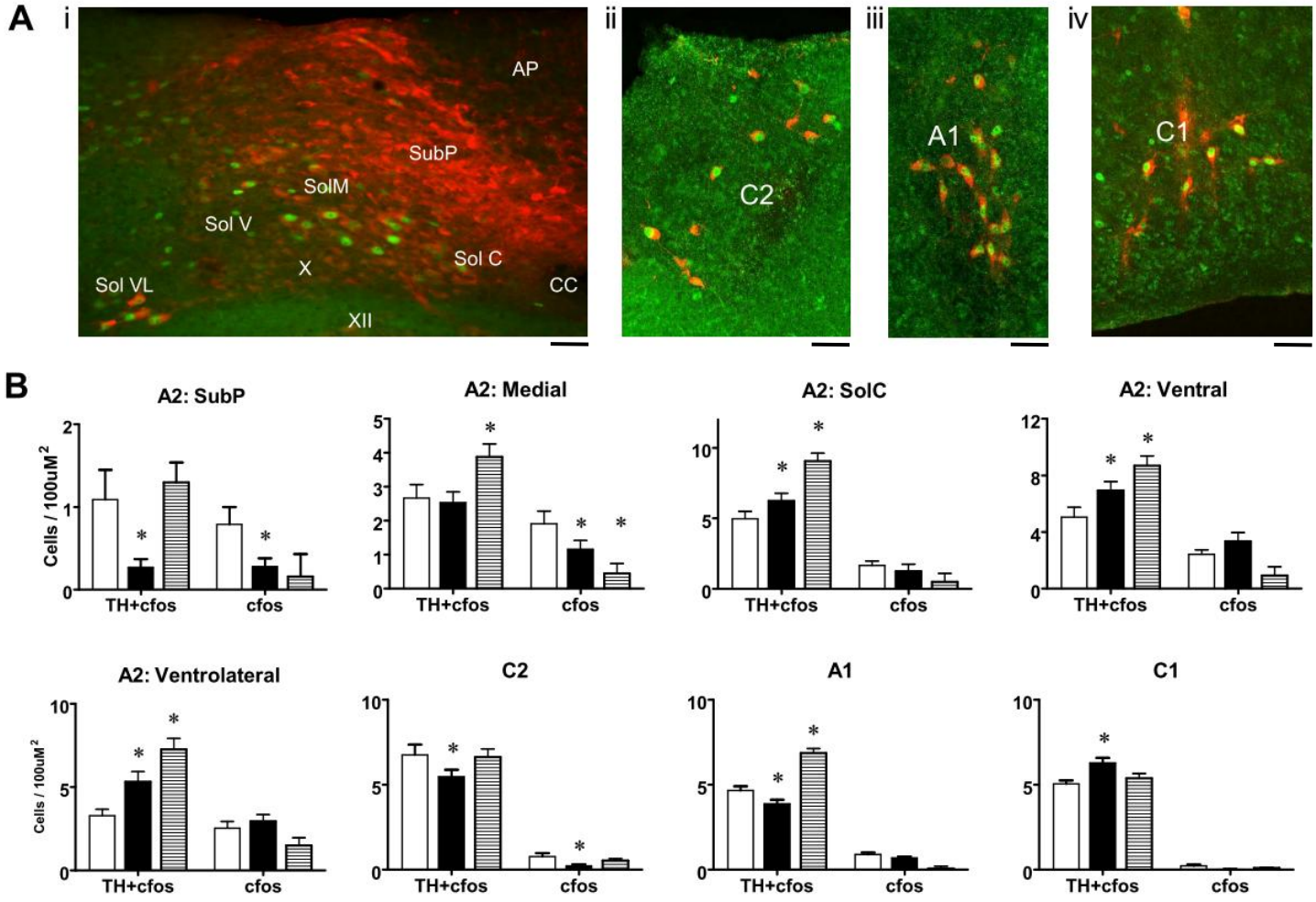


**Figure 2.11. For legend see next page**

**Figure 2.11 (previous page). A,** Representative examples of TH+ve (red), c-Fos +ve (green) and double-labelled neurons in the NTS region (i), C2 region (ii), A1 region (iii) and C1 region (iv) of the brainstem. Scale bars, 50 μm. **B,** Counts of TH+ve c-Fos+ve double-labelled cells, and c-Fos only cells, in each region of interest (as shown in Figure 2.9), normalised to cells/100$\mu m^2$ in relation to area of the region of interest. Open bars, AMPK Dflox (control) animals; filled bars, AMPK DKO animals; hatched bars, $\alpha$2-KO animals. (* =group significantly different from the controls , $P< 0.05$) Abbreviations as in Figure 2.9.

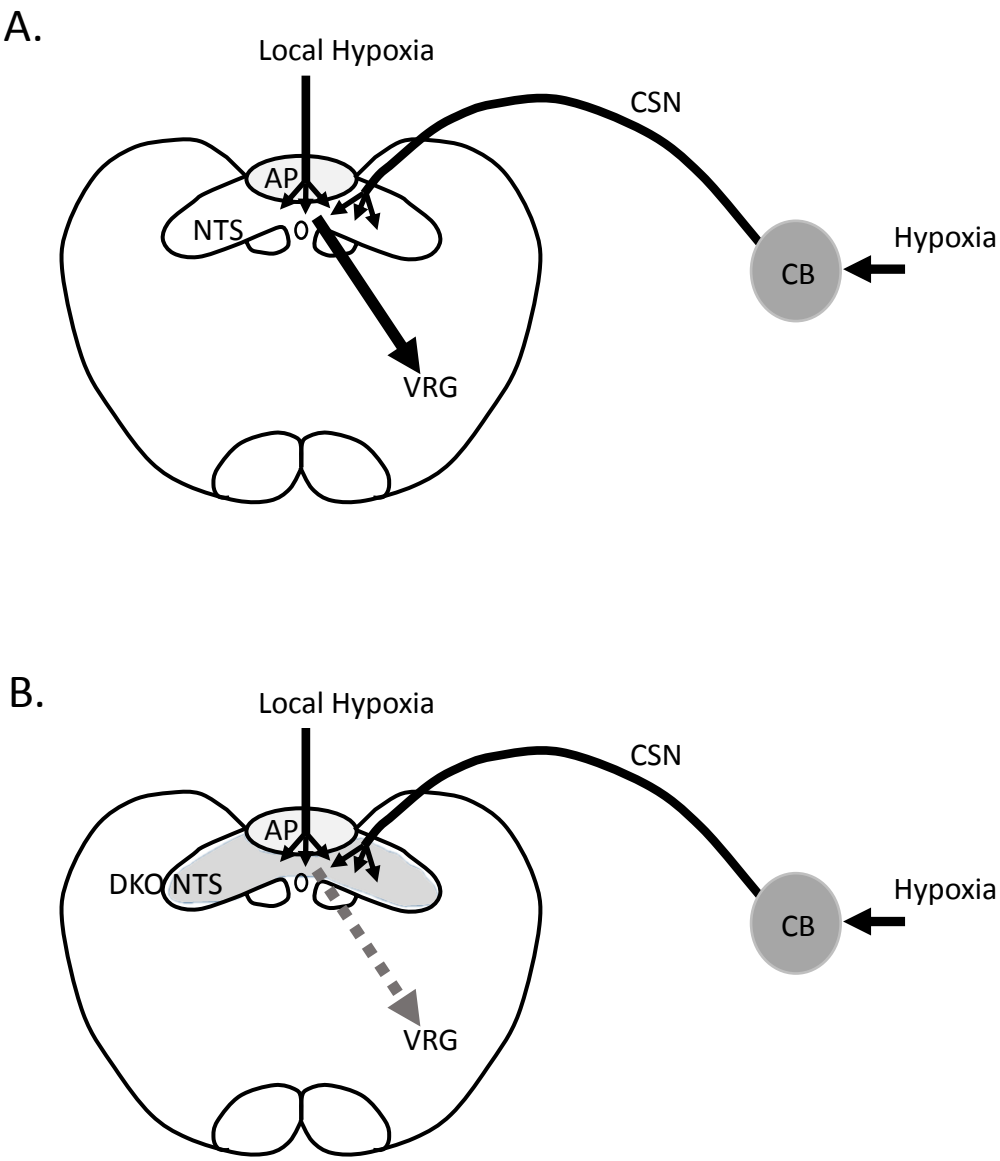


**Figure 2.12. Summary diagram showing the hypothesised effects of AMPK deletion on the hypoxic ventilatory response. A,** in normal animals, hypoxia activates the carotid body afferents in the carotid sinus nerve (CSN), which project to the caudal NTS neurons in the dorsal brainstem. The CSN afferent input is integrated with a hypothesised local hypoxia signal in the NTS. The NTS neurons stimulate hypoxic hyperventilation through their strong modulation of the ventral respiratory group (VRG) neurons. **B,** by contrast in DKO animals, deletion of AMPK in catecholaminergic neurons in the NTS (gray) results in hypoxic hypoventilation and apnoeas, even though the CSN afferent input is normal, indicating that AMPK is required for the correct integration of the local hypoxia signal in the NTS, and for the normal modulation of the VRG neurons. (Adapted from Mahmoud et al., 2015b)

# Chapter Three

## The effects of AMPK deletion on the peripheral carotid body

### *3.1 Introduction*

A definitive index of the carotid body response to hypoxia is its chemosensory signal that serves as the final common output to the central nervous system (Kumar, 2007). Previous classical electrophysiological studies have shown that the carotid body arterial $PO_2$ – response curve is sigmoid in nature with the chemosensory discharge starting to rise gradually at about 400-140mmHg arterial $PO_2$ up to approx.100mmHg by which time the slope increases and then rises sharply at about 70-75mmHg arterial $PO_2$ before attaining its maximum activity at approx. 20-30mmHg (Kumar, 2007).

Interestingly physiological recordings in vitro from isolated carotid bodies from both DKO and DFlox mice showed similar patterns as described above (see Fig 3.2 ; Mahmoud et al. 2015b), an observation that confirms that the CSN afferent responses to hypoxia are normal in both groups of animals.

The chemosensory synaptic transmission at the level of the carotid body during hypoxia involves the interplay of both excitatory and inhibitory neurotransmitters and neuromodulators as earlier discussed in chapter 1. Key examples of these transmitters are catecholamines (e.g dopamine and norepinephrine), acetylcholine, ATP and 5-Hydroxytryptamine (Nurse, 2005; Lahiri et al., 2006).

In the DKO mice the AMPKα1 and α2 isoforms were deleted from all TH-expressing (catecholaminergic) cells, including the glomus cells in the carotid body and it is unknown whether there is a loss of TH+ve (catecholaminergic) cells in the peripheral carotid body of DKO animals, as a result of the deletion of the AMPK gene even though their CSN in vitro physiological recordings are normal.

Therefore in this section of my work, I carried out experiments to examine the morphology of the carotid bodies in the AMPK DKO mice and compared it to the carotid bodies of DFlox mice with the aim of determining whether the deletion of AMPK had any effect on the total numbers of TH+ve (catecholaminergic) cells present in the carotid body of these mice.

Accordingly in this part of my work I examined the numbers of TH+ve cells in carotid bodies taken from DKO and DFlox animals.

### *3.2 Materials and Methods*

A total of 3 AMPK DKO mice and 4 AMPK DFlox mice were used in this study. The animals were kindly provided by Prof. Mark Evans. Dr Oluseye Ogunbayo was responsible for the management of the breeding programme and the genotyping of the animals, as described in Chapter 2. All experiments were carried out in concordance with the Home Office legislation.

Under terminal anaesthesia (0.2 ml pentobarbital, i.p.), the thorax was opened and the heart and ascending aorta were visualized under a dissecting microscope. The aortic

arch and the common carotid artery up to and including the carotid bifurcation, were gently cleared and excised. The dissection procedure was carried out by Dr. Jorge Navarro Dorado (Centre for Integrative Physiology, University of Edinburgh). Unlike in the rat and other animals (De Caro et al 2013), in the mouse the carotid bodies are not gathered together in a single identifiable mass, but instead are found in relatively small diffuse clusters attached to the bifurcation of the internal carotid arteries. A particular challenge in these experiments was to dissect out and identify the carotid bodies in the mice, as described below. In order to keep the internal carotid arteries stretched out, so that the anatomy could be recognised subsequently, the aorta and carotid arteries were suspended with a small weight in a vial of 4% paraformaldehyde in 0.01M PBS for 1h at 4ºC. The tissue blocks were then washed three times (15 minutes each) in 0.01M PBS, and transferred to 20% sucrose in 0.01M PBS plus 0.01%$NaN_3$ until needed. Prior to immunohistochemistry the carotid artery blocks were cut using a Cryostat (Bright 5040 microtome, Cryostat Instrument Company Ltd, Huntingdon, UK). The sections were collected and placed directly onto poly-l-lysine pre-coated slides (Superfrost®plus, Thermoscientific, UK). Thereafter the slides were incubated in 37ºC for 2hrs, and stored for immunolabelling at -80ºC.

The carotid body sections were stained for TH-immunoreactivity using the same methods as described in Chapter 2. Images of the carotid body sections were acquired using a Leica digital camera, controlled by Leica acquisition software (AIS) attached to an upright Leica microscope (LEICA DMR). Images were captured with both x10 and x20 objectives. The x20 images were used for the counting of the TH-immunopositive cells.

TH-immunoreactivity was visualized using the Alex Fluor 568 secondary antibody (Life Technologies Ltd, UK), using the red channel of the imaging system, in the same way as for the brainstem sections in Chapter 2. In addition, the auto-fluorescence of the arterial wall epithelial cells was visualized using the green channel (see Figure 3.1). Each section was searched for a recognizable length of the carotid arteries, and specifically for a section through the bifurcation of the internal carotid arteries. Clusters of TH+ve cells were searched for in the region of the bifurcation where it was found, corresponding to the carotid bodies. The larger mass of the superior cervical ganglion (SCG) was also strongly TH+ve, and this was usually recognizable as a large structure separate from the arterial walls (see for example Figure 3.1).

Regions of interest were drawn around clusters of TH- positive cells in each section of the carotid body where it was found, and the counts from each region of interest per section were normalized to cells/ 100$\mu m^2$.

## *3.3 Results*

### *3.3.1 Catecholaminergic cells in the carotid body*

Unfortunately after sectioning of the fixed dissected tissue, the carotid body bifurcation could only be clearly identified in 3 of the 4 DFlox mice preparations, and 2 of the 3 DKO mice preparations. In the remaining preparations it was not possible to confidently identify any groups of TH+ve cells as a cluster that could represent the carotid body, and so these were excluded from analysis.

In each of the identified carotid bodies of the DKO and DFlox carotid bodies there was a robust presence of TH+ve cells, as illustrated for one DKO animal in Figure 3.1. Cell counts of TH+ve cells in each group are shown in Table 3-1. From the cell counts it is apparent that the mean number of TH+ve cells in the carotid bodies from DKO animals is reduced, compared to that in the DFlox controls.

**Table 3.1: Total number of TH+ve cells in the carotid bodies of DFlox and DKO animals**

| | N | TH+ve cells/ 100$\mu^2$ |
|---|---|---|
| DFlox | 7 sections, from 3 animals | 131.51 ± 16.14 |
| DKO | 4 sections, from 2 animals | 60.16 ± 15.28 |

However, the small number of preparations available (with the DKO results coming from only two animals), means that it is difficult to reliably draw a conclusion from a statistical comparison of the DKO animals with controls. Although the mean numbers of TH+ve carotid body cells in the two DKO animals is clearly lower than the mean count in DFlox animals (Table 3-1), more data from additional DKO animals is required

before it can be concluded whether or not there is a significant decrease in TH+ve cells in the carotid bodies of DKO animals.

### *3.4 Discussion*

The small number of animals involved in this part of the work, and the limited number of sections in which the carotid bifurcation and the carotid bodies could be identified with confidence, means that a clear conclusion to the question of whether there is a change in the number of TH+ve cells in the carotid bodies of DKO animals or not, cannot be drawn from the present study. The likely reason for the difficulty in recognizing the carotid bodies in some of the sections is the twisting and deformation of the dissected tissue blocks during the fixing procedure, so that it was difficult to identify the carotid bifurcation. Further experiments to improve the fixation step to hold the tissue in a standard orientation, to avoid this from happening, are necessary. Unfortunately because of time constraints, and because of the fixed number of animals available from the mouse colony breeding programme for this part of the study, it was not possible to try alternative ways of fixing the tissue blocks.

The finding of significant numbers of TH+ve cells in the carotid bodies of both of the DKO mice included in this study, however, suggests that the morphology of the carotid bodies in DKO mice might not have been affected by the deletion of AMPK in the glomus cells. However if further work confirms the observed reduction in the number of TH+ve cells in the carotid bodies of the DKO animals, this will raise interesting questions relating to how the deletion of AMPK causes the loss of these cells in the

carotid bodies. In addition, although the role of TH neurotransmission in the sensing and transduction of hypoxia in the carotid body is not entirely clear (as discussed in Chapter 1), the *in vitro* results from isolated carotid body-CSN preparations (Mahmoud et al 2015b) show that the afferent firing evoked by hypoxia is not different from normal. Therefore, if further experiments confirm the a loss of TH+ve cells in the peripheral carotid bodies after AMPK deletion, as indicated by the present results, the mechanisms by which the normal afferent response to hypoxia is maintained, will need to be investigated. In addition it will be interesting to determine how the deletion of AMPK in the peripheral carotid bodies leads to a loss of TH+ve cells, while by contrast in the brain (Chapter 2), AMPK deletion leads to a hyperplasia of TH+ve neurons in the dorsal brainstem. Further work is therefore necessary to obtain more definitive results, regarding the effects AMPK deletion on the TH+ve cells in the peripheral carotid bodies of the DKO animals.

The possibility of a 2-fold reduction in the number of catecholaminergic (TH-expressing) cells in the carotid body of the AMPK DKO mice as opposed to the DFlox animals (although more work is needed) appears to be obvious probably due to the action of nitric oxide (NO). Nitric oxide is one of the neurotransmitters that are expressed by the glomus cells of the carotid body (Kumar, 2007). It is synthesised by the enzyme nitric oxide synthase (NOS) which exists in three isoforms; neuronal (nNOS), endothelial (eNOS) and inducible (iNOS) (Lira et al. 2007). nNOS and eNOS produce nitric oxide at lower concentrations and at such levels it plays a role in promoting cell growth and survival in many tissues but conversely iNOS produces nitric

oxide at higher levels leading to cellular damage including DNA damage and inhibition of oxidative metabolism (Lira et al., 2007; Meares et al., 2011).

Interestingly AMPK activation causes the inhibition of iNOS expression in many cell types including myocytes, adipocytes and macrophages while it phosphorylates and activates nNOS and eNOS isoforms (Pilon et al., 2004; Lira et al., 2007) (see Figure 3.3).

Thus the deletion of AMPK in the DKO mice may lead to an increase in the expression of iNOS in the carotid body with a resultant production of high levels of nitric oxide leading to the damage of the catecholaminergic cells in these animals.

On the other hand it is worth noting that nitric oxide has a facilitatory influence on the actions of AMPK either via the inhibition of AMPK phosphatases or activation of AMPK kinases (Lira et al., 2007) (see Figure 3.3).

Intriguingly if there is a loss of catecholaminergic cells in the carotid body of the DKO mice coupled with the demonstration that the discharge from the CSN is normal in these animals during hypoxia (see Mahmoud et al. 2015b) then it is plausible that there is a certain degree of redundancy in the physiology of the carotid body with regards to response to hypoxia i.e. it may not be necessary for all the glomus cells to be activated before a full discharge is recorded in the CSN during hypoxia alternatively there is a possibility that the cells that might have been loss following AMPK deletion are a subset of the glomus cells which may not be involved in mediating the hypoxic chemosensory process in the carotid body. Kumar and Prabhakar (2012), have reported attempts to classify glomus cells into types A and B with the type A cells being the presynaptic

elements that transmit hypoxic signals into the afferent nerve (CSN) while the type B cells are non-innervated glomus cells which may not be involved in the response to hypoxia. Taken together if these results are confirm it shows that although AMPK deletion may cause a reduction in the total glomus cell counts it has no effect on the TH–expressing chemistry of these cells.

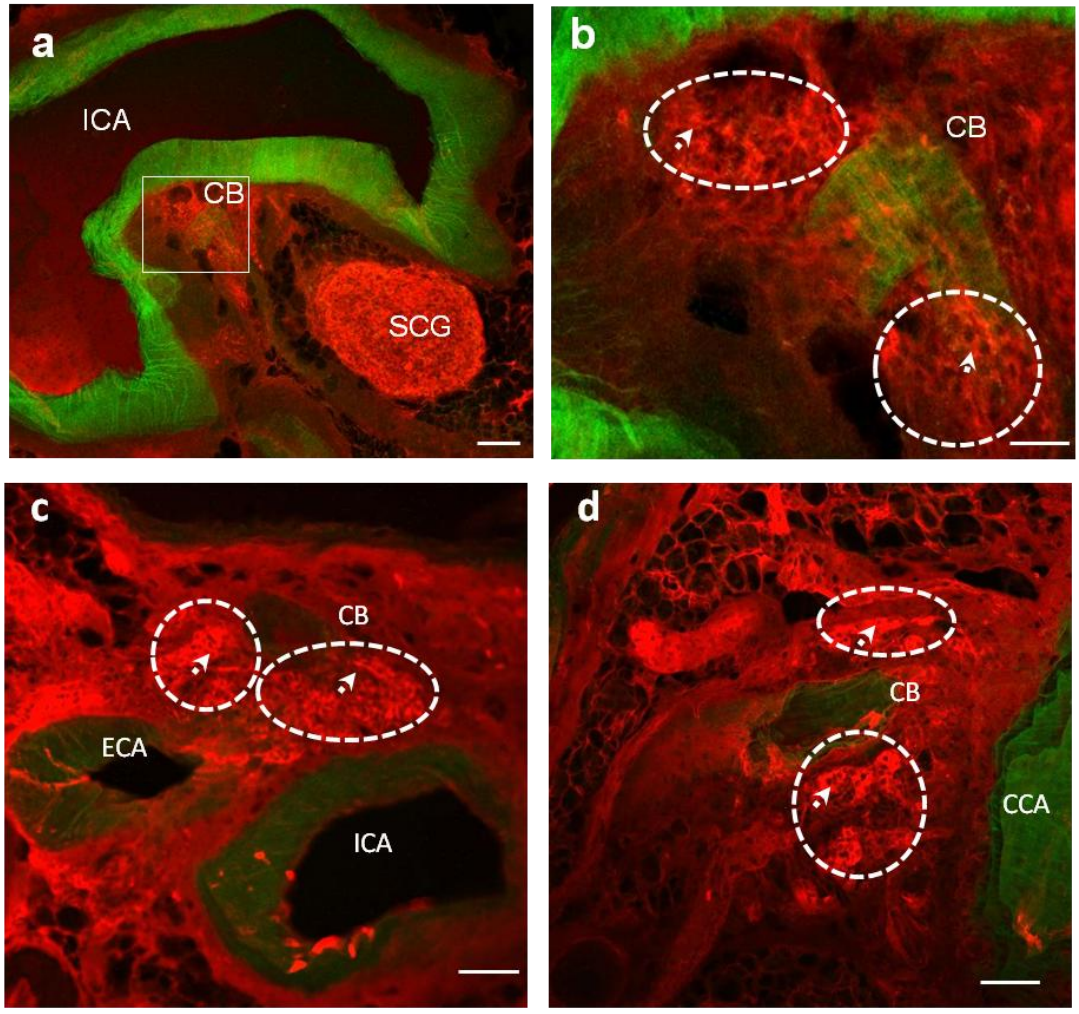


**Figure 3.1:** .(**a**) Tyrosine Hydroxylase (TH) immunostaining (red) of carotid body (CB) and superior cervical ganglion (SCG) in a DKO animal. Autofluorescence (green) of the arterial wall of the internal carotid artery indicates the location of the CB adjacent to the carotid bifurcation. Scale bar, 100µm. (**b**), higher magnification view of the rectangular area indicated in (a), showing clusters of TH+ve cells (in circles, were cells were counted). Arrows indicate TH-ve cells within the carotid body. Scale bars, 25µm. (**c**) and (**d**), show TH immunofluorescence staining of the glomus cells of the carotid body in a DFlox mice. Circles indicate clusters of TH+ve cells in areas where cells were counted. Arrows indicate TH-ve cells within the carotid body. Scale bars are 25µm(c,d). Abbreviations: CCA, Common carotid artery; ICA, Internal carotid artery; ECA, External carotid artery.

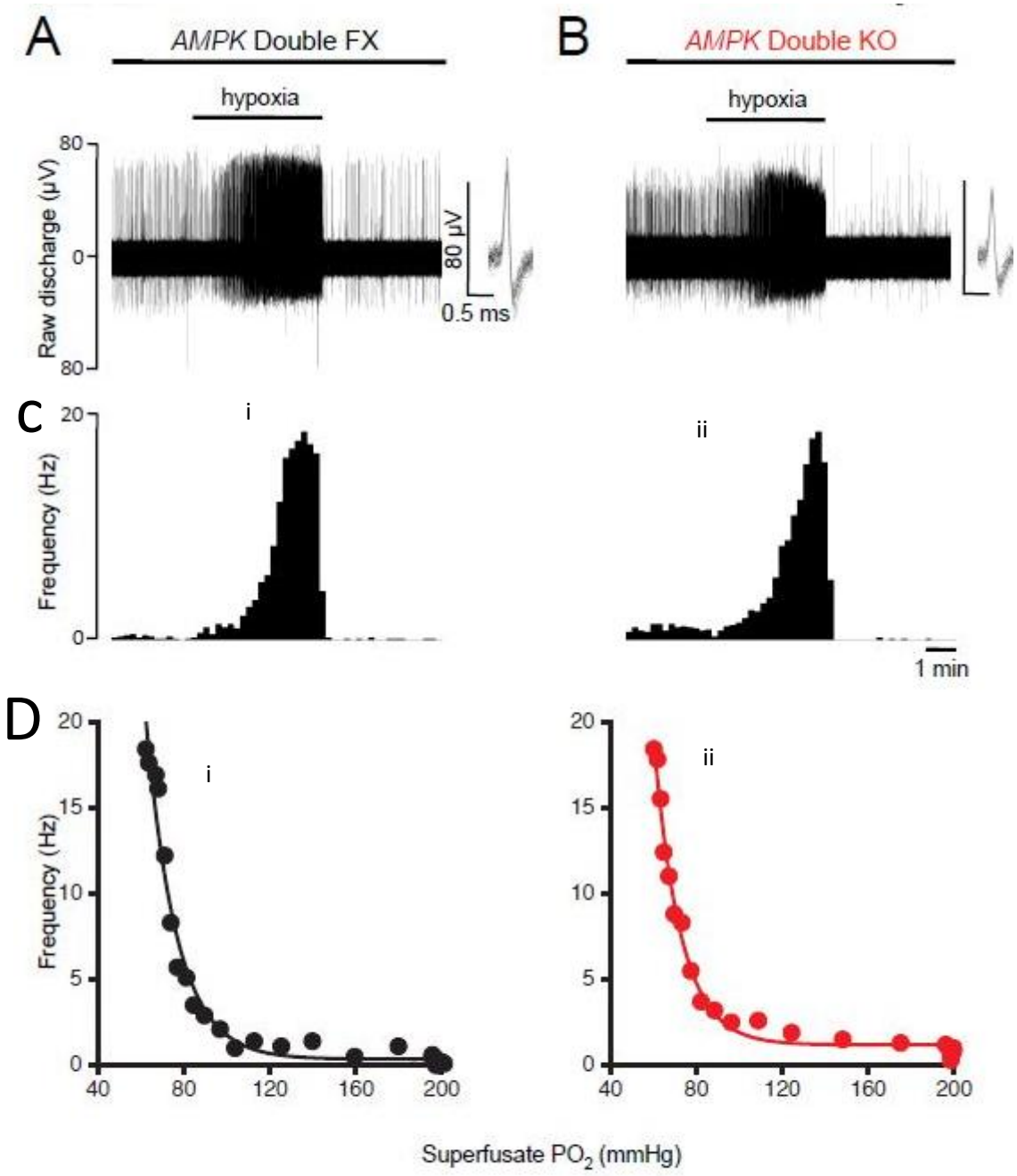


Mahmoud et al., 2015b

**Figure 3.2: (A&B)** Show extracellular recordings of single fibre chemosensory firing versus $PO_2$ for DFLOX and DKO mice respectively. Inset, shows single fibre discrimination. The middle panel **(c)** shows the frequency- time histogram for fibre chemoafferent discharge for DFLOX mice (**i**) and DKO animals (**ii**). **(D)** Sigmoid graphs showing the $PO_2$ – response curves of the glomus cells in **(i)** DFLOX mice and **(ii)** DKO animals. Observe (lower panel) the exponential rise in chemoafferent discharge frequency following reductions in superfusate $PO_2$ in both the DKO and DFLOX carotid bodies with a peak frequency at a $PO_2$ of approx. 74mmHg and measuring at 12.5 ±1.6 Hz for the control mice and 13.9±1.5Hz for the DKO group. (n=10 for DFlox; n=8 for DKO, P≤0.001). (Mahmoud et al., 2015b).

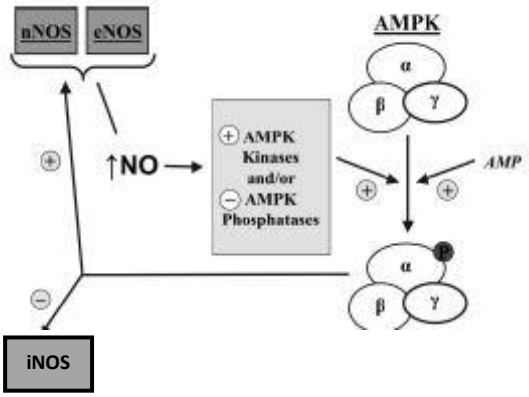


**Figure 3.3:** A proposed schematic diagram showing the interaction between AMPK and NO (e.g in skeletal muscles).Θ= Inhibition; ⊕ = activation; ● = AMPK activation. **nNOS**= neuronal nitric oxide synthase; **eNOS**= endothelial nitric oxide synthase; **iNOS**= Inducible nitric oxide synthase; **↑NO** = increased levels of nitric oxide (Adapted from Lira et al., 2007).

# Chapter Four

## Pilot Study to develop virus-induced targeted AMPK knock-out in brain areas

### *4.1 Introduction*

Previous work in this thesis has shown altered respiratory responses to hypoxia in AMPK DKO mice when compared to control DFlox animals. As shown in Chapter 2, these mice also presented systematic changes in the activation of brainstem catecholaminergic neuronal groups that are known to be involved in the control of respiration, suggesting that AMPK has an important role to play in these brainstem areas in the normal hypoxic hyperventilatory response. In the absence of AMPK in these brainstem areas, the animals show the observed respiratory abnormalities.

However, the above work was carried out in animals where the AMPK gene had been globally knocked-out in catecholaminergic cells (using a Cre-lox system under the control of a TH-promoter).

For further and more specific investigation of the neuronal mechanisms involved in the respiratory abnormalities following AMPK deletion, it would be beneficial to develop methodology to selectively delete AMPK in the brain only (i.e. Leaving other catecholaminergic cells, such as the glomus cells in the carotid body, unaffected). In addition, attempts could be made to target specific brainstem areas, to localise the effects of AMPK deletion in the different brainstem nuclei involved in the control of respiration.

Therefore, this pilot study was designed to elucidate, whether a localised (targeted) knock-out of the genes carrying the α1 and α2 isoforms of the α-catalytic subunit of

AMPK in the brainstem of AMPK DFlox mice, would reproduce the same abnormal ventilatory responses as observed in the AMPK DKO mice.

The recombinant viral vector technology, using adeno-associated virus (AAV), which allows for the targeting of localised populations of neurons or other cell types within a specific part of the nervous system (Kootstra and Verma, 2003; Zincarelli et al., 2008; Schultz and Chamberlain, 2008; Lentz et al., 2012; Aschauer et al., 2013; Holehonnur et al., 2014), was used for this work.

### *4.1.1 Recombinant viral vector technology*

#### *Background*

The roles of various molecules in the development and function of the nervous system can be studied by using mice carrying conventional null mutations of the genes for these molecules (Ahmed et al., 2004). This conventional transgenic animal technology alters the genetic makeup of the cells or the tissue types and so the expression of the molecules concerned (Gordon et al., 1980; Palmiter and Brinster, 1986; Gu et al., 1994; Glueck and Dzau, 2002; Haruyama, 2009; Miao, 2013; Holehonnur et al., 2014).

Research using transgenic animal technology started in 1974, following the work of Janeisch and Mintz (1974), who generated transgenic animals by microinjection of viral DNA into blastocysts (Miao, 2013). This was followed by the generation of the first transgenic mouse by Gordon et al. (1980) through the pronuclear injection of a foreign gene into the mouse oocytes (Haruyama, 2009; Miao, 2013). One of the major approaches in generating conventional knockout animals is the Cre –loxP recombinase technique, which involves the use of Cre-recombinase to remove loxP-

flanked segments of DNA (Sauder and Henderson, 1988; Gu et al., 1994; Tsien et al., 1996; Ahmed, et al., 2004). This technique has been previously discussed in detail in Chapter 2.

While in the conventional Cre-lox system the knock-out animals are generated through the breeding of Cre-expressing mice with mice in which the gene of interest has been flanked by loxP sequences, recent progress in genetic engineering and neuroscience has made it possible to deliver Cre–recombinase directly to specific groups of neurons in adult animals *in vivo,* using viral vectors such as adeno-associated virus, lentivirus, herpes virus and adenovirus carrying the Cre sequence with resultant recombination (Stec, et al., 1999; Brooks et al., 2002; Kaspar et al., 2002; Ahmed et al., 2004; Sinnayah et al., 2004; Holehonnur et al, 2014). This technique is referred to as the recombinant viral vector technology.

*Recombinant viral vector technology*

Recombinant viral technology allows for the targeting of discrete populations of neurons or other cell types within specific regions of the brain, using recombinant viruses ( McCown et al., 1996; Kasparov and Paton, 2000 ; Sinnayah et al., 2002; Sinnayah et al., 2004; Holehonnur et al., 2014). These viruses are genetically engineered to carry transgenes of interest (for example, Cre- recombinase) and when injected into desired regions of the central nervous system, mediate the delivery and stable transduction of these genes into the cells of the region (Blomer et al., 1997; Naldini, 1998; Zufferey et al., 1998; Ahmed et al., 2004; Sinnayah et al., 2004; Lentz et al., 2012; Daya and Berns , 2008; Holehonnur et al., 2014). One of the advantages of this technology over the conventional transgenic animal technology is that it permits genes to be manipulated at virtually any point in the animal's life span

relatively quickly and easily (Pitkow et al., 2001; Ahmed, et al, 2004; Sinnayah et al., 2004; Lentz et al., 2012; Holehonnur et al, 2014). Also, unlike the conventional knock out animals, mice exposed to this technique do not suffer from such limitations as embryonic or perinatal lethality and the compensatory regulation of other genes, which may result in altered observed abnormalities (Ahmed et al, 2004). Another advantage of the recombinant viral vectors is that they allow for selective delivery of Cre-recombinase to specific brain targets in which specific promoters have not yet been identified, as opposed to the conventional genetic knock–out technique that requires highly specific promoters for selective gene deletion and where these are not available, the technique is limited (Kilby et al., 1993; Stec, et al., 1999; Brooks, et al., 2000; Kaspar et al., 2002; Sinnayah et al., 2004). A further consideration in the use of conventional transgenic animal technology is also in relation to the breeding and maintenance of mouse lines, but this shortcoming is greatly reduced in the recombinant vector approach since it only requires the generation and breeding of the Floxed mouse line.

Although several recombinant viral vectors have been used for selective delivery of transgenes into mice *in vivo* (Connolly, 2002; Sinnayah et al., 2004; Ahmed, et al., 2004; Holehonnur et al., 2014), the two most widely used viral vectors are the adeno-associated virus (AAV) and lentivirus (LV) ( Flotte et al., 1993; Peel et al., 1997; Connolly, 2002; Wright et al., 2003; Ahmed, et al, 2004; Vasileva and Jessberger,2005; Daya and Berns, 2008; Holehonnur et al., 2014). These viruses have the ability to deliver and transduce genes into both dividing and non-dividing cells in the nervous system, without causing immune responses in the host animal.

*Adeno-associated virus vector*

Adeno- associated virus (AAV) vectors occupy a preeminent position in neuroscience research, in terms of gene delivery to adult mice brains and also have potential as a vector for human gene therapy for several genetic disorders like haemophilia, cystic fibrosis and muscular dystrophies (Vasileva and Jessberger, 2005; Ahmed, et al, 2004; Broekman et al.,2006; Honaramooz et al., 2008; Daya and Berns, 2008; Schultz and Chamberlain, 2008; Zincarelli et al., 2008; Aschauer et al., 2013 Chakrabarty et al., 2013 ; Holehonnur et al., 2014).

AAV mediated gene delivery has been shown to be a safe and efficient method for extensive transduction of neurons and long-term expression of transgenes in the brain. The unique characteristics of AVV of not being toxic in vivo, lack of pathogenic ability, non- inducement of significant inflammatory and immune responses and the ease of its production within the laboratory at required titres, make it an ideal virus for in vivo use (Wright et al., 2003; Broekman et al., 2006; Daya and Berns, 2008; Zincarelli et al., 2008; Holehonnur et al., 2014).

Lentiviral vectors are equally useful in gene delivery to cells as AAV (Connoly, 2002; Ikawa et al., 2003). Lentivirus has the ability to integrate into non–dividing cells, such as neurons and provides stable and long–term gene expression *in vivo*. However one of the major advantages of the recombinant AAV vectors over the lentivirus is that they present low risk of insertional mutagenesis, due to their low integrating property with the host cell genome (Connolly, 2002; Ikawa et al.,2003 ; Daya and Berns.2008:;Schultz and Chamberlain, 2008; Chandrashekran et al., 2014).

In this pilot study, a commercially available adeno-associated virus vector, AAV-DJ (Vector Biolabs, Phiadelphia.USA) was used. This vector expresses an improved Cre transgene (iCre) under the influence of a cytomegalovirus (CMV) promoter, together with an enhanced green fluorescent protein (eGFP) as a reporter. The vector was used based on the fact that the technology and expertise for its effective injection into desired brain regions was available in Prof. Matthew Nolan's laboratory, Centre of integrative Physiology, University of Edinburgh. The virus vector was injected into the brainstem of AMPK DFlox mice, in order to induce the knock-out of AMPK α1 and α2 genes in the virally infected neurons.

The success of the deletion of the AMPKα1 and /or α2 cataytic subunits in the brainstem catecloaminergic neurons was confirmed by culturing AMPK DFlox mouse brain tissues with the AAV vector after which real-time quantitative PCR (qPCR) was carried out following the protocol as discussed in chapter 2 (all procedures were carried out by members of the Evans laboratory, Centre for Integrative Physiology, University of Edinburgh).

### *4.2 Materials and Methods*

*Animals*

A total of 6 AMPK DFlox mice (5 males and 1 females), weighing between 20-29g (9-10 weeks old), were used for this pilot study. All mice (a gift from Prof. Mark Evans, with the mice colony under the management of Dr.Oluseye Ogunbayo) were bred and housed in the BRR animal facility, Centre for Integrative Physiology, School of Biomedical Sciences. All procedures were carried out in accordance with

the University of Edinburgh guidelines for animal research in conformity with the UK Animals (Scientific procedures) Act 1986.

*Surgery / Stereotaxic Injections*

All surgeries were performed by Dr Marlies Oostland (Centre for Integrative Physiology, University of Edinburgh). The mice were anaesthetised with isofluorane (Abbot Laboratories ltd, Berkshire, UK), placed in a stereotaxic frame, and local anaesthetic (Vetergesic, 0.03 ml of 0.03mg/ml buprenorphine per animal) was injected subcutaneously at the incision sites. The skin was swabbed with Betadine antiseptic solution (povidone-iodine 10%, Ecolab, Leeds, UK).

The foramen magnum was exposed by gently pulling aside the muscles and overlying fascia. The dura between the foramen magnum and first cervical vertebra (C1) was opened with a small bent needle. Injections were made through this opening using glass pipettes which were slowly lowered into the brainstem using a micromanipulator attached to the stereotaxic frame. In terms of anatomical guidance for the injection sites, coordinates in relation to bregma or lambda were not used, but the midline and distance from the base of the skull were used, since injection were performed through the foramen magnum.

The virus was injected using pulled glass pipettes with a tip diameter of 6-10µm. 50nl of the virus was injected per injection site, totalling 800nl for 8 injection sites on each side of the brainstem. The virus titre used was $1.0x10^{13}$ GC/ml, based on the titres which were used routinely by Dr. Marlies Oostland for injection into the inferior olive and related structures (Oostland, unpublished, personal communication).

*Dorsal injections*

The dorsal brainstem was targeted by lowering the pipettes into the foramen magnum at an angle of 30-35$^{o}$ to the vertical. A series of injections were carried out with the first injection at a depth of 3.5 mm, before being slowly raised to the next injection sites at 3.0, 2.5, 2.0,1.5.1.0, 0.5 and 0.2mm depth. The pipette was left in place in each position for 3mins. At the last site the pipette was left in place for 5 mins following the injection before being fully retracted very slowly. Bilateral injections were made at 0.1 mm lateral on each side of the midline.

*Ventral injections*

The ventral areas of the brainstem were targeted by lowering the pipettes into the foramen magnum at an angle of 45-50$^{o}$ to the vertical. A series of injections were carried out as described above. Bilateral injections were made at 10 and 13 mm lateral to the midline, on each side.

The surgeries typically lasted for 2-2.5 hours. Mice were closely monitored for a full recovery after anaesthesia and returned to their home cage when fully awake. They remained in their home cage for two weeks before the next experiments were carried out.

*Plethysmorgraphy/ Immunohistochemistry*

Respiratory responses to hypoxia in the virus injected mice were recorded by using an unrestrained whole- body plethysmography as earlier described (Chapter 2). Three recording sessions were carried out for each mouse at 2 weeks, 3 weeks and 3.5 weeks after the surgery. At the end of the third plethysmographic run the

animals were deeply anaesthetised and transcardially perfused, and the brain was removed and processed for immunohistochemistry, as described in Methods, Chapter 2. Images of the brainstem sections were then acquired using a Leica digital camera as earlier described. The x20 images were used for the counting of the immunopositive cells.

Virus infected cells were identified as those expressing GFP, while TH+ve neurons were visualised using the red channel of the imaging microscope as before. TH+ve neurons, and double-labelled neurons, were counted in the brainstem areas of interest (the NTS subdivisions, C2, A1 and C1 regions) using image J software (Fiji; an open source platform for biological–image analysis). The percentage viral transfection for each nucleus was then calculated, as the percentage of total TH+ve cells that were also co-labelled with GFP, and normalised by the area to give cells per 100 $um^2$.

### *4.3 Results*

#### *Hypoxia responses in virus-vector injected mice*

Fig. 4.1 shows the measured ventilatory response (left column) and the number of apnoeas per minute (right column) in each of the animals in this study, during the 5 minutes of exposure to hypoxia (8% $O_2$, 0.05% $CO_2$, balanced with $N_2$). In the first experimental run 2 weeks after surgery three of the animals (mice 834, 840 and 844) showed a higher incidence of hypoxia-induced apnoeas (Fig. 4.1, upper panel). This is suggestive of the apnoeas observed in DKO mice during hypoxia (Chapter 2, Results, Figure 2.8). However the ventilatory response in these three virus-injected animals appears to be normal and no different from that seen in the other animals in the group. In subsequent runs (weeks 3 and 3.5 after surgery) these three animals no

longer showed the increased incidence of apnoeas (Fig. 4.1, middle and lower panel). Thus the apnoeas observed in the first exposure to hypoxia at 2 weeks post-surgery were not sustained. The ventilatory response to hypoxia in all of the animals also appeared to be normal, and none of the animals showed an evidence of hypoxia-induced hypoventilation similar to that seen in DKO animals (Chapter 2).

***Transfection of brainstem neurons by Cre –virus vector injection***

Injection of the Cre-recombinase viral vector into both the dorsal and ventral portions of the brainstem resulted in varying degree of transfection of brainstem catecholaminergic neuronal populations after 3.5 weeks (Figures 4.2 – 4.7).

*Mouse 844:* This mouse received dorsal and ventral injections of the Cre-recombinase viral vector. There was a 43% transfection of the TH+ve A2 neurons in the SubP subdivision of the NTS, and 70% transfection of these neurons in the medial subdivision of the NTS, while that of the SolC, ventral and ventrolateral portions of the NTS were 61%, 76% and 85% respectively. There was no transfection of the C2 adrenergic neurons. Ventrally, there was a poor transfection of A1 neurons (9%) and 95 % transfection of the C1 adrenergic neurons (Figure 4.2). Interestingly this mouse showed a higher number of apnoeas in the first exposure to hypoxia (Figure 4.1), but this was not maintained and the respiratory responses to subsequent exposures to hypoxia were no different from normal animals (Figure 4.1).

*Mouse 836:* This mouse received dorsal and ventral injections of the Cre-recombinase viral vector. After a period of 3.5 weeks, there was only a 33% transfection in the A2 neurons of the ventral subdivision of the NTS; 32% in the

ventrolateral subdivision; 19% in the SolC subdivision; 4% in the medial subdivision and 0% in the SubP subdivision. There was also no infection in the C2 neurons. On the other hand, 56% transfection of the A1 noradrenergic neurons was observed (Figure 4.3).

*Mouse 834:* Injection of the Cre-recombinase viral vector into the dorsal brainstem of this mouse showed widespread transfection of the A2 neurons in many subdivisions of the NTS after 3.5 weeks: 96% transfection was seen in the ventrolateral subdivision; 97% in the ventral subdivision; 96% in the SolC subdivision; 94% in the medial subdivision and 35% in the SubP subdivision. A 30% transfection of the C2 neurons was also observed and there was no virus spread to the ventrally located A1 and C1 neurons (Figure 4.4). This mouse also showed a higher number of apnoeas in the first exposure to hypoxia (Figure 4.1), but this was not maintained and the respiratory responses to subsequent exposures to hypoxia were no different from normal animals (Figure 4.1).

*Mouse 835:* Injection of the Cre-recombinase viral vector into the dorsal brainstem of this mouse resulted in the transfection of the rostral C3 adrenergic neurons located in the midline of the brainstem after 3.5 weeks. There was no transfection of other catecholaminergic neuronal groups in the brainstem (Figure 4.5).

*Mouse 840:* Transfection of the catecholaminergic neurons in the ventral portion of the brainstem of the above mouse was observed when the ventral region of its brainstem was injected with the Cre- recombinase viral vector. After a period of 3.5 weeks, 95% transfection was observed in the A1 neuronal population, while 79% transfection was seen in the C1 adrenergic neurons. There was no virus spread to the A2 and C2 cell groups (Figure 4.6). This mouse also showed a higher number of

apnoeas in the first exposure to hypoxia (Figure 4.1), but as with mouse 834 this was not maintained and the respiratory responses to subsequent exposures to hypoxia were no different from normal animals (Figure 4.1).

*Mouse 842:* Injection of the Cre-recombinase viral vector into the ventral portion of the brainstem of mouse 842 resulted in the transfection of the ventrally located A1 and C1 neuron groups after 3.5 weeks, with no transfection of other catecholaminergic cell groups in the brainstem (Figure 4.7).

### *4.4 Discussion*

Injection of an AAV viral vector carrying the Cre-recombinase sequence into the brainstem of AMPK DFlox mice, to induce AMPK knockout in virally infected neurons, resulted in varying levels of viral infection in different brainstem areas in the six animals used in this pilot study. Unfortunately this did not result in a corresponding respiratory phenotype as that observed in the AMPK DKO mice, in any of these animals (Figure 4.1).

Although a high number of hypoxia-induced apnoeas were observed in three animals during their first exposure to the hypoxia challenge (Figure 4.1, upper panel), this was not accompanied by a hypoventilation as seen in the DKO animals. In addition, the virally infected regions of the brainstem were not consistent between these three animals (Figures 4.2, 4.4 and 4.6), and the hypoxia-induced apnoeas were not observed in the subsequent exposures of the same animals to hypoxia (Figure 4.1). This indicates that the apnoeas were not due to a virally-induced knockout of AMPK in key neurons that produce the phenotype seen in DKO animals, but instead they were probably due to some mechanical damage or trauma to the brainstem of these animals, which gradually healed over the period of 2-3 weeks after surgery.

The lack of a DKO-like respiratory phenotype in any of the virally-injected animals could be due to the titre of virus injected not being high enough for adequate transfection of the targeted brainstem regions, thereby limiting the deletion of AMPK in these neuronal populations. It is of interest to note that there was a poor or no viral transfection of the A2 neurons in the SubP region of the NTS, in the mice that had dorsally-targeted injections (mice 834, 35%; 836, 0%; 844, 43%), perhaps because of its highly vascularised structure in close proximity to the AP. Thus it is

plausible that such low or no of transfection of the SubP neurons, which may play a crucial role in mediating the hypoxic hypo-ventilatory response as discussed in Chapter 2, might explain the lack of the abnormal respiratory phenotype in virally-injected animals.

On the other hand, it is interesting to note that in a number of animals receiving ventrally-targeted virus injections, there was a high percentage of virally infected cells in the ventral A1 and C1 regions (e.g. mouse 840). Nevertheless, these animals did not show any abnormal hypoxia-induced respiratory phenotype. This indicates that the knockout of AMPK in these ventral regions is not sufficient to induce the hypoxia-induced apnoeas and hypoventilation observed in DKO animals. This is additional suggestive evidence that AMPK plays an important role in the dorsal brainstem neurons, in particular the SubP neurons in the NTS, as opposed to the ventral brainstem regions, in generating the hypoxia-induced apnoeas and hypoventilation in DKO animals (Chapter 2).

Also, it is reasonable to argue that the absence of a similar respiratory phenotype in the virally – injected mice as compared to the conditional AMPK knock out animals could be due to some compensatory changes / responses that have occurred during the development and growth of the conditional DKO mice. The ability of AMPK in coupling the energy status of the cell to its metabolic processes is achieved through the acute modulation of major metabolic enzymes (direct phosphorylation) and via slower transcriptional changes within the cell, thus AMPK controls the expression of quite a number of genes especially those involved in mitochondrial biogenesis, energy production and oxidative stress response (Canto and Auwerx, 2010). Therefore it is expected that lack of AMPK from the onset of the mice development (as in the conditional AMPK DKO mice) may results in compensatory genetic

modulation of the downstream targets of AMPK leading to the expression of the respiratory phenotype in these mice as opposed to the virally –induced AMPK knock-out mice. Other compensatory responses may include changes in cell-cell communication between the AMPK deficient catecholaminergic neurons within the SubP and other regions of NTS with the non- catecholaminergic neurons in these areas resulting in the observed phenotype. Furthermore the lack of a corresponding phenotype in the virally –induced AMPK knock-out mice in comparison to the conditional DKO upon exposure to hypoxia may be due to the fact that a simultaneous deletion of AMPK in all the catecholaminergic neuronal cells and that of the carotid body is required for the full expression of this phenotype.

Intriguingly this pilot study if extended will open research doors for further elucidation of the specific brainstem neuronal groups (and their roles) in the central control of oxygen sensing as well as their interaction with the peripheral carotid body. For example, the relationship between the peripheral carotid body and these central (brainstem) oxygen sensors during hypoxia could be investigated via the use an *in situ* dual perfused animal preparation which allows for separate perfusion (with varying $PO_2$ ) of the central and peripheral oxygen sensing components of the body (Day and Wilson, 2007; Dutia, 2012 {lab preparation}). Also the specific group(s) or sets of brainstem neurons (including those of the SubP) that are involved in oxygen sensing during hypoxia could be ascertained by using optogenetics procedure which involves the use of light to manipulate the neural activity of these functionally defined cells (Packer et al., 2013). Other techniques that could be utilised to further investigate specific key oxygen sensing neuronal populations within the central loci (brainstem) include electrophysiological methods and double/triple immunohistochemical procedures that target specific protein(s) that are expressed

only by an identified group of neurons in a region ( e.g the SubP subregion of the NTS).

Overall the results of this pilot study are encouraging and with more precise targeting of brainstem areas, using higher virus titres, fewer injection sites per animal and a simultaneous deletion of all the catecholaminergic cells in the brainstem and that of the carotid body, it is possible that better replication of the DKO phenotype could be obtained. However the high vascularisation of the AP and the neighbouring SubP region of the NTS, may make it difficult to deliver sufficient viral titres to achieve a 100% infection of SubP neurons but this challenge may be circumvented by the utilisation of some of the earlier mentioned techniques to further investigate and established the oxygen sensing function of the SubP neurons as well as that of the other identified brainstem regions. Interestingly further studies are presently underway to extend these pilot observations and the results from such studies will throw more light on the role of the SubP neurons as well as other brainstem catecholaminrgic cells in oxygen sensing.

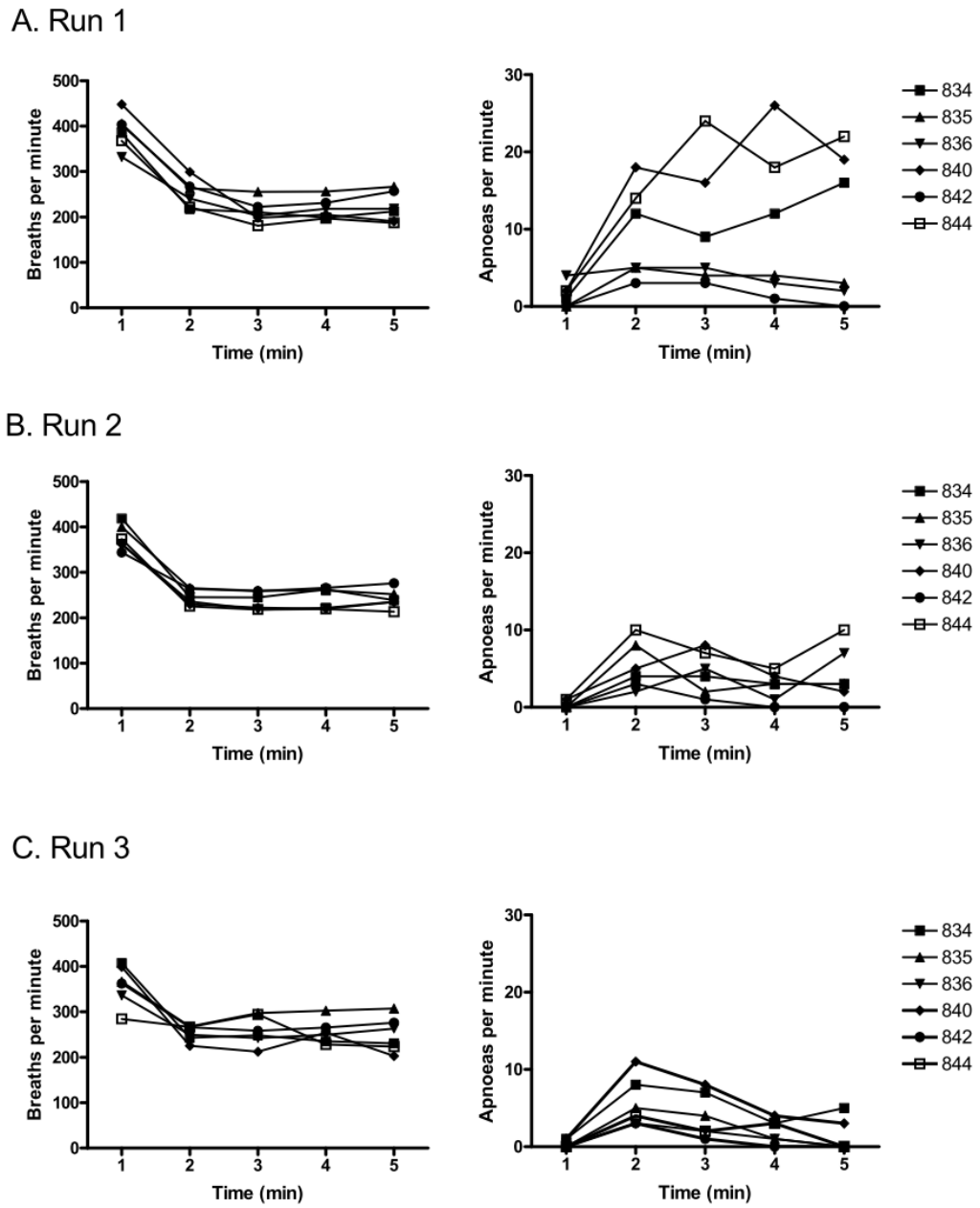


**Figure 4.1 : Respiratory responses to hypoxia in virus-injected mice.** The breathing rate (breaths/minute), left column, and the number of apnoeas/minute (right column) are shown for each animal in the pilot study. **A**, Run1 two weeks after virus injection. **B,** Run 2, 3 weeks post-injection and **C,** 3.5 weeks post-injection. Note the high incidence of apnoeas in three of the six animals in Run 1 (A, right) but which returned to normal subsequently.

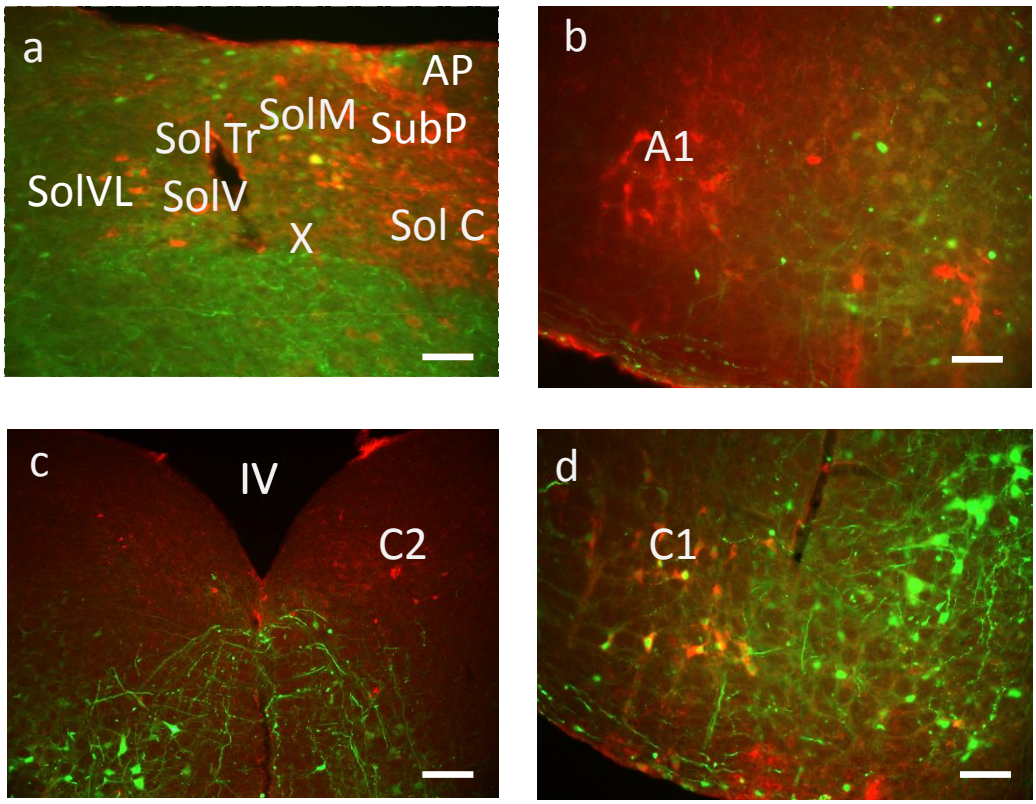


e

| Mouse 844 | TH+ve cells per 100 um² | | | |
|---|---|---|---|---|
| | Total | Virus(-) | Virus(+) | |
| | N | N | N | % Transfection |
| A2 | | | | |
| SubP | 10.6 | 6.1 | 4.6 | 43 |
| Medial | 10.0 | 3 | 7.0 | 70 |
| SolC | 9.3 | 3.7 | 5.7 | 61 |
| Ventral | 7.1 | 1.6 | 5.4 | 76 |
| Ventrolateral | 5.5 | 0.8 | 4.7 | 85 |
| A1 | 3.2 | 2.9 | 0.3 | *9* |
| C1 | 4.4 | 0.2 | 4.2 | 95 |
| C2 | 3.5 | 3.5 | 0 | *0* |

**Figure 4.2** : Immunohistochemistry of Cre- virus-injected transfection of brainstem catecholaminergic neurons in mouse 844. **(a**) shows co-localization of cre-virus (green)/ TH+ve neuron(red) in the different subdivisions of the NTS region, **(b)** the A1 region, **(c)** the C2 region and **(d)** the C1 region. **(e)** table, showing % transfection of each of these brainstem areas . Scale bars in (a), (b), (d) 20 µm, 40µm in (c).

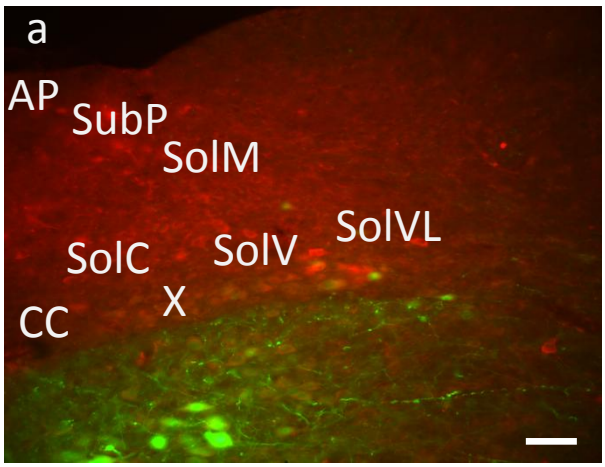


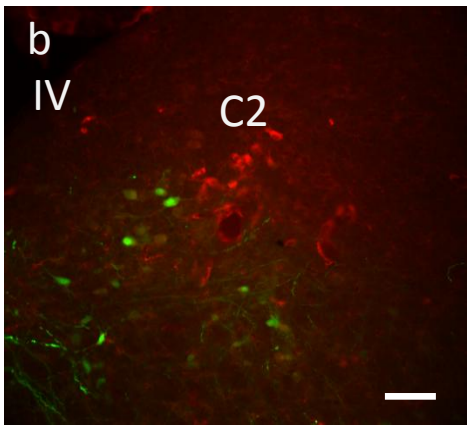


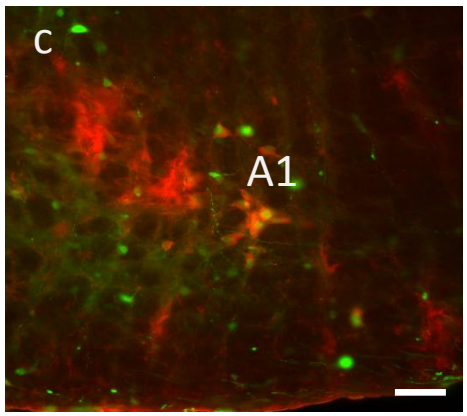


| Mouse 836 | TH+ve cells per 100 um² | | | |
|---|---|---|---|---|
| d | Total | Virus(-) | Virus(+) | |
| | N | N | N | % Transfection |
| A2 | | | | |
| SubP | 20.2 | 20.2 | 0 | 0 |
| Medial | 14.8 | 14.2 | 0.5 | 4 |
| SolC | 19.4 | 15.8 | 3.7 | 19 |
| Ventral | 20.6 | 13.7 | 6.9 | 33 |
| Ventrolateral | 18.3 | 12.5 | 5.8 | 32 |
| A1 | 7.1 | 3.1 | 4 | 56 |
| C1 | - | - | - | - |
| C2 | 5.1 | 5.1 | 0 | *0* |

**Figure 4.3** : Immunohistochemistry of Cre- virus transfection of brainstem catecholaminergic neurons in mouse 836. **(a**) shows co-localization of cre-virus (green)/ TH+ve neuron(red) mostly in the ventrolateral subdivision of the NTS region, **(b)** the C2 region, **(c)** the A1 region. **(d)** table, showing % transfection of different brainstem nuclei . Scale bars for (a), (b) and (c) 20 µm.

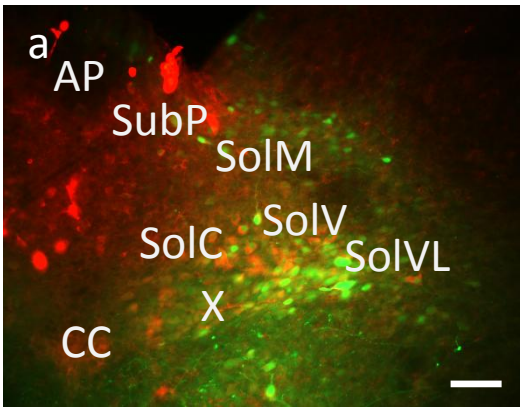


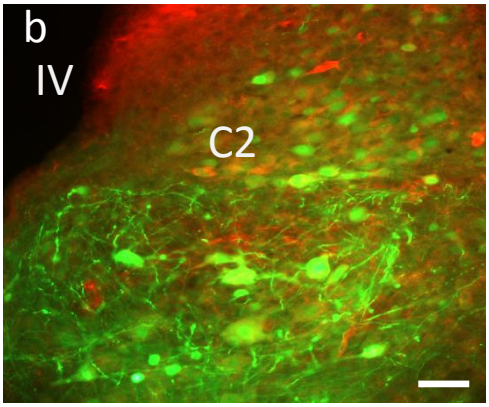


C

Mouse 834

| | TH+ve cells per 100 um² | | | |
|---|---|---|---|---|
| | Total | Virus(-) | Virus(++) | |
| | N | N | N | %Transfecoion |
| A2 | | | | |
| SubP | 6.8 | 4.4 | 2.4 | 35 |
| Medial | 7.9 | 0.5 | 7.4 | 94 |
| SolC | 7.6 | 0.3 | 7.3 | 96 |
| Ventral | 9.4 | 0.3 | 9.1 | 97 |
| Ventrolateral | 8.9 | 0.3 | 8.4 | 96 |
| A1 | - | - | - | - |
| C1 | - | - | - | - |
| C2 | 8.6 | 6 | 2.6 | *30* |

**Figure 4.4** : Immunohistochemistry of Cre- virus-injected transfection of brainstem catecholaminergic neurons in mouse 834. **(a**) shows co-localization of Cre-virus (green)/ TH+ve neuron(red) in different subdivisions of the NTS, **(b)** the C2 region, and **(c)** table, showing % transfection of different brainstem regions . Scale bars in (a) and (b), 20 µm.

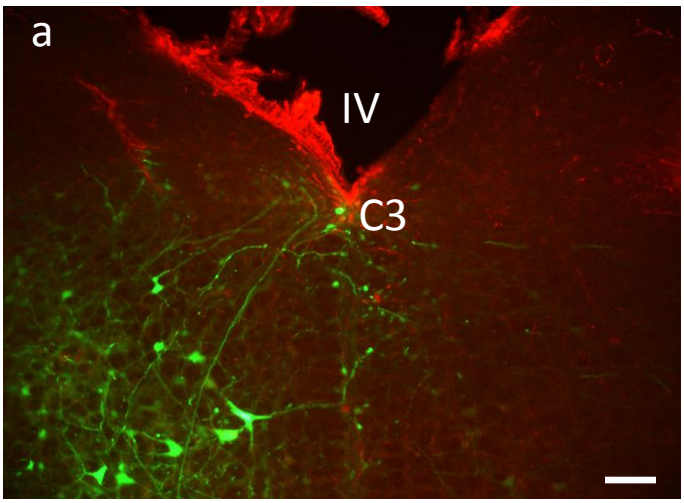


b

| Mouse 835 | TH+ve cells per 100 um² | | | |
|---|---|---|---|---|
| | Total | Virus(-) | Virus(+) | |
| | N | N | N | % Transfection |
| A2 | | | | |
| SubP | - | - | - | - |
| Medial | - | - | - | - |
| SolC | - | - | - | - |
| Ventral | - | - | - | - |
| Ventrolateral | - | - | - | - |
| A1 | - | - | - | - |
| C1 | - | - | - | - |
| C2 | - | - | - | - |
| C3 | 9.3 | 0.2 | 9.1 | 98 |

**Figure 4.5** : Immunohistochemistry of Cre- virus-injected transfection of C3 catecholaminergic neurons in mouse 835 **(a). (b)** table, showing % transfection of neurons observed in the different brainstem regions. Scale bar in (a), 20 µm .

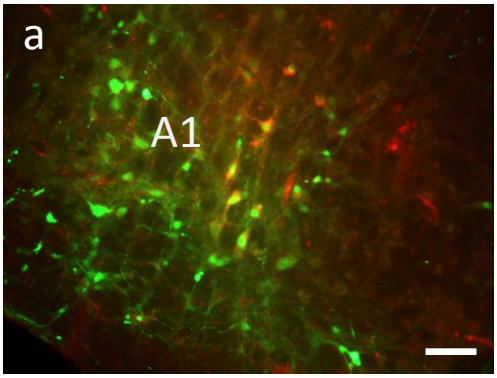


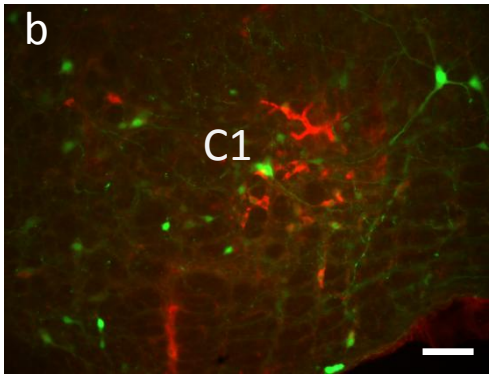


c

| Mouse 840 | TH+ve cells per 100 um² | | | |
|---|---|---|---|---|
| | Total | Virus(-) | Virus(+) | |
| | N | N | N | % Transfection |
| A2 | | | | |
| SubP | - | - | - | - |
| Medial | - | - | - | - |
| SolC | - | - | - | - |
| Ventral | - | - | - | - |
| Ventrolateral | - | - | - | - |
| A1 | 4.0 | 0.2 | 3.8 | 95 |
| C1 | 4.9 | 1 | 3.8 | 79 |
| C2 | - | - | - | - |

**Figure 4.6** : Immunohistochemistry of Cre- virus-injected transfection of brainstem catecholaminergic neurons in mouse 840. **(a**) and **(b)** show the A1 and C1 regions respectively. **(c)** table, showing % transfection of TH+ve cells by cre-virus in the different regions of the brainstem. Scale bars in (a) and (b), 20 µm.

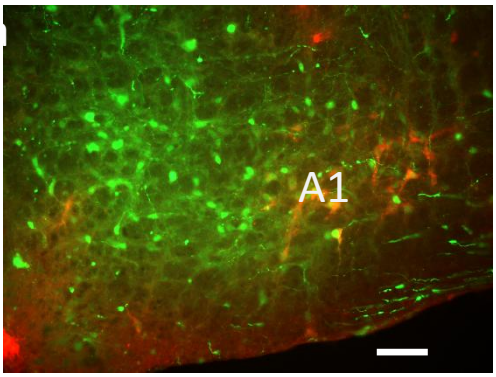


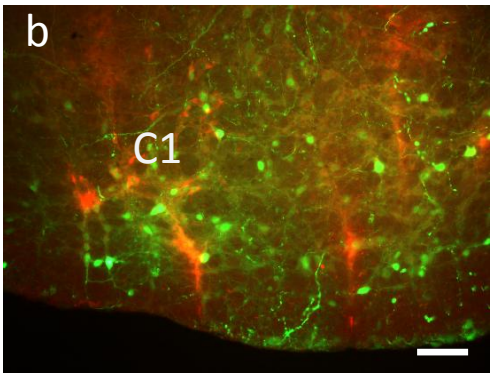


C

| Mouse 842 | TH+ve cells per 100 um² | | | |
|---|---|---|---|---|
| | Total | Virus(-) | Virus(+) | |
| | N | N | N | % Transfection |
| A2 | | | | |
| SubP | - | - | - | - |
| Medial | - | - | - | - |
| SolC | - | - | - | - |
| Ventral | - | - | - | - |
| Ventrolateral | - | - | - | - |
| A1 | 4.1 | 0.6 | 3.5 | 85 |
| C1 | 4.7 | 0 | 4.6 | 100 |
| C2 | - | - | - | - |

**Figure 4.7** : Immunohistochemistry of Cre-virus-injected transfection of brainstem catecholaminergic neurons in mouse 840. **(a**) and **(b)** show the A1 and C1 regions respectively, **(c)** table, showing % transfection of TH+ve cells by Cre-virus in the different brainstem regions of interest. Scale bars for (a) and (b), 20 µm.

# Chapter Five

## General Discussion

The work in this thesis has shown that conditional deletion of the α1 and α2 isoforms of the α-catalytic subunit of AMPK in catecholaminergic (TH+ve) cells in mice resulted in marked abnormalities in their ventilatory response to hypoxia. The observed abnormalities included hypoventilation in association with prolonged and frequent apnoeas, confirming the earlier findings of Mahmoud et al. (2015a, b).

Investigation into the possible physiological basis of the above respiratory abnormalities revealed that, in spite of the fact that the response of the carotid body afferents to hypoxia in these mice is normal (Mahmoud et al 2015b), there was a significant decrease in the activation of specific catecholaminegic neuronal populations in the dorsal brainstem that are known to be involved in the control of breathing (Results, Chapter 2). Prominent reductions in activation, indicated by c-Fos expression, were seen in the A2 noradrenergic neurons in the SubP region of the nucleus tractus solitarius (NTS), and in the C2 adrenergic neurons of the dorsal brainstem. This finding implies that AMPK in these catecholaminergic neurons has an important role in regulating their responsiveness to the afferent excitatory inputs they receive from the carotid sinus nerve, so that in the absence of AMPK these neurons fail to respond adequately to the otherwise normal carotid nerve afferent firing.

The NTS is a critical integrating centre which mediates chemosensory afferent information from the peripheral carotid bodies to the ventral brainstem areas that are involved in the regulation of breathing. Catecholaminergic neurons in the brainstem play a fundamentally important role in the control of respiration, as evidenced by the profound and ultimately fatal respiratory arrhythmias and breath-holding that result from the loss of these neurons in, for example, Rett syndrome (Viemari et al., 2006; Stettner et al., 2007; Smith et al., 2013). The hypoventilation and apnoeas observed in AMPK-null mice may therefore be causally linked to the reduced response and decreased activation of the dorsal brainstem catecholaminergic neurons during hypoxia. Thus, while in Rett syndrome the irreversible loss of the catecholaminergic neurons causes profoundly disordered breathing, the reduced activation of the catecholaminergic neurons in AMPK-null mice may cause the less profound signs of hypoventilation and prolonged apnoeas during hypoxia, as first observed by Mahmoud (2015a) and also in this work.

Indeed the present work identifies for first time that the A2 catecholaminergic neurons in the SubP region of the NTS, in particular, may be crucial in mediating the hypoxia-induced hyperventilatory response in normal animals. Of all the brainstem catecholaminergic neuronal groups, the most marked reduction in activation was observed in this region, along with a lesser effect in C2 region, in AMPK-null mice after exposure to hypoxia. By contrast, catecholaminergic neurons in the other regions of the dorsal brainstem showed either no change or an

increase in activation (Figure 2.11). As discussed in Chapter 2, the SubP neurons lie in close proximity to the highly vascularised area postrema (AP), and share an intimate specialised blood supply with it (Fodor et al., 2007; McGinnis et al., 2013), putting them in a very suitable position to respond to changes in systemic $pO_2$.

The present results, which show that a markedly reduced activation of the SubP neurons is associated with the hypoxic hypoventilation and prolonged apnoeas in AMPK-null mice, indicate that the deletion of AMPK in these neurons reduces or prevents their normal activation by hypoxia. As suggested in Figure 2.12, the normal hypoxia-induced hyperventilatory response therefore appears to require both the normal carotid body afferent excitatory input to the NTS neurons, and simultaneously a local, AMPK-dependent response to the hypoxic stimulus. In AMPK-null mice the failure of the local hypoxic response after AMPK deletion, results in a reduced activation of these cells and may thus explain the respiratory abnormalities observed in these animals.

The convergence of the carotid body afferent inputs and the local hypoxic AMPK-dependent response may occur in the same neuronal population (likely SubP neurons), or alternatively this may involve efferent projections from the SubP neurons to other regions of the NTS which receive the excitatory inputs from the carotid body afferents. Presently little is known of the micro-circuitry of the SubP and the other sub-regions of the NTS, and the corresponding areas of termination of the carotid body afferent axons.

Interestingly the result from this work synchronises and aligns well with earlier reports from functional magnetic resonance imaging studies (fMRI) in the brain of anesthetised AMPK mutant mice during hypoxia (Mahmoud et al., 2015b). From their work they showed that upon exposure to hypoxia (8% $O_2$) AMPK DKO mice brains in contrast to the control DFlox mice displayed reduction in $O_2$-consumption (as indicated by a decrease in the BOLD signal) in two –well defined dorsal (DAR) and ventral (VAR) active regions of the brainstem (see Figure 5.1; Mahmoud et al., 2015b). The dorsal region was shown to be consistent with the caudal subdivisions of the NTS containing A2 noradrenergic neurons as well as the C2 region which comprises adrenergic neurons (areas which showed reduction in c-fos expression in this work) both of which receive sensory inputs from the carotid body while the ventral active area equally aligns well with the A1/C1 catecholaminergic cells of the ventral medulla (notice in Figure 2.10 ; the decrease in c-fos expression in A1 cells in this work) that receives afferent chemosensory information from the carotid body relayed via the NTS (Figure 5.1; Mahmoud et al., 2015b). Therefore the result from this work corroborating with this earlier study allows for a proper identification of the specific areas or loci of the brainstem chemosensory circuit that might have been interrupted during hypoxia by the deletion of AMPK resulting in the respiratory phenotype that was seen in these mice. Furthermore it enhances the understanding of the role of AMPK in mediating the oxygen sensing function of these identified catecholaminegic brainstem neurons during the period of hypoxic stress.

In the light of the above, Mahmoud et al. (2015b) have argued that the hypoventilatory response observed in AMPK DKO mice during hypoxia may be due to failure in central integration and transduction of chemosensory inputs from the carotid body as a results of the inability of these brainstem catecholaminergic neurons to respond appropriately to metabolic stresses because of the lack of AMPK. A postulated new mechanism of the integration by AMPK at the level of the brainstem of the local and metabolic stresses during hypoxia is as shown in Figure 5.2 (Mahmoud et al., 2015b).

The identification of the SubP and to a lesser extent the C2 regions of the dorsal brainstem as key areas in which a local, AMPK-dependent response to hypoxia is required for normal breathing, is likely to be important in understanding the mechanisms underlying some breathing disorders in humans. In particular, breathing disorders during sleep (sleep apnoeas) are a significant health concern. While the majority of sleep apnoeas are believed to be obstructive (due to the muscles and soft tissues in the throat collapsing sufficiently during sleep to cause a blockage of the airway), some sleep apnoeas have also a central origin, in a reduced or interrupted drive to breathe (central sleep apneas, or mixed complex apneas). Central sleep apnoeas constitute about 11% of the total apnoeas (both obstructive and non-obstructive) that are experienced by the adult population, while in children and infants its prevalence rises to about 40 - 90% (Nakamura and Kuwaki, 2003). Presently the mechanisms involved in central sleep apnoeas are largely unknown. The present results, which for the first time demonstrate that an

AMPK-dependent hypoxic response of dorsal NTS (SubP and C2) neurons is necessary for the normal respiratory modulation, suggest a potential brainstem mechanism that may be involved in central sleep apnoeas. Thus, disorders in AMPK regulation or function in dorsal NTS catecholaminergic neurons may precipitate apnoeas and hypoventilation in patients with mild obstructive apnoeas, where partial blockage of the airway and consequent hypoxia induces the abnormal respiratory phenotype observed in AMPK-null animals in this work. The localisation of the SubP and C2 regions of the NTS as potentially key regions where central sleep apnoeas could arise, offers new avenues for investigation of the underlying mechanisms, and also in the longer term the potential for targeted diagnostic and therapeutic interventions based on an understanding of the role of AMPK in mediating the response to hypoxia in these neurons.

Interestingly, comparison of the activation of SubP A2 neurons in AMPK-null animals with that in AMPK α2-null animals, showed that the marked reduction in activation was observed only in after the deletion of both α1 and α2 isoforms, while the activation of these neurons in AMPK α2-null animals was normal (Figure 2.11). This suggests that the AMPK α1 isoform has a particularly important role in SubP neurons, while loss of the AMPK α2 isoform has no effect. This could be explained for example by the selective expression of only the α1 isoform in the SubP neurons, so that deletion of the AMPK α2 isoform in the AMPK α2-null animals does not have any effect on these cells. By contrast, in the other regions of the NTS deletion of the AMPK α2 isoform in the AMPK α2-null animals results

in a significant hyperplasia of the catecholaminergic neurons compared to both the normal and AMPK-null animals (Figure 2.10). There is no hyperplasia in the SubP region when the AMPK α2-null mice are compared to the AMPK DKO, again suggesting that the AMPK α2 isoform may not be expressed in these neurons. At present there is no information about the relative expressions of the different α1 and α2 isoforms in these regions of the brainstem. In order to fully understand the role played by AMPK in mediating the local hypoxic response in these neurons, it will be important to clarify the expression profile of each of these isoforms in the different brainstem areas.

The hyperplasia of catecholaminergic neurons in the AMPK α2-null animals is in line with the known function of AMPK in inhibiting cell proliferation, both in non-malignant and tumor cells (e.g hepatoma). Currently AMPK is postulated to be a plausible therapeutic target for proliferative disorders such as atherosclerosis and cancers such as glioblastoma, melanoma and advanced prostate cancer (Motoshima, et al., 2006), because of its role in regulating cell proliferation. In the present work, marked hyperplasia was observed in the dorsal brainstem NTS neurons as well as those of the ventral A1 region (but not in the other catecholaminergic cell groups), specifically after deletion of the AMPK α2 isoform (Figure 2.10). Indeed the hyperplasia in AMPK α2-null animals was greater than in AMPK-null (DKO) animals. This is an interesting finding as it suggests that the selective deletion of the AMPK α2 isoform, presumably leaving intact the selective expression of only the AMPK α1 isoform, appears to simulate the hyperplasia in

the dorsal NTS neurons. Thus the cell proliferation stimulated by AMPK appears to involve the AMPK α1 isoform, while the AMPK α2 isoform, when it is present, appears to inhibit cell proliferation and prevents hyperplasia. In addition, it is not clear why the hyperplasia is observed in the noradrenergic cell groups (A1and A2, but not in adrenergic cell groups (C1 and C2) (Figure 2.10). As noted above the expression profile of these isoforms in the brainstem neurons is presently not known, so the interpretation of the present findings remains speculative. Understanding the possible different roles of the two AMPK isoforms however, may be an important step in determining how they regulate cell proliferation in central neurons.

In an attempt to develop a methodology to further investigate the role of AMPK and its selective targeted deletion in specific areas of the brainstem, the pilot study was carried out in the work to use a virus vector injected into the target areas to produce the localised deletion of AMPK in these areas (Chapter 4). In these initial experiments, a number of injections of virus were made into either the dorsal, ventral or both dorsal and ventral areas of the brainstem, in order to produce a widespread deletion of AMPK and determine if the respiratory phenotype of prolonged apnoeas and hypoventilation could be produced, similar to that seen in the AMPK-null animals. In the event it proved difficult to achieve consistently high transfection rates of the catecholaminergic neurons in the targeted areas, and the respiratory phenotype of the AMPK-null mice was not observed in any of the injected animals. Given the suggested crucial importance of

the dorsal brainstem SubP and C2 neurons in mediating the normal ventilatory response to hypoxia, as discussed above, it was of particular interest to achieve a high transfection rate and AMPK deletion in these specific areas. However, perhaps because of the high vascularity of the AP region in close proximity to the SubP neurons, this was not achieved in any of the animals, even those that received virus injections targeted towards the dorsal brainstem. This could explain why the respiratory phenotype of the AMPK-null animals was not observed in any of the injected animals, if the knock-out of AMPK in SubP neurons is essential for the effects to be observed. Interestingly, in animals that received ventrally-targeted injections, high transfection rates were achieved in the A1 and C1 ventral catecholaminergic neuron groups, but this did not result in the prolonged apnoeas and hypoxic-hypoventilation seen in AMPK-null animals (Chapter 4). This supports the notion that it is the deletion of AMPK in the dorsal NTS neurons, particularly in the SubP region, that results in the abnormal hypoxic ventilatory response, while AMPK deletion in the ventral catecholaminergic cell groups has no effect on the breathing pattern.

In contrast to the effects of AMPK deletion observed in the central catecholaminergic neurons, the limited results obtained in this work in the peripheral carotid bodies (Chapter 3) suggest that in AMPK-null animals there is a reduction in the number of TH+ve catecholaminergic cells compared to normal. Unfortunately the number of animals from which useful data was obtained is too small to allow a firm conclusion to be made. Indeed it is likely that, because of the

dispersed nature of the carotid bodies in the mouse, the observed result may be explained by experimental bias in selecting the clusters of TH+ve cells that were counted in the histological sections. If indeed there is a loss of peripheral carotid body cells after AMPK deletion in AMPK-null mice, it will be interesting to identify the role of AMPK in these cells and contrast this with the better-known effects of AMPK in regulating cell proliferation, as discussed above. Thus in a range of tissues, including the dorsal NTS neurons as observed in this work, AMPK inhibition or deletion leads to the stimulation of cell proliferation, while in the peripheral carotid bodies there would appear to be the opposite effect. Furthermore, it will also be interesting to determine how the afferent discharge and hypoxia-evoked firing of the carotid body afferents recorded in the carotid sinus nerve *in vitro* remains normal in AMPK-null animals (Mahmoud et al 2015b), if there is indeed a loss of catecholaminergic cells in the carotid bodies. Thus for the moment the question of the effects of AMPK deletion on the catecholaminergic cells in the peripheral carotid bodies remains open, and awaits further investigation.

Overall the findings of this work contribute to the understanding of the role of AMPK, a key regulator of energy metabolism in cells and tissues, in the control of respiration during hypoxia. The demonstration of the importance of AMPK in dorsal brainstem neurons in mediating the response to hypoxia, particularly in the A2 SubP and the C2 regions, indicates for the first time a specific central site of action of AMPK in central respiratory control. These findings may be of relevance

in further understanding the mechanisms involved in central disorders of breathing, as in central or mixed complex sleep apnoeas, and may offer in the longer term opportunities to develop therapeutic interventions in managing such disorders.

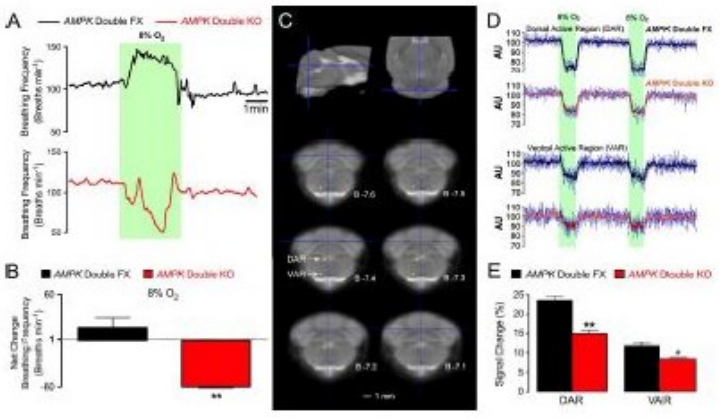


**Figure 5.1:** Functional magnetic imaging demonstrating that AMPK deletion inhibits activation by hypoxia of the dorsal and ventral regions of the brainstem. (A) Shows records of frequency (breaths/min) versus time during hypoxia (8% $O_2$) for anaesthetised AMPK DFlox (black, n=6) and AMPK DKO (red, n=6) mice. (B) Bar charts showing the mean±SEM for change in breathing frequency during hypoxia; $p<0.01$. (C) Dorsal (DAR) and ventral (VAR) active regions of the brainstem that showed significantly lower signal change ($p< 0.005$) during hypoxia in DKO mice compared to DFlox controls. (D) Variability of signal time courses for DAR and VAR in blue for each individual mouse ( same mice for A lower panel) overlaid on mean signal for DFox mice (black) and DKO mice (red line). AU = arbitrary units. (E) Mean±SEM percentage signal changes for DAR and VAR during hypoxia in DFlox versus DKO mice (same mice as for A, lower panel).*= $p<0.05$; **=$p<0.01$ (Mahmoud et al.,2015b).

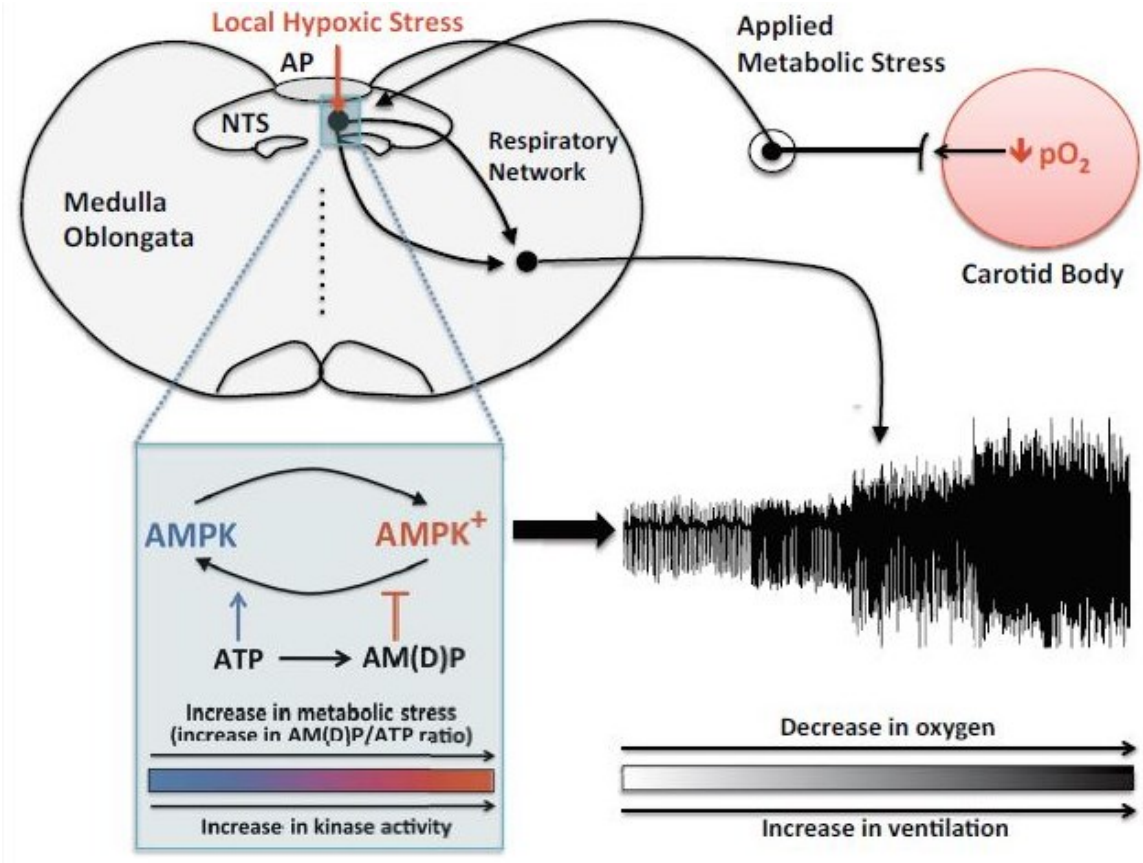


**Figure 5.2. Figure legend on the next page**

**(**Mahmoud et al., 2015b)

**Figure 5.2.** A schematic diagram showing the new hypothesis on the integration by AMPK of local and applied metabolic stresses during hypoxia. AMPK is activated by increase in AM(D)P/ATP ratio as a result of local hypoxic stress within the NTS (decreased ATP supply) alongside with applied metabolic stress (increased ATP usage) and /or increased cytoplasmic $Ca^{2+}$ (not shown) delivered through sensory input from the carotid bodies which is in turn relayed to the ventrolateral A1 neurons . The sensory input and brainstem hypoxia could thus jointly determine the set point at which the AMPK and invariably the brainstem respiratory network are activated during hypoxia. AMPK thereafter modulates cellular metabolism, ion channels, neuronal firing frequency and /or neurotransmitter release with a resultant facilatatory effect on efferent output leading to an increased drive to breathe in a manner that could be impaired or augmented by appropriate control of AMPK expression (Mahmoud et al., 2015b).

## Reference list


Ahmed BY, Chakravarthy S, Eggers R, Hermens W, Zhang JY, et al. 2004. Efficient delivery of Cre-recombinase to neurons in vivo and stable transduction of neurons using adeno-associated and lentiviral vectors. *BMC Neuroscience* 5:4. doi:10.1186/1471-2202-5-4

Alheid GF, Jiao W, McCrimmon DR. 2011. Caudal nuclei of the rat nucleus of the solitary tract differentially innervate respiratory compartments within the ventrolateral medulla. *Neuroscience* 190: 207-27

Andersson U, Filipsson K, Abbott CR, Woods A, Smith K, et al. 2004. AMP-activated protein kinase plays a role in the control of food intake. *Journal of Biological Chemistry* 279: 12005-08

Andresen MC, Mendelowitz D. 1996. Sensory afferent neurotransmission in caudal nucleus tractus solitarius - Common denominators. *Chemical Senses* 21(3): 387-95

Aschauer DF, Kreuz S, Rumpel S. 2013. Analysis of Transduction Efficiency, Tropism and Axonal Transport of AAV Serotypes 1, 2, 5, 6, 8 and 9 in the Mouse Brain. *Plos One* 8, e76310. doi:10.1371/journal.pone.0076310

Barnes BR, Marklund S, Steiler TL, Walter M, Hjalm G, et al. 2004. The 5 '-AMP-activated protein kinase gamma 3 isoform has a key role in carbohydrate and lipid metabolism in glycolytic skeletal muscle. *Journal of Biological Chemistry* 279(37): 38441-47

Bateman A. 1997. The structure of a domain common to archaebacteria and the homocystinuria disease protein. *Trends in Biochemical Sciences* 22(1): 12-13

Bathina CS, Rajulapati A, Franzke M, Yamamoto K, Cunningham JT, Mifflin S. 2013. Knockdown of tyrosine hydroxylase in the nucleus of the solitary tract reduces elevated blood pressure during chronic intermittent hypoxia. *American Journal of Physiology-Regulatory Integrative and Comparative Physiology* 305(9): R1031-R39

Bigham AW, Julian CG, Wilson MJ, Vargas E, Browne VA, Shriver MD, Moore LG. 2014. Maternal PRKAA1 and EDNRA genotypes are associated with birth weight, and PRKAA1 with uterine artery diameter and metabolic homeostasis at high altitude. *Physiological Genomics*, 46(18):687-697

Blanco Martinez de Morentin P, Gonzalez CR, Saha AK, Martins L, Dieguez C, et al. 2011. Hypothalamic AMP-activated protein kinase as a mediator of whole body energy balance. *Reviews in endocrine & metabolic disorders* 12(3): 127-40

Blomer U, Naldini L, Kafri T, Trono D, Verma IM, Gage FH. 1997. Highly efficient and sustained gene transfer in adult neurons with a lentivirus vector. *Journal of Virology* 71(9): 6641-49

Braga VA, Soriano RN, Braccialli AL, de Paula PM, Bonagamba LGH, et al. 2007. Involvement of L-glutamate and ATP in the neurotransmission of the sympathoexcitatory component of the chemoreflex in the commissural nucleus tractus solitarii of awake rats and in the working heart-brainstem preparation. *Journal of Physiology-London* 581(3): 1129-45. doi: 10.1113/jphysiol.2007.129031

Broekman MLD, Comer LA, Hyman BT, Siena-Esteves M. 2006. Adeno-associated virus vectors serotyped with AAV8 capsid are more efficient than AAV-1 or-2 serotypes for widespread gene delivery to the neonatal mouse brain. *Neuroscience* 138(2): 501-10.

Brooks AI, Stein CS, Hughes SM, Heth J, McCray PM, et al. 2002. Functional correction of established central nervous system deficits in an animal model of lysosomal storage disease with feline immunodeficiency virus-based vectors. *Proceedings of the National Academy of Sciences of the United States of America* 99(9): 6216-21. doi: 10.1073/pnas.082011999

Buckler KJ, Vaughanjones RD. 1994. Effects of hypoxia on membrane-potential and intracellular calcium in rat neonatal carotid-body type-I cells. *Journal of Physiology-London* 476(3): 423-28

Buller KM, Wixey JA, Pathipati P, Carty M, Colditz PB, et al. 2008. Selective losses of brainstem catecholamine neurons after hypoxia-ischemia in the immature rat pup. *Pediatric Research* 63(4): 364-69. doi:10.1203/PDR.0b013e3181659774

Canto C, Auwerx J. 2010. AMP-activated protein kinase and its downstream transcriptional pathways. *Cellular and Molecular Life Sciences*, 67(20):3407-3423

Carling D. 2004. The AMP-activated protein kinase cascade - a unifying system for energy control. *Trends in Biochemical Sciences* 29(1): 18-24. doi: http://dx.doi.org/10.1016/j.tibs.2003.11.005

Carling D, Mayer FV, Sanders MJ, Gamblin SJ. 2011. AMP-activated protein kinase: nature's energy sensor. *Nature Chemical Biology* 7(8): 512-18 doi:10.1038/nchembio.610

Carling D, Sanders MJ, Woods A. 2008. The regulation of AMP-activated protein kinase by upstream kinases. *International Journal of Obesity* 32(4): S55-S59 doi:10.1038/ijo.2008.124

Carling D, Thornton C, Woods A, Sanders MJ. 2012. AMP-activated protein kinase: new regulation, new roles? *Biochemical Journal* 445(1): 11-27. doi: 10.1042/BJ20120546

Celenza JL, Carlson M. 1986. A yeast gene that is essential for release from glucose repression encodes a protein kinase. *Science* 233(4759): 1175-80. doi: 10.1126/science.3526554

Chakrabarty P, Rosario A, Cruz P, Siemienski Z, Ceballos-Diaz C, et al. 2013. Capsid Serotype and Timing of Injection Determines AAV Transduction in the Neonatal Mice Brain. *Plos One* 8(6): e67680-e67680. doi: 10.1371/journal.pone.0067680

Chandrashekran A, Sarkar R, Thrasher A, Fraser SE, Dibb N, et al. 2014. Efficient generation of transgenic mice by lentivirus-mediated modification of spermatozoa. *Faseb Journal* 28(2): 569-76. doi: 10.1096/fj.13-233999

Cheung PCF, Salt IP, Davies SP, Hardie DG, Carling D. 2000. Characterization of AMP-activated protein kinase gamma-subunit isoforms and their role in AMP binding. *Biochemical Journal* 346(3): 659-69. doi: 10.1042/bj3460659

Connolly JB. 2002. Lentiviruses in gene therapy clinical research. *Gene Therapy* 9(24): 1730-34. doi: 10.1038/sj.gt.3301893

Corton JM, Gillespie JG, Hawley SA, Hardie DG. 1995. 5-aminoimidazole-4-carboxamide ribonucleoside - a specific method for activating amp-activated protein-kinase in intact-cells. *European Journal of Biochemistry* 229(2): 558-65

Cruz JdC, Bonagamba LGH, Stern JE, Machado BH. 2010. Fos expression in the NTS in response to peripheral chemoreflex activation in awake rats. *Autonomic Neuroscience-Basic & Clinical* 152(1-2): 27-34. doi:10.1016/j.autneu.2009.08.016

Davies SP, Helps NR, Cohen PTW, Hardie DG. 1995. 5'-AMP inhibits dephosphorylation, as well as promoting phosphorylation, of the AMP-

activated protein kinase. Studies using bacterially expressed human protein phosphatase-2C alpha and native bovine protein phosphatase-2A(c). *Febs Letters* 377(3): 421-25. doi:10.1016/0014-5793(95)01368-7

Day TA, Wilson RJA. 2007. Brainstem P-CO2 modulates phrenic responses to specific carotid body hypoxia in an in situ dual perfused rat preparation. *Journal of Physiology-London*, 578(3):843-857

Daya S, Berns KI. 2008. Gene Therapy Using Adeno-Associated Virus Vectors. *Clinical Microbiology Reviews* 21(4): 583-93.doi: 10.1128/CMR.00008-08

Dean JB, Nattie EE. 2010. Central CO2 chemoreception in cardiorespiratory control. *Journal of Applied Physiology* 108(4): 976-78. doi: 10.1152/japplphysiol.00133.2010.

De Caro R, Macchi V, Sfriso MM, Porzionato A. 2013. Structural and neurochemical changes in the maturation of the carotid body. *Respiratory Physiology & Neurobiology* 185(1): 9-19. do**i:** 10.1016/j.resp.2012.06.012

DeLorme MP, Moss OR. 2002. Pulmonary function assessment by whole-body plethysmography in restrained versus unrestrained mice. *Journal of Pharmacological and Toxicological Methods* 47(1): 1-10. doi:10.1016/S1056-8719(02)00191-0

Deng C. 2012. The use of cre-loxP technology and inducible systems to generate mouse models of cancer. In Genetically engineered mice for cancer research: design, analysis, pathways, validation and pre-clinical testing edited by Green JE &Reid TH. Springer Science + Media, LLC. New York: 17-36. dio:10:10071/978-0-387-69805-2_2

Dutia MB. 2012. A working heart-brainstem preparation (Prof. Dutia lab, Centre for Integrative Physiology, University of Edinburgh)

Emerling BM, Weinberg F, Snyder C, Burgess Z, Mutlu GM, et al. 2009. Hypoxic activation of AMPK is dependent on mitochondrial ROS but independent of an increase in AMP/ATP ratio. *Free Radical Biology and Medicine* 46(10): 1386-91. doi:10.1016/j.freeradbiomed.2009.02.019

Erickson JT, Millhorn DE. 1994. Hypoxia and electrical-stimulation of the carotid-sinus nerve induce fos-like immunoreactivity within catecholaminergic and serotoninergic neurons of the rat brain-stem. *Journal of Comparative Neurology* 348(2): 161-82. doi:10.1002/cne.903480202

Evans AM. 2006. AMP-activated protein kinase and the regulation of Ca2+ signalling in O-2-sensing cells. *Journal of Physiology-London* 574(1): 113-23. doi:10.1113/jphysiol.2006.108381

Evans AM, Hardie DG, Peers C, Wyatt CN, Viollet B, et al. 2009. Ion Channel Regulation by AMPK The Route of Hypoxia-Response Coupling in the Carotid Body and Pulmonary Artery. Hypoxia and Consequences from Molecule to Malady. *Annual New York Acadamy of Sciences* 1177: 89-100 doi: 10.1111/j.1749-6632.2009.05041.x.

Evans AM, Mustard KJW, Wyatt CN, Peers C, Dipp M, et al. 2005. Does AMP-activated protein kinase couple inhibition of mitochondrial oxidative phosphorylation by hypoxia to calcium signaling in O-2-sensing cells? *Journal of Biological Chemistry* 280(50): 41504-11. doi: 10.1074/jbc.M510040200

Fisslthaler B, Fleming I. 2009. Activation and Signaling by the AMP-Activated Protein Kinase in Endothelial Cells. *Circulation Research* 105: 114-27

Flotte TR, Afione SA, Conrad C, McGrath SA, Solow R, et al. 1993. Stable in-vivo expression of the cystic-fibrosis transmembrane conductance regulator with an adeno-associated virus vector. *Proceedings of the National Academy of Sciences of the United States of America* 90(22): 10613-17

Fodor M, Palkovits M, Gallatz K. 2007. Fine structure of the area subpostrema in rat. Open gate for the medullary autonomic centers. *Ideggyogyaszati szemle* 60(3-4): 83-8

Frederich M, O'Rourke MR, Furey NB, Jost JA. 2009. AMP-activated protein kinase (AMPK) in the rock crab, *Cancer irroratus*: an early indicator of temperature stress. Journal of Experimental Biology 212 (5): 722-30. doi: 10.1242/jeb.021998

Fryer LGD, Carling D. 2005. AMP-activated protein kinase and the metabolic syndrome. *Biochemical Society Transactions* 33(2): 362-66

Furuya WI, Bassi M, Menani JV, Colombari E, Zoccal DB, Colombari DSA. 2014. Differential modulation of sympathetic and respiratory activities by cholinergic mechanisms in the nucleus of the solitary tract in rats. *Experimental Physiology* 99(5): 743-58. doi: 10.1113/expphysiol.2013.07679

Gao YJ, Ji RR.2009. c-Fos and pERK, which is a better marker for neuronal activation and central sensitization after noxious stimulation and tissue injury? Open Pain Journal 1(2):11-17. doi:10.2174/1876386300902010011

Garcia AJ, III, Zanella S, Koch H, Doi A, Ramirez J-M. 2011. Networks within networks: The neuronal control of breathing. Progress in Brain Research 188: 31-50. doi:10.1016/B978-0-444-53825-3.00008-5

Garcia-Gil M, Pesi R, Perna S, Allegrini S, Giannecchini M, et al. 2003. 5 '-aminoimidazole-4-carboxamide riboside induces apoptosis in human neuroblastoma cells. *Neuroscience* 117(4): 811-20. doi:10.1016/S0306-4522(02)00836-9

Gaveriaux-Ruff C, Kieffer BL. 2007. Conditional gene targeting in the mouse nervous system: Insights into brain function and diseases. *Pharmacology & Therapeutics* 113(3): 619-34. doi:10.1016/j.pharmthera.2006.12.003

Glaab T, Taube C, Braun A, Mitzner W. 2007. Invasive and noninvasive methods for studying pulmonary function in mice. *Respiratory Research* 8:63

Goldring MB, Goldring SR. 1991. CYTOKINES AND CELL GROWTH CONTROL. *Critical Reviews in Eukaryotic Gene Expression*, 1(4):301-326

Gordon JW, Scangos GA, Plotkin DJ, Barbosa JA, Ruddle FH. 1980. Genetic-transformation of mouse embryos by micro-injection of purified DNA. *Proceedings of the National Academy of Sciences of the United States of America-Biological Sciences* 77(12): 7380-84

Greenberg HE, Sica AL, Scharf SM, Ruggiero DA. 1999. Expression of c-fos in the rat brainstem after chronic intermittent hypoxia. *Brain Research* 816(2): 638-45. doi:10.1016/S0006-8993(98)01222-0

Gu H, Marth JD, Orban PC, Mossmann H, Rajewsky K. 1994. Deletion of a DNA-polymerase-beta gene segment in T-cells using cell-type-specific gene targeting. *Science* 265(5168): 103-06. doi: 10.1126/science.8016642

Guyenet PG, Stornetta RL, Bochorishvili G, DePuy SD, Burke PGR, Abbott SBG. 2013. C1 neurons: the body's EMTs. *American Journal of Physiology-Regulatory Integrative and Comparative Physiology* 305(3): R187-R204. doi: 10.1152/ajpregu.00054.2013

Han F, Zhang YF, Li YQ. 2003. Fos expression in tyrosine hydroxylase-containing neurons in rat brainstem after visceral noxious stimulation: an

immunohistochemical study. *World Journal of Gastroenterology* 9(5): 1045-50

Hardie DG. 2004. AMP-activated protein kinase: the guardian of cardiac energy status. *Journal of Clinical Investigation* 114(4): 465-68. doi: 10.1172/JCI200422683

Hardie DG. 2011. Signal transduction: How cells sense energy. *Nature* 472(7342): 176-77. doi:10.1038/472176a

Hardie DG. 2013. AMPK: A Target for Drugs and Natural Products With Effects on Both Diabetes and Cancer. *Diabetes* 62(7): 2164-72. doi: 10.2337/db13-0368

Hardie DG, Carling D, Carlson M. 1998. The AMP-activated/SNF1 protein kinase subfamily: Metabolic sensors of the eukaryotic cell? *Annual Review of Biochemistry* 67: 821-55. doi: 10.1146/annurev.biochem.67.1.821

Hardie DG, Carling D, Halford N. 1994. Roles of the SNf1/Rkin1/AMP-activated protein kinase family in the response to environmental and nutritional stress. *Seminars in Cell Biology* 5(6): 409-16. doi:10.1006/scel.1994.1048

Hardie DG, Ross FA, Hawley SA. 2012. AMPK: a nutrient and energy sensor that maintains energy homeostasis. *Nature Reviews Molecular Cell Biology* 13(4): 251-62. doi**:** 10.1038/nrm3311

Hardie DG, Sakamoto K. 2006. AMPK: A key sensor of fuel and energy status in skeletal muscle. *Physiology* 21: 48-60. doi**:** 10.1152/physiol.00044.2005

Hardie DG, Salt IP, Hawley SA, Davies SP. 1999. AMP-activated protein kinase: an ultrasensitive system for monitoring cellular energy charge. *Biochemical Journal* 338(3): 717-22. doi:10.1042/0264-6021:3380717

Hardie DG, Scott JW, Pan DA, Hudson ER. 2003. Management of cellular energy by the AMP-activated protein kinase system. *Febs Letters* 546(1): 113-20. doi**:** 10.1016/S0014-5793(03)00560-X

Haruyama N, Cho A, Kulkarni AB. 2009. Overview: engineering transgenic constructs and mice. *Current protocols in cell biology:* Chapter 19: 10. doi**:**10.1002/0471143030.cb1910s42

Hawley SA, Pan DA, Mustard KJ, Ross L, Bain J, et al. 2005. Calmodulin-dependent protein kinase kinase-beta is an alternative upstream kinase for AMP-

activated protein kinase. *Cell Metabolism* 2(1): 9-19. doi: 10.1016/j.cmet.2005.05.009

Heymans C, Bouckaert JJ, Dautrebande L. 1931. Sinus carotidien et reflexes respiratoires. III. Sensibilite des sinus carotidiens aux substances chimiques. Action stimulante respiratoire reflexe du sulfure de sodium, du cyanure de potassium, de la nicotine et de la lobeline. *Arch Internat Pharmacodyn Et Therap* 40: 54-91. Cited in Wyatt CN, Evans AM. 2007. AMP-activated protein kinase and chemotransduction in the carotid body. *Respiratory Physiology & Neurobiology* 157: 22-29

Hirooka Y, Polson JW, Potts PD, Dampney RAL. 1997. Hypoxia-induced Fos expression in neurons projecting to the pressor region in the rostral ventrolateral medulla. *Neuroscience* 80(4): 1209-24. doi: 10.1016/S0306-4522(97)00111-5

Hoffman GE, Smith MS, Verbalis JG. 1993. C-fos and related immediate-early gene-products as markers of activity in neuroendocrine systems. *Frontiers in Neuroendocrinology* 14(3): 173-213. doi: 10.1006/frne.1993.1006

Holehonnur R, Luong JA, Chaturvedi D, Ho A, Lella SK, et al. 2014. Adeno-associated viral serotypes produce differing titers and differentially transduce neurons within the rat basal and lateral amygdala. *BMC Neuroscience* 15:28. doi**:** 10.1186/1471-2202-15-28

Honaramooz A, Megee S, Zeng W, Destrempes MM, Overton SA, et al. 2008. Adeno-associated virus (AAV)-mediated transduction of male germ line stem cells results in transgene transmission after germ cell transplantation. *Faseb Journal* 22(2): 374-82. doi: 10.1096/fj.07-8935com

Hudson ER, Pan DA, James J, Lucocq JM, Hawley SA, et al. 2003. A novel domain in AMP-activated protein kinase causes glycogen storage bodies similar to those seen in hereditary cardiac arrhythmias. *Current Biology* 13(10): 861-66. doi: 10.1016/S0960-9822(03)00249-5

Hurley RL, Anderson KA, Franzone JM, Kemp BE, Means AR, Witters LA. 2005. The Ca2+/calmodulin-dependent protein kinase kinases are AMP-activated protein kinase kinases. *Journal of Biological Chemistry* 280 (32): 29060-66. doi: 10.1074/jbc.M503824200

Ikawa M, Tanaka N, Kao WWY, Verma IM. 2003. Generation of transgenic mice using lentiviral vectors: A novel preclinical assessment of lentiviral vectors for gene therapy. *Molecular Therapy* 8(4): 666-73. doi: 10.1016/S1525-0016(03)00240-5

Iseli TJ, Walter M, van Denderen BJW, Katsis F, Witters LA, et al. 2005. AMP-activated protein kinase beta subunit tethers alpha and gamma Subunits via its C-terminal sequence (186-270). *Journal of Biological Chemistry* 280(14): 13395-400. doi: 10.1074/jbc.M412993200

Jaenisch R, Mintz B. 1974. Simian virus 40 DNA sequences in DNA of healthy adult mice derived from preimplantation blastocysts injected with viral DNA. *Proceedings of the National Academy of Sciences of the United States of America* 71(4): 1250-54. doi: 10.1073/pnas.71.4.1250

Kahn BB, Alquier T, Carling D, Hardie DG. 2005. AMP-activated protein kinase: Ancient energy gauge provides clues to modern understanding of metabolism. *Cell Metabolism* 1(1): 15-25. doi: 10.1016/j.cmet.2004.12.003

Kaspar BK, Vissel B, Bengoechea T, Crone S, Randolph-Moore L, et al. 2002. Adeno-associated virus effectively mediates conditional gene modification in the brain. *Proceedings of the National Academy of Sciences of the United States of America* 99(4): 2320-25. doi:10.1073/pnas.042678699

Kasparov S, Paton JFR. 2000. Somatic gene transfer: implications for cardiovascular control. *Experimental Physiology* 85(6): 747-55. doi: 10.1111/j.1469-445X.2000.02144.x

Kilby NJ, Snaith MR, Murray JAH. 1993. Site-specific recombinases- tools for genome engineering. *Trends in Genetics* 9(12): 413-21. doi: 10.1016/0168-9525(93)90104-P

King TL, Heesch CM, Clark CG, Kline DD, Hasser EM. 2012. Hypoxia activates nucleus tractus solitarii neurons projecting to the paraventricular nucleus of the hypothalamus. *American Journal of Physiology-Regulatory Integrative and Comparative Physiology* 302(10): R1219-R32. doi: 10.1152/ajpregu.00028.2012

Kola B, Boscaro M, Rutter GA, Grossman AB, Korbonits M. 2006. Expanding role of AMPK in endocrinology. *Trends in Endocrinology and Metabolism* 17: 205-15

Kola B, Grossman AB, Korbonits M. 2008. The role of AMP-Activated protein kinase in obesity. *Obesity and Metabolism* 36: 198-211

Kootstra NA, Verma IM. 2003. Gene therapy with viral vectors. *Annual Review of Pharmacology and Toxicology* 43: 413-39. doi**:** 10.1146/annurev.pharmtox.43.100901.140257

Kos CH. 2004. Cre/loxP system for generating tissue-specific knockout mouse models. *Nutrition Reviews* 62(6): 243-46. **doi:** 10.1301/nr.2004.jun.243-246

Kovacs KJ. 1998. c-Fos as a transcription factor: a stressful (re)view from a functional map. *Neurochemistry International* 33(4): 287-97. doi: 10.1016/S0197-0186(98)00023-0

Kumar P. 2007. Sensing hypoxia in the carotid body: from stimulus to response. Essays in Biochemistry 43:43-60

Kumar P, Prabhakar NR. 2012. Peripheral Chemoreceptors: Function and Plasticity of the Carotid Body. *Comprehensive Physiology*, 2(1):141-219

Lahiri S. 2000. Historical perspectives of cellular oxygen sensing and responses to hypoxia. *Journal of Applied Physiology* 88(4): 1467-73

Lahiri S, Roy A, Baby SM, Hoshi T, Semenza GL, Prabhakar NR. 2006. Oxygen sensing in the body. *Progress in Biophysics & Molecular Biology* 91(3): 249-86. doi: 10.1016/j.pbiomolbio.2005.07.001

Lentz TB, Gray SJ, Samulski RJ. 2012. Viral vectors for gene delivery to the central nervous system. *Neurobiology of Disease* 48(2): 179-88. doi: 10.1016/j.nbd.2011.09.014

Li A, Emond L, Nattie E. 2008. Brainstem catecholaminergic neurons modulate both respiratory and cardiovascular function. Integration in Respiratory Control: from Genes to Systems. *Advances in Experimental Medicine and Biology* 605: 371-76

Li AH, Nattie E. 2006. Catecholamine neurones in rats modulate sleep, breathing, central chemoreception and breathing variability. *Journal of Physiology-London* 570(2): 385-96. doi**:** 10.1113/jphysiol.2005.099325

Lim R, Zavou MJ, Milton P-L, Chan ST, Tan JL, et al. 2014. Measuring Respiratory Function in Mice Using Unrestrained Whole-body Plethysmography. *Jove-Journal of Visualized Experiments* 90: e51755 doi: 10.3791/51755

Lira VA, Soltow QA, Long JHD, Betters JL, Sellman JE, Criswell DS. 2007. Nitric oxide increases GLUT4 expression and regulates AMPK signaling in skeletal muscle. *American Journal of Physiology-Endocrinology and Metabolism*, 293(4):E1062-E1068.

Liu YZ, Ji ES, Xiang SL, Tamisier R, Tong JL, et al. 2009. Exposure to cyclic intermittent hypoxia increases expression of functional NMDA receptors in

the rat carotid body. *Journal of Applied Physiology* 106(1): 259-67. doi: 10.1152/japplphysiol.90626.2008

Lopez-Barneo J. 2003. Oxygen and glucose sensing by carotid body glomus cells. *Current Opinion in Neurobiology* 13(4): 493-99. doi**:** 10.1016/S0959-4388(03)00093-X

Lopez-Barneo J, Ortega-Saenz P, Pardal R, Pascual A, Piruat JI. 2008. Carotid body oxygen sensing. *European Respiratory Journal* 32(5): 1386-98. doi: 10.1183/09031936.00056408

Lopez-Barneo J, Ortega-Saenz P, Pardal R, Pascual A, Piruat JI, et al. 2009. Oxygen Sensing in the Carotid Body. Hypoxia and Consequences from Molecule to Malady. *Annals of the New York Academy of Sciences* 1177: 119-31. doi: 10.1111/j.1749-6632.2009.05033.x

Lopez-Barneo J, Pardal R, Ortega-Saenz P. 2001. Cellular mechanisms of oxygen sensing. *Annual Review of Physiology* 63: 259-87. doi: 10.1146/annurev.physiol.63.1.259

Ma S, Mifflin SW, Cunningham JT, Morilak DA. 2008. Chronic intermittent hypoxia sensitizes acute hypothalamic-pituitary-adrenal stress reactivity and Fos induction in the rat locus coeruleus in response to subsequent immobilization stress. *Neuroscience* 154(4): 1639-47. doi: 10.1016/j.neuroscience.2008.04.068

Mahlapuu M, Johansson C, Lindgren K, Hjalm G, Barnes BR, et al. 2004. Expression profiling of the gamma-subunit isoforms of AMP-activated protein kinase suggests a major role for gamma 3 in white skeletal muscle. *American Journal of Physiology-Endocrinology and Metabolism* 286(2): E194-E200. doi: 10.1152/ajpendo.00147.2003

Mahmoud AD. 2015a. The loss of LKB1 and the AMPK-activated protein kinase in catecholaminergic cells and effect on the ventilatory response to hypoxia and hypercapnia. Phd Thesis, University of Edinburgh, UK.

Mahmoud AD Lewis S, Juričić L, Udoh U, Hartmann S, Jansen MA, Ogunbayo OA, P Puggioni P, Navarro-Dorado J, Foretz M, Viollet B, Dutia MB, Marshall I, Evans AM. 2015b. AMPK deficiency blocks the regulation of breathing by hypoxia and thus precipitates hypoventilation and apnoea. American Journal of Respiratory and Critical Care Medicine, under review.

Mayer CA, Wilson CG, MacFarlane PM. 2015. Changes in carotid body and nTS neuronal excitability following neonatal sustained and chronic intermittent

hypoxia exposure. *Respiratory Physiology & Neurobiology* 205: 28-36**.** doi: 10.1016/j.resp.2014.09.015

McCown TJ, Xiao X, Li J, Breese GR, Samulski RJ. 1996. Differential and persistent expression patterns of CNS gene transfer by an adeno-associated virus (AAV) vector. *Brain Research* 713(1-2): 99-107. doi: 10.1016/0006-8993(95)01488-8

McGinnis WR, Audhya T, Edelson SM. 2013. Proposed Toxic and Hypoxic Impairment of a Brainstem Locus in Autism. *International Journal of Environmental Research and Public Health* 10(2): 6955-7000. doi: 10.3390/ijerph10126955

Meares GP, Hughes KJ, Naatz A, Papa FR, Urano F, Hansen PA, Benveniste EN, Corbett JA. 2011. IRE1-Dependent Activation of AMPK in Response to Nitric Oxide. *Molecular and Cellular Biology*, 31(21):4286-4297

Meares GP, Qin H, Liu Y, Holdbrooks AT, Benveniste EN. 2013. AMP-Activated Protein Kinase Restricts IFN-gamma Signaling. *Journal of Immunology*, 190(1):372-380**.**

Merrill GF, Kurth EJ, Hardie DG, Winder WW. 1997. AICA riboside increases AMP-activated protein kinase, fatty acid oxidation, and glucose uptake in rat muscle. *American Journal of Physiology* 273: E1107-E12

Metzger D, Chambon P. 2001. Site- and time-specific gene targeting in the mouse. *Methods* 24(1): 71-80. **doi:** 10.1006/meth.2001.1159

Miao X. 2013. Recent advances in the development of new transgenic animal technology. *Cellular and Molecular Life Sciences* 70(5): 815-28. doi**:** 10.1007/s00018-012-1081-7

Mills E, Jobsis FF. 1972. Mitochondrial respiratory chain of carotid-body and chemoreceptor response to changes in oxygen-tension. *Journal of Neurophysiology* 35(4): 405-428

Minokoshi Y, Alquier T, Furukawa N, Kim YB, Lee A, et al. 2004. AMP-kinase regulates food intake by responding to hormonal and nutrient signals in the hypothalamus. *Nature* 428(6982): 569-74. doi**:** 10.1038/nature02440

Miyamoto T, Rho E, Sample V, Akano H, Magari M, et al. 2015. Compartmentalized AMPK Signaling Illuminated by Genetically Encoded Molecular Sensors and Actuators. *Cell Reports* 11(4): 657-70. doi**:** 10.1016/j.celrep.2015.03.057

Momcilovic M, Hong S-P, Carlson M. 2006. Mammalian TAK1 activates Snf1 protein kinase in yeast and phosphorylates AMP-activated protein kinase in vitro. *Journal of Biological Chemistry* 281(35): 25336-43. doi**:** 10.1074/jbc.M604399200

Montoro RJ, Urena J, FernandezChacon R, deToledo GA, LopezBarneo J. 1996. Oxygen sensing by ion channels and chemotransduction in single Glomus cells. *Journal of General Physiology* 107(1): 133-43. doi**:** 10.1085/jgp.107.1.133

Morgan JI, Curran T. 1991. Stimulus-transcription coupling in the nervous-system – involvement of the inducible protooncogenes Fos and Jun. *Annual Review of Neuroscience* 14: 421-51. doi**:** 10.1146/annurev.ne.14.030191.002225

Motoshima H, Goldstein BJ, Igata M, Araki E. 2006. AMPK and cell proliferation - AMPK as a therapeutic target for atherosclerosis and cancer. *Journal of Physiology-London* 574: 63-71

Nakamura A, Kuwaki T. 2003. Sleep apnea in mice: a useful animal model for study of SIDS? Early Human Development 75: S167-S74. doi: 10.1016/j.earlhumdev.2003.08.019

Naldini L. 1998. Lentiviruses as gene transfer agents for delivery to non-dividing cells. *Current Opinion in Biotechnology* 9(5): 457-63. doi**:** 10.1016/S0958-1669(98)80029-3

Nattie E. 1999. CO(2), brainstem chemoreceptors and breathing. *Progress in Neurobiology* 59(4): 299-331. doi**:** 10.1016/S0301-0082(99)00008-8

Neubauer JA, Sunderram J. 2004. Oxygen-sensing neurons in the central nervous system. *Journal of Applied Physiology* 96(1): 367-74. doi: 10.1152/japplphysiol.00831.2003

Neurath KM, Keough MP, Mikkelsen T, Claffey KP. 2006. AMP-dependent protein kinase alpha 2 isoform promotes hypoxia-induced VEGF expression in human glioblastoma. *Glia* 53(7): 733-43. doi**:** 10.1002/glia.20326

Nurse CA. 2005. Neurotransmission and neuromodulation in the chemosensory carotid body. *Autonomic Neuroscience-Basic & Clinical* 120(1-2): 1-9. doi: 10.1016/j.autneu.2005.04.008

Oakhill JS, Chen Z-P, Scott JW, Steel R, Castelli LA, et al. 2010. beta-Subunit myristoylation is the gatekeeper for initiating metabolic stress sensing by AMP-activated protein kinase (AMPK). *Proceedings of the National*

*Academy of Sciences of the United States of America* 107(45): 19237-41. doi**:** 10.1073/pnas.1009705107

Packer AM, Roska B, Haeusser M. 2013. Targeting neurons and photons for optogenetics. *Nature Neuroscience*, 16(7):805-815

Palmiter RD, Brinster RL. 1986. Germ-line transformation of mice. *Annual Review of Genetics* 20: 465-99

Pardal R, Ortega-Saenz P, Duran R, Lopez-Barneo J. 2007. Glia-like stem cells sustain physiologic neurogenesis in the adult mammalian carotid body. *Cell* 131(2): 364-77. doi**:** 10.1016/j.cell.2007.07.043

Parenti A, Macchi V, Snenghi R, Porzionato A, Scaravilli T, et al. 2005a. Selective stroke of the solitary tract nuclei in two cases of central sleep apnoea. *Clinical Neuropathology* 24(5): 239-46

Paxinos G, Watson C. 1998. The rat brain - In stereotaxic coordinates . *Rat Brain in Stereotaxic Coordinates, Fourth Ed.*: Elsevier Academic Press INC, 525 B Street, Suite 1900, San Diego, CA 92101-4495 USA.

Peel AL, Zolotukhin S, Schrimsher GW, Muzyczka N, Reier PJ. 1997. Efficient transduction of green fluorescent protein in spinal cord neurons using adeno-associated virus vectors containing cell type-specific promoters. *Gene Therapy* 4(1): 16-24. doi**:** 10.1038/sj.gt.3300358

Peers C, Buckler KJ. 1995. Transduction of chemostimuli by the type-I carotid-body cell. *Journal of Membrane Biology* 144(1): 1-9

Peers C, Wyatt CN, Evans AM. 2010. Mechanisms for acute oxygen sensing in the carotid body. *Respiratory Physiology & Neurobiology* 174(3): 292-98. doi**:** 10.1016/j.resp.2010.08.010

Peltohuikko M, Dagerlind A, Kononen J, Lundberg JM, Villar M, et al. 1995. Neuronal regulation of C-Fos C-Jun, and JunB immediate-early genes in rat adrenal-medulla. *Journal of Neuroscience* 15(3): 1854-68

Peng ZC, Chen S, Bentivoglio M. 1995. A sensitive double immunostaining protocol for Fos-immunoreactive neurons. *Brain Research Bulletin* 36(1): 101-05. doi**:** 10.1016/0361-9230(94)00125-K

Pilon G, Dallaire P, Marette A.2004. Inhibition of inducible nitric-oxide synthase by activators of AMP-activated protein kinase - A new mechanism of action of

insulin-sensitizing drugs. *Journal of Biological Chemistry*, 279(20):20767-20774

Pitkow LJ, Sharer CA, Ren XL, Insel TR, Terwilliger EF, Young LJ. 2001. Facilitation of affiliation and pair-bond formation by vasopressin receptor gene transfer into the ventral forebrain of a monogamous vole. *Journal of Neuroscience* 21(18): 7392-96

Polekhina G, Gupta A, Michell BJ, van Denderen B, Murthy S, et al. 2003. AMPK beta subunit targets metabolic stress sensing to glycogen. *Current Biology* 13(10): 867-71. doi**:** 10.1016/S0960-9822(03)00292-6

Prabhakar NR. 2000. Oxygen sensing by the carotid body chemoreceptors. *Journal of Applied Physiology* 88(6): 2287-95

Prabhakar NR, Peng YJ. 2004. Peripheral chemoreceptors in health and disease. *Journal of Applied Physiology* 96(1): 359-66. doi: 10.1152/japplphysiol.00809.2003

Putnam RW. 2010. CO2 chemoreception in cardiorespiratory control. *Journal of Applied Physiology* 108(6): 1796-802. doi**:** 10.1152/japplphysiol.01169.2009

Putnam RW, Filosa JA, Ritucci NA. 2004. Cellular mechanisms involved in CO(2) and acid signaling in chemosensitive neurons. *American Journal of Physiology-Cell Physiology* 287(6): C1493-C526. doi**:** 10.1152/ajpcell.00282.2004

Ravn K, Nielsen JB, Skjeldal OH, Kerr A, Hulten M, Schwartz M. 2005. Large genomic rearrangements in MECP2. *Human mutation* 25(3): 324-24 doi**:**10.1002/humu.9320.

Reis DJ, Golanov EV, Ruggiero DA, Sun MK. 1994. Sympathoexcitatory neurons of the rostral ventrolateral medulla are oxygen sensors and essential elements in the tonic and reflex control of the systemic and cerebral circulations. *Journal of Hypertension* 12 (10): S159-S80

Roux J-C, Villard L. 2010. Biogenic Amines in Rett Syndrome: The Usual Suspects. *Behavior Genetics* 40(1): 59-75. doi**:** 10.1007/s10519-009-9303-y

Ruderman NB, Carling D, Prentki M, Cacicedo JM. 2013. AMPK, insulin resistance, and the metabolic syndrome. *Journal of Clinical Investigation* 123(7): 2764-72. doi**:** 10.1172/JCI67227

Sagar SM, Sharp FR, Curran T. 1988. Expression of c-fos protein in brain –metabolic mapping at the cellular-level. *Science* 240 (4857): 1328-31. doi**:** 10.1126/science.3131879

Salt I, Celler JW, Hawley SA, Prescott A, Woods A, et al. 1998. AMP-activated protein kinase: greater AMP dependence, and preferential nuclear localization, of complexes containing the alpha 2 isoform. *Biochemical Journal* 334: 177-87

Sanders MJ, Grondin PO, Hegarty BD, Snowden MA, Carling D. 2007. Investigating the mechanism for AMP activation of the AMP-activated protein kinase cascade. *Biochemical Journal* 403: 139-48. doi**:** 10.1042/BJ20061520

Sauer B, Henderson N. 1988. Site-specific DNA Recombination in mammalian-cells by the cre recombinase of Bacteriophage-P1. *Proceedings of the National Academy of Sciences of the United States of America* 85(14): 5166-70. doi: 10.1073/pnas.85.14.5166

Schultz BR, Chamberlain JS. 2008. Recombinant adeno-associated virus transduction and integration. *Molecular Therapy* 16(7): 1189-99.doi**:** 10.1038/mt.2008.103

Sica AL, Greenberg HE, Scharf SM, Ruggiero DA. 2000. Immediate-early gene expression in cerebral cortex following exposure to chronic-intermittent hypoxia. *Brain Research* 870(1-2): 204-10. doi**:** 10.1016/S0006-8993(00)02170-3

Sinnayah P, Lindley TE, Staber PD, Cassell MD, Davidson BL, Davisson RL. 2002. Selective gene transfer to key cardiovascular regions of the brain: Comparison of two viral vector systems. *Hypertension* 39(2): 603-08. doi**:** 10.1161/hy0202.103295

Sinnayah P, Lindley TE, Staber PD, Davidson BL, Cassell MD, Davisson RL. 2004. Targeted viral delivery of Cre recombinase induces conditional gene deletion in cardiovascular circuits of the mouse brain. *Physiological Genomics* 18(1): 25-32. doi**:** 10.1152/physiolgenomics.00048.2004

Smith JC, Abdala APL, Borgmann A, Rybak IA, Paton JFR. 2013. Brainstem respiratory networks: building blocks and microcircuits. *Trends in Neurosciences* 36(3): 152-62

Soliz J, Soulage C, Borter E, van Patot MT, Gassmann M. 2008. Ventilatory responses to acute and chronic hypoxia are altered in female but not male Paskin-deficient mice. *American Journal of Physiology-Regulatory*

*Integrative and Comparative Physiology* 295(2): R649-R58. doi: 10.1152/ajpregu.00876.2007

Song P, Wang S, He C, Wang S, Liang B, et al. 2011. AMPK alpha 2 Deletion Exacerbates Neointima Formation by Upregulating Skp2 in Vascular Smooth Muscle Cells. *Circulation Research* 109(11): 1230-U91. doi: 10.1161/CIRCRESAHA.111.250423

Stec DE, Davisson RL, Haskell RE, Davidson BL, Sigmund CD. 1999. Efficient liver-specific deletion of a floxed human angiotensinogen transgene by adenoviral delivery of Cre recombinase in vivo. *Journal of Biological Chemistry* 274(30): 21285-90. doi: 10.1074/jbc.274.30.21285

Stein SC, Woods A, Jones NA, Davison MD, Carling D. 2000. The regulation of AMP-activated protein kinase by phosphorylation. *Biochemical Journal* 345(3): 437-43. doi: 10.1042/0264-6021:3450437

Steinberg GR, Kemp BE. 2009. AMPK in Health and Disease. *Physiological Reviews* 89(3): 1025-78. doi: 10.1152/physrev.00011.2008

Stettner G, Dutschmann M, Gaertner J, Huppke P. 2007. Breathing dysfunctions associated with impaired control of postinspiratory activity in Mecp2(-/y) knockout mice. *Journal of physiology-London*, 579(3): 863-876. doi: 10.1113/jphysiol.2006.119966

Suter M, Riek U, Tuerk R, Schlattner U, Wallimann T, Neumann D. 2006. Dissecting the role of 5 '-AMP for allosteric stimulation, activation, and deactivation of AMP-activated protein kinase. *Journal of Biological Chemistry* 281(43): 32207-16. doi: 10.1074/jbc.M606357200

Teppema LJ, Dahan A. 2010. The Ventilatory Response to Hypoxia in Mammals: Mechanisms, Measurement, and Analysis. *Physiological Reviews* 90(2): 675-754. doi: 10.1152/physrev.00012.2009

Teppema LJ, Veening JG, Kranenburg A, Dahan A, Berkenbosch A, Olievier C. 1997. Expression of c-fos in the rat brainstem after exposure to hypoxia and to normoxic and hyperoxic hypercapnia. *Journal of Comparative Neurology* 388(2): 169-90. doi: 10.1002/(SICI)1096-9861(19971117)388:2<169::AID-CNE1>3.0.CO;2-#

Thiele TE, Cubero I, van Dijk G, Mediavilla C, Bernstein IL. 2000. Ethanol-induced c-Fos expression in catecholamine- and neuropeptide Y-producing neurons in rat brainstem. *Alcoholism-Clinical and Experimental Research* 24(6): 802-09. doi: 10.1111/j.1530-0277.2000.tb02059.x

Towler MC, Hardie DG. 2007. AMP-activated protein kinase in metabolic control and insulin signaling. *Circulation Research* 100(3): 328-41. doi**:** 10.1161/01.RES.0000256090.42690.05

Townley R, Shapiro L. 2007. Crystal structures of the adenylate sensor from fission yeast AMP-activated protein kinase. *Science* 315(5819): 1726-29. doi**:** 10.1126/science.1137503

Tsien JZ, Chen DF, Gerber D, Tom C, Mercer EH, et al. 1996. Subregion- and cell type-restricted gene knockout in mouse brain. *Cell* 87(7): 1317-26. doi: 10.1016/S0092-8674(00)81826-7

Turnley AM, Stapleton D, Mann RJ, Witters LA, Kemp BE, Bartlett PF. 1999. Cellular distribution and developmental expression of AMP-activated protein kinase isoforms in mouse central nervous system. *Journal of Neurochemistry* 72(4): 1707-16. doi**:** 10.1046/j.1471-4159.1999.721707.x

Urena J, Fernandezchacon R, Benot AR, Detoledo GA, Lopezbarneo J. 1994. Hypoxia induces voltage-dependent $Ca^{2+}$ entry and quantal dopamine secretion in carotid-body glomus cells. *Proceedings of the National Academy of Sciences of the United States of America* 91(21): 10208-11. doi**:** 10.1073/pnas.91.21.10208

Vasileva A, Jessberger R. 2005. Precise hit: Adeno-associated virus in gene targeting. *Nature Reviews Microbiology* 3(11): 837-47. doi**:** 10.1038/nrmicro1266

Viemari JC, Roux JC, Tryba AK, Saywell R, Burnet H, et al. 2005. Mecp2 deficiency disrupts norepinephrine and respiratory systems in mice. *Journal of Neuroscience* 25(50): 11521-30. doi**:** 10.1523/JNEUROSCI.4373-05.2005

Viollet B, Horman S, Leclerc J, Lantier L, Foretz M, et al. 2010. AMPK inhibition in health and disease. *Critical Reviews in Biochemistry and Molecular Biology* 45(4): 276-95. doi**:** 10.3109/10409238.2010.488215

Watt MJ, Dzamko N, Thomas WG, Rose-John S, Ernst M, et al. 2006. CNTF reverses obesity-induced insulin resistance by activating skeletal muscle AMPK. *Nature Medicine* 12(5): 541-48 .doi**:** 10.1038/nm1383

Weir EK, Lopez-Barneo J, Buckler KJ, Archer SL. 2005. Mechanisms of disease - Acute oxygen-sensing mechanisms. *New England Journal of Medicine* 353(19): 2042-55. doi**:** 10.1056/NEJMra050002

Whipp BJ. 1994. Carotid-bodies and breathing in humans. *Thorax* 49(11): 1081-84. doi**I:** 10.1136/thx.49.11.1081

Woods A, Dickerson K, Heath R, Hong SP, Momcilovic M, et al. 2005. Ca2+/calmodulin-dependent protein kinase kinase-beta acts upstream of AMP-activated protein kinase in mammalian cells. *Cell Metabolism* 2(1): 21-33. doi**:** 10.1016/j.cmet.2005.06.005

Woods A, Johnstone SR, Dickerson K, Leiper FC, Fryer LGD, et al. 2003. LKB1 is the upstream kinase in the AMP-activated protein kinase cascade. *Current Biology* 13(22): 2004-08. **doi:** 10.1016/j.cub.2003.10.031

Woods A, Munday MR, Scott J, Yang XL, Carlson M, Carling D. 1994. Yeast SNF1 is functionally related to mammalian AMP-activated protein-kinase and regulates acetyl-coA carboxylase in-vivo. *Journal of Biological Chemistry* 269 (30): 19509-15

Wright JF, Qu G, Tang CL, Sommer JM. 2003. Recombinant adeno-associated virus: Formulation challenges and strategies for a gene therapy vector. *Current Opinion in Drug Discovery & Development* 6 (2): 174-78

Wyatt CN, Evans AM. 2007. AMP-activated protein kinase and chemotransduction in the carotid body. *Respiratory Physiology & Neurobiology* 157(1): 22-29. doi**:** 10.1016/j.resp.2007.01.021

Wyatt CN, Mustard KJ, Pearson SA, Dallas ML, Atkinson L, et al. 2007. AMP-activated protein kinase mediates carotid body excitation by hypoxia. *Journal of Biological Chemistry* 282(11): 8092-98. doi: 10.1074/jbc.M608742200

Xiao B, Heath R, Saiu P, Leiper FC, Leone P, et al. 2007. Structural basis for AMP binding to mammalian AMP-activated protein kinase. *Nature* 449(7161): 496-U14. doi**:** 10.1038/nature06161

Xiao B, Sanders MJ, Underwood E, Heath R, Mayer FV, et al. 2011. Structure of mammalian AMPK and its regulation by ADP. *Nature* 472(7342): 230-33. doi**:** 10.1038/nature09932

Xie M, Zhang D, Dyck JRB, Li Y, Zhang H, et al. 2006. A pivotal role for endogenous TGF-beta-activated kinase-1 in the LKB1/AMP-activated protein kinase energy-sensor pathway. *Proceedings of the National Academy of Sciences of the United States of America* 103(46): 17378-83. doi**:** 10.1073/pnas.0604708103

Yamauchi T, Kamon J, Minokoshi Y, Ito Y, Waki H, et al. 2002. Adiponectin stimulates glucose utilization and fatty-acid oxidation by activating AMP-activated protein kinase. *Nature Medicine* 8(11): 1288-95. doi**:** 10.1038/nm788

Zincarelli C, Soltys S, Rengo G, Rabinowitz JE. 2008. Analysis of AAV serotypes 1-9 mediated gene expression and tropism in mice after systemic injection. *Molecular Therapy* 16(6): 1073-80. doi: 10.1038/mt.2008.76

Zoccal DB, Furuya WI, Bassi M, Colombari DSA, Colombari E. 2014. The nucleus of the solitary tract and the coordination of respiratory and sympathetic activities. *Frontiers in Physiology* 5:234. doi**:** 10.3389/fphys.2014.00238

Zufferey R, Dull T, Mandel RJ, Bukovsky A, Quiroz D, et al. 1998. Self-inactivating lentivirus vector for safe and efficient in vivo gene delivery. *Journal of Virology* 72(12): 9873-80